Review article

Efficient integration of covalent triazine frameworks (CTFs) for augmented photocatalytic efficacy: A review of synthesis, strategies, and applications

Shuqi Li [a,b,*], Yintian Mao [c], Jian Yang [a], Yin Li [a], Jun Dong [a], Zhen Wang [a], Lixian Jiang [a], Shilong He [b]

[a] *Ecology and Health Institute, Hangzhou Vocational & Technical College, Hangzhou, China*
[b] *School of Environment and Spatial Informatics, China University of Mining and Technology, Xuzhou 221116, China*
[c] *Hangzhou Environmental Group Company, Hangzhou, China*

ABSTRACT

Heterogeneous photocatalysis emerges as an exceptionally appealing technological avenue for the direct capture, conversion, and storage of renewable solar energy, facilitating the generation of sustainable and ecologically benign solar fuels and a spectrum of other pertinent applications. Heterogeneous nanocomposites, incorporating Covalent Triazine Frameworks (CTFs), exhibit a wide-ranging spectrum of light absorption, well-suited electronic band structures, rapid charge carrier mobility, ample resource availability, commendable chemical robustness, and straightforward synthetic routes. These attributes collectively position them as highly promising photocatalysts with applicability in diverse fields, including but not limited to the production of photocatalytic solar fuels and the decomposition of environmental contaminants. As the field of photocatalysis through the hybridization of CTFs undergoes rapid expansion, there is a pressing and substantive need for a systematic retrospective analysis and forward-looking evaluation to elucidate pathways for enhancing performance. This comprehensive review commences by directing attention to diverse synthetic methodologies for the creation of composite materials. And then it delves into a thorough exploration of strategies geared towards augmenting performance, encompassing the introduction of electron donor–acceptor (D-A) units, heteroatom doping, defect Engineering, architecture of Heterojunction and optimization of morphology. Following this, it systematically elucidates applications primarily centered around the efficient generation of photocatalytic hydrogen, reduction of carbon dioxide through photocatalysis, and the degradation of organic pollutants. Ultimately, the discourse turns towards unresolved challenges and the prospects for further advancement, offering valuable guidance for the potent harnessing of CTFs in high-efficiency photocatalytic processes.

1. Introduction

Amidst the rapid proliferation of contemporary industrialization and the burgeoning global population, there has emerged a set of enduring and formidable challenges concerning energy and environmental matters [1–5]. As a response to these pressing concerns,

there exists an ongoing and persistent endeavor towards the exploration of solar energy utilization, driven by its environmentally sustainable and inexhaustible characteristics [6–9]. As a novel approach for harnessing solar energy, semiconductor photocatalysis technology has garnered significant attention within the realm of scientific inquiry due to its environmentally friendly and energy-efficient attributes when contrasted with biological and chemical methodologies (Fig. 1) [10–14]. The domain of photocatalysis has witnessed an expanding array of semiconductor materials, encompassing but not limited to TiO_2 [15,16], $g-C_3N_4$ [17,18], Bi_2WO_6 [19,20], boron nitride [21,22], Covalent Triazine Frameworks (CTFs) [23–25] and black phosphorus [26,27], all of which have been explored extensively for their applications in photocatalysis. In addition to hydrogen (H_2) production [7,28,29], these materials have found diverse utility in the degradation of organic pollutants [30–32], carbon dioxide reduction [33–35], disinfection [15,36] and so on. Nonetheless, a majority of contemporary photocatalytic systems are comprised of heavy metal constituents, thus warranting endeavors for enhancement in cost-effectiveness and mitigation of biotoxicity associated with the catalyst [37]. Furthermore, there remain challenges such as suboptimal sunlight utilization rates, limited flexibility in band gap adjustment, and heightened rates of recombination among photogenerated carriers. These factors collectively impose significant constraints on the overall quantum efficiency and real-world applicability of photocatalytic processes.

The CTFs comprises a metal-free conjugated semiconductor structure formed by nitrile aromatic units, characterized by its graphitic layered configuration, remarkable physicochemical stability, and substantial nitrogen content [23–25]. In recent years, CTF has emerged as a prominent entity in the realm of photocatalysis, owing to its favorable attributes encompassing physical and chemical stability, biocompatibility, a bandgap energy (Eg) of approximately 2.6 eV, capacity for visible light absorption, and a diverse compositional profile [38,39]. Since the pioneering work by Niu and colleagues in 2014 on the photocatalytic degradation of methylene blue using CTFs, the utilization of CTFs in photocatalytic applications has witnessed a substantial annual upsurge (inset of Fig. 1). These inherent characteristics have rendered CTF highly applicable across a spectrum of domains, encompassing gas adsorption and storage [24,25,38], catalysis [39–41], and energy storage [42,43]. However, in the pursuit of industrial applicability, CTF encounters certain limitations that curtail its efficacy as an exceptionally efficient photocatalyst. These limitations encompass: i) restrictions in the current synthetic methodologies for CTF; ii) limited capacity for visible light absorption; iii) relatively constrained specific surface area; and iv) a suboptimal intrinsic quantum efficiency. To address these challenges encountered in the utilization of CTF within the domain of photocatalysis, numerous research investigations have placed emphasis on the modulation of morphology, incorporation of defects, creation of heterophane structures, and the development of composite materials.

These methodologies have the potential to substantially broaden the inherent band gap of the material by inducing alterations in its physicochemical, optical, and electronic attributes. Such modifications serve to enhance the capacity of material for light capture and utilization, particularly in the visible light spectrum. Concurrently, the introduction of alterations in the donor-acceptor (D-A) conjugated ligands or the establishment of heterostructures through chemical bonding [41,44], π-π stacking and electron attraction interactions proves effective in promoting the efficient separation of photogenerated electron-hole pairs within the CTF framework, thereby expediting their transfer [45–47]. Consequently, when juxtaposed with the performance of pristine CTF, CTF derivatives subjected to diverse modifications have exhibited augmented photocatalytic activity, which exists a profound interest in harnessing the entirety of the solar spectrum for multifarious photocatalytic applications. Although there have been some excellent reviews of CTFs in recent years, majority of them are concentrated on synthetic methods and applications in certain fields, while lack of a systematic discussion on intrinsic charge density and bandgap-promoted photogenerated carrier segregation-migration strategies.

In this review, we present a comprehensive discussion on strategies for the preparation of CTFs, focusing on the modulation of intrinsic charge density and band gap. Subsequently, the comprehensive advancements in the application of modified CTFs in areas such as clean energy production (e.g., H_2 production [30,48–51], clean energy applications [52–55]) and environmental remediation (e.g., organic pollutant degradation [56–59], CO_2 reduction [60–63], and nitrogen fixation [31,64,65]) are discussed. It has been
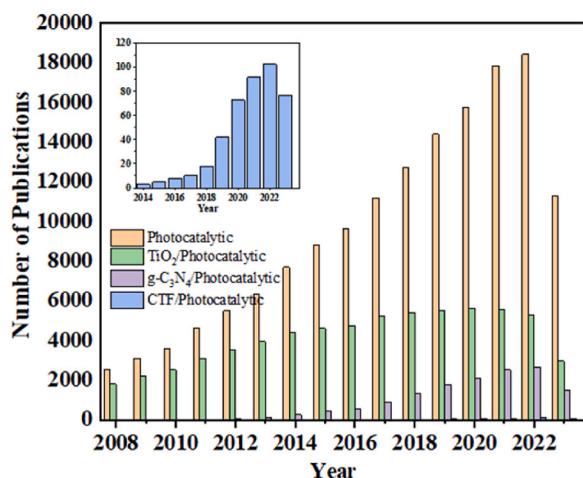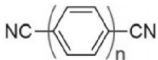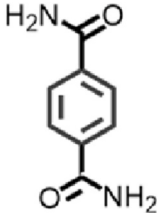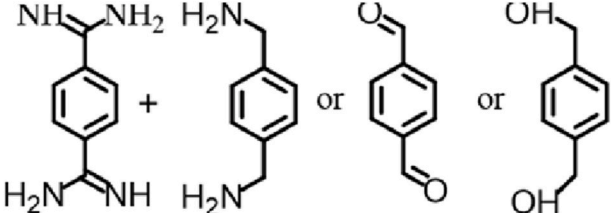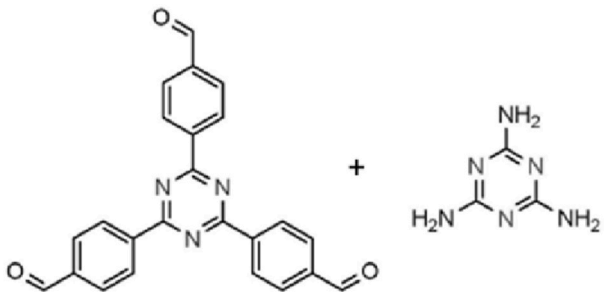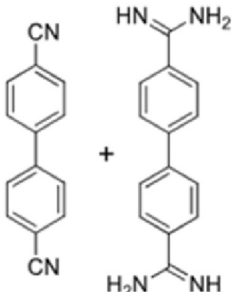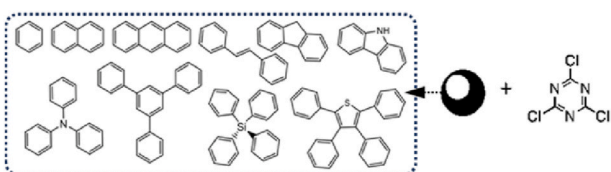

Fig. 1. The annual number of publications containing the word "TiO_2*", $g-C_3N_4$* or CTFs*" in the title and "photocatalytic*" in the topic since 2008. (Using Web of Science, date of search: Sep 19, 2023).

Table 1
Typical monomers used to build CTFs.

Catalysts	Monomer	Preparation condition	Ref.
CTFs		ZnCl$_2$, 300 °C	[43]
CTFs		CF$_3$SO$_3$H/H$_6$P$_4$O$_{13}$	[67]
pCTF-1		P$_2$O$_5$, 400 °C	[60]
CTFs		DMSO, Cs$_2$CO$_3$, 120 °C	[68]
TCMP-3		DMF, 100 °C	[69]
CTF-B		Cs$_2$CO$_3$, 180 °C	[70]
CTFs		AlCl$_3$	[71]

Table 1 (*continued*)

Catalysts	Monomer	Preparation condition	Ref.
NiPor-CTF		ZnCl$_2$, 400 °C	[72]

demonstrated that the synthesis method significantly affects the morphology, charge density, and band gap of CTFs. Precise modifications can effectively accelerate the separation of photogenerated electron-hole pairs and the transfer of photogenerated carriers, thereby enhancing their photocatalytic performance. This review aims to provide insights and strategies for the synthesis of CTF-based derivatives with strong visible light response and excellent photocatalytic properties, facilitating their controlled preparation and subsequent utilization within commercial applications.

2. Synthesis of CTFs

The crystalline nature and utility of CTFs are notably contingent upon the approach employed for their synthesis and monomers (Table 1). Since the pioneering work of Thomas and collaborators in 2008 [66], several methods have emerged for the direct synthesis of CTFs (Fig. 2), including ZnCl$_2$-catalyzed ionothermal method, amidine based polycondensation method, superacid-catalyzed method, coupling method, and P$_2$O$_5$-catalyzed method. Broadly, the synthetic approach exerts a significant influence on the physical characteristics and photocatalytic efficacy of CTFs, consequently bearing implications for their subsequent utilization in diverse applications.
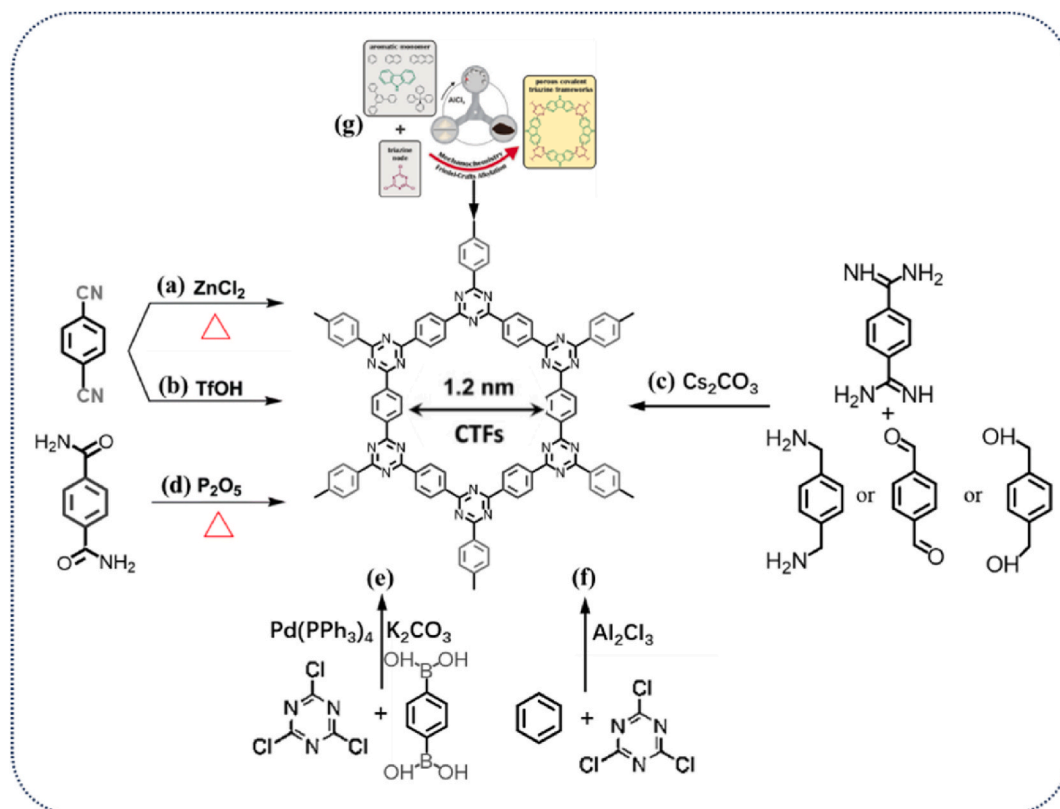

Fig. 2. Cyclization- and coupling-based synthesis of CTFs.

2.1. Ionothermal methods

Since 2008, researchers have employed a method involving the use of readily available aromatic nitrile compounds as monomers to synthesize a series of high-performance CTFs. These syntheses occur under the catalytic influence of $ZnCl_2$ in ionic thermal conditions, with reaction temperatures exceeding 400 °C, and are characterized by both regular and irregular porosity (Fig. 2a) [66,73–77]. $ZnCl_2$ proves to be a highly efficient catalyst, facilitating the requisite reversibility of the triazine ring formation under elevated temperatures and self-induced pressure, thereby enabling the development of CTFs with well-defined, long-range ordered structures. Consequently, the monomer-to-$ZnCl_2$ ratio and the planarity of the monomer wield significant influence over porosity and crystallinity. While CTFs synthesized using this method exhibit a commendable degree of crystalline order, a narrow pore size distribution, and an exceptionally high specific surface area, the elevated reaction temperatures lead to partial carbonization, limiting practical applications. Moreover, the resulting material manifests in the form of black powder, devoid of an electronic band gap, potentially rendering it unsuitable for certain photophysical applications. Additionally, these high-temperature reactions consume a considerable amount of energy and selectively exclude structural units other than the most stable ones, imposing constraints on scalability and synthetic diversification.

Recently, Wang et al. [77] have introduced an ionothermal synthesis approach to fabricate photocatalysts based on CTFs, employing a ternary NaCl–KCl–$ZnCl_2$ eutectic salt (ES) mixture characterized by a melting point of approximately 200 °C. This operating temperature, notably lower than the pure $ZnCl_2$ counterpart (318 °C), offers a conducive milieu for the polycondensation process, thus averting the carbonization of the polymeric scaffold. Consequently, the resultant CTF-ES200 material demonstrates augmented optical and electronic characteristics, ultimately manifesting exceptional efficacy in the photocatalytic process, particularly in the context of the hydrogen evolution reaction (HER).

However, though CTFs possess considerable BET surface areas, their photocatalytic performance is compromised by high-temperature carbonization. Moreover, their large-scale synthesis is impeded by the requirement for high-pressure, time-consuming reaction conditions, and inert atmospheres (e.g., handling within gloveboxes and Parr reactors). Additionally, their assembly into films or pellets faces significant limitations.

2.2. Superacid-catalyzed methods

In 2012, Dai and Cooper group [25,38] pioneered the synthesis of CTFs bearing biphenyl and triphenyl spacer nitriles (Fig. 2b) under acidic conditions, facilitated by trifluoromethanesulfonic acid (CF_3SO_3H) as a catalyst. This methodology effectively catalyzed the dynamic formation and dissociation of triazine bonds, resulting in the attainment of CTFs characterized by a moderate degree of crystallinity. Additionally, the utilization of superacid catalysis conferred the advantage of lower reaction temperatures, yielding finely colored powders, thereby broadening the potential utility, especially within the realms of optics and optoelectronics.

However, it is important to note that this approach tended to yield polymeric materials with a propensity for bulk formation, consequently resulting in a reduced specific surface area. Concurrently, the strong corrosive properties and relatively high cost associated with superacid catalysts imposed certain limitations on their widespread scalability. To address these challenges, Xu and collaborators [78]. introduced an innovative synthetic route employing polyphosphate ($H_6P_4O_{13}$) as a catalyst for nitrile trimerization. This pioneering strategy facilitated the economic and efficient large-scale production of kilogram-scale crystalline CTFs for the first time. Substantiating this development, density functional theory calculations and meticulous controlled experiments demonstrated the superior catalytic activity of polyphosphate compared to its analogs such as H_3PO_4, underscoring its significant potential for applications in environmental remediation.

Nevertheless, CTFs prepared using various super-acidic catalysts exhibit favorable visible-light activity. However, the strong corrosiveness and high cost of trifluoromethanesulfonic acid limit their large-scale application. Although polyphosphoric acid also faces limitations due to partial carbonization at elevated temperatures, its light color powder nature endows it with commendable visible-light activity. Furthermore, its low-cost materials have enabled the preparation of kilogram-scale highly crystalline CTFs. Nonetheless, the strong acidity and corrosiveness of the acidic reagents lied on heightened requirements of synthetic equipment.

2.3. Aldehydes and amidines polycondensation methods

In pursuit of enhanced control over polymer synthesis, Cooper [68] introduced a novel strategy in 2017, involving the condensation reaction between aldehydes and hydrazides for the construction of CTFs under mild conditions (≤120 °C) and in the absence of strong acids (Fig. 2c). This reaction, facilitated by the solvent dimethyl sulfoxide and the alkaline catalyst cesium carbonate (Cs_2CO_3), yielded CTFs characterized by vibrant colors, layered structures, high surface areas, tunable functionalities, and diverse geometries, all achieved at relatively low temperatures (120 °C). The condensation method employed in this approach follows a reversible Michael addition and Schiff base formation, following the irreversible cascade condensation involving dehydrogenation and cyclization. This irreversible/reversible stepwise condensation method serves to lock in an ordered structure, subsequently transforming it into a steady triazine-ring, which forms the foundational basis for the development of highly ordered CTFs. And also, this versatile approach allows for the facile scalability of CTFs production to the multigram level without the need for specialized equipment. Additionally, these materials typically manifest as yellow or orange powders, retaining their optical bandgap, indicative of their potential applications in photophysical domains.

Remarkably, this strategy also enables the fabrication of CTFs in a variety of shapes beyond powders, such as core-shell hollow spheres [79–81], nanosheets [82–85], and free-standing film [86]. This layered structure opens pathways for novel nitrogen-doped layered materials with promising prospects in photocatalysis and energy storage applications, including the catalytic production of

H_2 through sacrificial water splitting and the formation of anodes for sodium-ion batteries [87].

However, the relatively mild polymerization method in an open system circumvents harsh conditions such as high temperatures, inherent pressures, corrosive acids, and inert environments, providing a potential pathway for large-scale industrial production. Furthermore, this approach enables the fabrication of CTFs into various shapes beyond powders, including nanosheets and core-shell structures, significantly expanding their applications.

2.4. Phosphorus pentoxide-catalyzed methods

In 2018, Baek and colleagues [60] developed a phosphorus pentoxide (P_2O_5)-catalyzed condensation reaction conducted at elevated temperatures to synthesize pCTF-1 (Fig. 2d) using diphenylmethane as a precursor. The pCTF-1 exhibited a high degree of crystallinity and a large specific surface area (2034.1 $m^2\ g^{-1}$). In comparison to metal catalysts or superacids, the P_2O_5-catalyzed method offers a relatively environmentally friendly approach, thereby expanding the array of available monomers for the CTFs family. However, it is worth noting that this method displays a notable temperature dependence, with crystallinity and thermal stability being superior at a calcination temperature of 400 °C as opposed to 300 °C. Samples synthesized at 450 °C and 550 °C undergo substantial carbonization, resulting in the formation of amorphous structures, with residual P_2O_5 physically retained within the polymer framework.

Compared to metal or superacids catalysts, the P_2O_5-catalytic method offers relatively environmentally friendly alternatives and a wider range of monomer options. However, the reaction requires high temperatures (~350 °C), inevitably leading to partial carbonization and affecting the visible-light performance.

2.5. Straightforward coupling methods

The synthesis of CTFs can be achieved through the direct creation of triazine nuclei alongside a diverse range of monomeric components. This approach holds a twofold significance: Firstly, it eliminates the requirement for stringent reaction conditions, encompassing elevated temperatures, highly acidic environments, and potent alkali agents. Secondly, it confers modular characteristics upon CTFs, thereby establishing an invaluable foundation for scrutinizing the impact of chemical composition on the photocatalytic performance of these materials, which is helpful in revealing the impact of their chemical composition on their performance in electrochemical applications. Recently,a multitude of CTFs have been synthesized employing C–C coupling reactions (Pd-based Sonogashira coupling [69], Ni-catalyzed Yamamoto coupling [88], and Suzuki cross-coupling reaction (Fig. 2e)), C–Se coupling [89], and CsPbBr$_3$ quantum dots coupling, *etc* [90]. Besides, Yu and colleagues employed cyanuric chloride in conjunction with tetrahedral building blocks, employing the Friedel–Crafts method under mild reaction conditions (Fig. 2f) [91–93]. This method is distinguished by its inherent simplicity, cost-effectiveness, and superior atom economy when contrasted with alternative pathways. Borchardt et al. [94] presented an innovative solvent-free mechanochemical Friedel–Crafts method (Fig. 2g), enabling the large-scale production of CTFs with practical feasibility. Additionally, the ensuing CTFs manifest remarkable thermodynamic and chemical resilience across a wide spectrum of aqueous and organic solvents. Furthermore, it enables the convenient incorporation of heteroatoms into the CTFs via heteroatom-containing aromatic compounds [95,96]. However, it is worth noting that the CTFs obtained via these methodologies tend to exhibit amorphous characteristics due to the kinetically controlled nature of these processes.

Even so, this method offers advantages of simplicity and low cost in the reaction process, enabling large-scale production of CTFs, the crystallinity of CTFs prepared by this method is compromised due to kinetic control of the reaction process.

According to the above, considering the concurrent evaluation of photocatalytic performance and manufacturing expenses, the Aldehydes and Amidines Polycondensation Method stands out as the most promising approach.
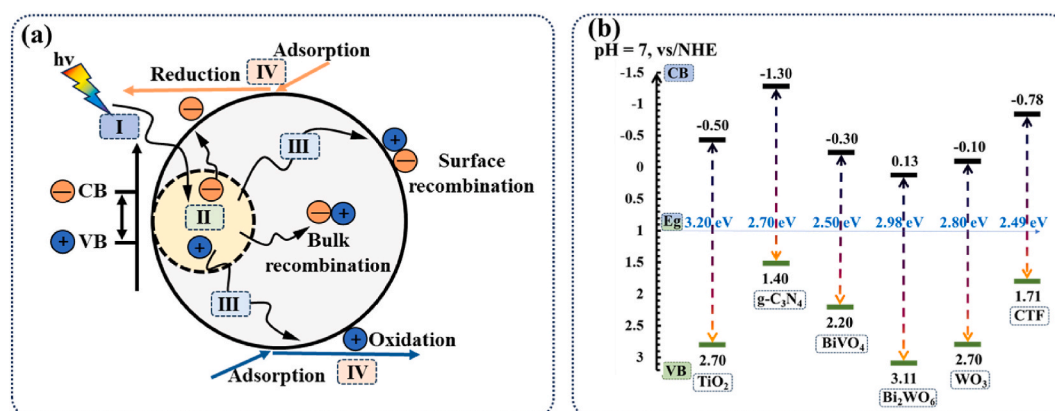

Fig. 3. Typical four-stage mechanism diagram of heterogeneous photocatalysis (a). Band gap structures of several typical photocatalysts (b).

3. Catalytic mechanism and modification strategy of CTFs photocatalyst

3.1. Catalytic mechanism of CTFs photocatalyst

To date, the fundamental mechanism underlying heterogeneous photocatalysis has been extensively elucidated, generally encompassing four principal stages (Fig. 3a): light absorption (Stage I); charge excitation (Stage II); charge separation (Stage III) and transfer; surface electrocatalytic reactions (Stage IV). Firstly, the efficacy of the light absorption process is intimately tied to the surface morphology and structure of the photocatalyst. This is often achieved through the construction of a hierarchical microporous or mesoporous architecture, which enhances light utilization via multiple reflection and scattering effects [39,97]. In this context, it is crucial to consider various dimensions, such as point, line, surface, and volume, in order to optimize light capture, as the flat and smooth surface obtained through the trifluoromethane method is not conducive to this objective. Secondly, the excitation of charge carriers in semiconductors is intrinsically linked to their distinctive electronic structures. Typically, under light irradiation with energy equal to or exceeding the Eg, electrons in the valence band (VB) of a semiconductor are elevated to its conduction band (CB), creating positive holes in the VB. The bandgap characteristics of several representative photocatalysts are summarized in Fig. 3b. Compared with TiO$_2$ [98], g-C$_3$N$_4$ [9], BiVO$_4$ [99], Bi$_2$WO$_6$ [100] and WO$_3$ [101], pristine CTFs [67] exhibit the more suitable bandgap (around 2.36–2.98 eV) for photocatalysis and a negatively positioned CB level, rendering it promising for extended application in visible light photocatalysis. Researchers have further reduced the bandgap of CTFs and adjusted its VB and CB positions through straightforward terminal defects, heteroatom doping, and heterojunction construction strategies [102]. Thirdly, the abundance of active surface/interface sites both within and on the semiconductor dictates the likelihood of charge recombination, separation, and transfer, which is a pivotal factor influencing the quantum efficiency of photocatalysis. In general, decreasing the diffusion distance of photogenerated carriers or establishing an interfacial electric field can effectively curtail the recombination rate, consequently enhancing photocatalytic activity. Strategies for enhancing CTFs performance are often approached from a modification perspective [40,49,103]. Lastly, and of utmost significance, only charge carriers with sufficient energy migrate to the semiconductor surface and are amenable to capture by surface-active sites or cocatalysts, thereby enabling subsequent catalytic reduction or oxidation reactions. Consequently, by effectively modifying the CB and VB levels of CTFs to render them more positive and negative, a broader range of reactants can be accommodated.

Given that the photocatalytic quantum efficiency (η_c) is predominantly contingent upon the cumulative effectiveness exhibited across all four successive stages, encompassing light absorption efficiency (η_{abs}), charge utilization efficiency (η_{cu}), charge migration and transport efficiency (η_{cmt}), and charge separation efficiency (η_{cs}), as delineated in Eq. (1) [102]:

$$\eta_c = \eta_{absolute} \times \eta_{cs} \times \eta_{cmt} \times \eta_{cu} \tag{1}$$

Hence, to devise efficacious photocatalysts tailored to diverse photocatalytic applications, it is imperative to thoroughly contemplate and refine each of these characteristic four-step processes. While considerable advancements have been achieved in the realm of heterogeneous photocatalysis, there persist substantial challenges associated with augmenting light absorption (particularly within the visible spectrum), optimizing carrier excitation, separation, and harnessing their potential effectively [7].

3.2. Strategies to enhance photocatalytic performance of CTFs

To enhance the absorption of visible light by derivatives of CTFs, along with the separation of e$^-$/h$^+$ pairs and the overall η_c, a spectrum of strategies has been devised to augment photocatalytic activity. These encompass the regulation of morphology and structure to expand specific surface area [39,81,104–108], the construction of defects [44,50,109–114], and the introduction of heteroatom doping [63,64,115–133] to tailor energy level configurations. Additionally, the fabrication of nanostructures and interfacial heterostructures has been employed to expedite carrier separation, among other approaches. These methodologies collectively induce alterations in the electronic structure and surface characteristics of CTFs, thereby amplifying its photocatalytic prowess. In the subsequent sections, we will enumerate and comprehensively discuss several representative strategies in this regard.

3.2.1. Electron donor–acceptor (D-A) units building

Incorporating electron-donating and electron-accepting (D-A) units with differing ionization potentials and electron affinities into the polymer matrix constitutes a highly effective strategy for robustly mitigating the rapid recombination of charge carriers during the photocatalytic process. This approach not only enables the rational design of CTFs with tailored band structures at the molecular level but also expedites the transfer of electrons from the highest occupied molecular orbital (HOMO) of the electron-donating unit to the lowest unoccupied molecular orbital (LUMO) of the adjacent electron-accepting unit, thereby engendering an internal electric field. Consequently, this facilitates the dissociation of excitons into liberated electrons and holes, while concurrently extending the carrier lifetime, thereby enhancing charge separation and transfer within the CTF [41,54,134–161]. These numerous benefits offer a plethora of opportunities for the synthesis and refinement of CTF derivatives that satisfy a wide range of uses.

3.2.1.1. Donating-accepting (D-A) units building.
Liu et al. [162] have presented a novel approach involving the incorporation of benzodithiophene (BDT) into CTFs, aimed at modifying the architecture and composition of the D-A components beyond conventional design paradigms. BDT exhibits promise as an electron donor, characterized by its conjugated C2 symmetric structure, while the triazine ring serves as an electron acceptor (Fig. 4a). Density functional theory (DFT) calculations reveal that the HOMO of BDT-CTF-1

predominantly resides within the BDT unit, distinguished by its conjugated C2 symmetric configuration (Fig. 4b). In contrast, the LUMO is primarily localized on the extensive ring formed by benzene and triazine moieties, with minimal orbital overlap between these two regions. This unique configuration within the D-A pore structure establishes an efficient conduit for electron transfer from BDT to the electron-acceptor region, facilitating effective charge separation. Experimental photophysical characterization further corroborates this phenomenon, demonstrating rapid electron transfer between D-A units that curtails the recombination rate of photogenerated charge carriers. This, in turn, extends the exciton lifetime and promotes charge generation and migration. Concurrently, precise control over the band positions and bandgap of the material is attainable through manipulation of the number and proportion of D-A units. It demonstrated that the nuanced control strategy of D-A units building offers the flexibility to finely regulate and enhance the photocatalytic performance as needed.

3.2.1.2. Electron-donating-π-accepting (D-π-A) units building. While the D-A binary configuration promotes efficient intramolecular charge separation, a prevailing challenge lies in the concomitant occurrence of reverse charge recombination, attributed to the mutual electrostatic attraction of charges and attenuated light absorption within the visible spectrum. These factors collectively contribute to a
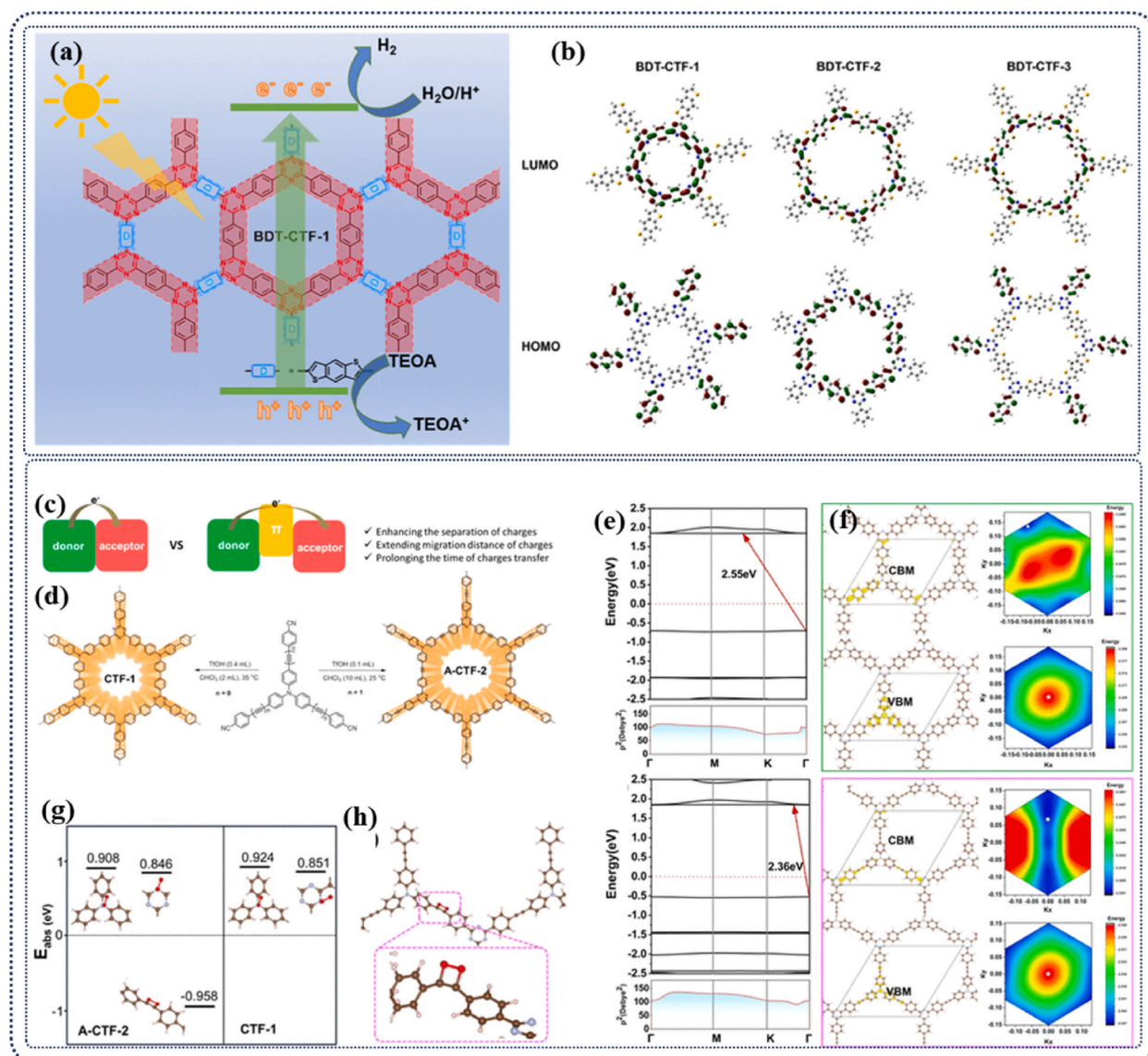
Fig. 4. (a) Synthesis Scheme of BDT-CTFs, (b) Charge density distribution of HOMO and LUMO for oligomer models of BDT-CTFs based on DFT methods. Reproduced with permission [162]. Copyright 2023, American Chemical Society. (c) Schematic diagram of the photoexcited electron-transfer process in the D–A system and D−π–A system. (d) Scheme of synthesis of CTF-1 and A-CTF-2 following acid-catalyzed trimerization. (e) Energy band gap structures and (f) spatial distributions of VBM and CBM of CTF-1 and A-CTF-2. (g) Adsorption energy barriers and (h) Adsorption model of O2 in different sites for CTF-1 and A-CTF-2. Reproduced with permission [134]. Copyright 2021, American Chemical Society.

decline in photocatalytic activity. Consequently, the imperative lies in the minimization of exciton binding energy within the CTFs while concurrently enhancing charge separation, ultimately culminating in the attainment of heightened quantum efficiency [107, 163–174].

Zhang et al. [134] undertook the synthesis of CTFs employing acetylene as a pivotal component within a π-conjugated donor-π-acceptor (D-π-A) motif (Fig. 4c and d), employing a low-temperature acid-catalyzed trimerization approach. A comprehensive examination alongside density functional theory (DFT) computations substantiates that the presence of the acetylene moiety in CTF plays an indispensable role in orchestrating the electronic structure and photoelectric attributes of the CTF. The incorporation of the alkyne group further contributes to the reduction of the energy associated with the lowest CB state (Fig. 4e and f), concomitantly curtailing the bandgap. In essence, this strategic integration of the π-conjugated acetylene unit, while retaining the D-A unit, serves to not only impede the forward migration of electrons but also mitigate reverse charge recombination, thereby diminishing the exciton binding energy. This concerted effect robustly advances the separation and transfer of charge carriers, significantly prolonging the migration lifespan of charge carriers from the donor to the acceptor, consequently promoting positive charge transfer/separation. Simultaneously, the acetylene component fulfills a dual role as an adsorption site, augmenting oxygen adsorption, and as a catalytic active site, effectively reducing the energy barrier associated with the visible-driven oxidative coupling process (Fig. 4g and h). It indicates that the D-π-A motif strategically optimizes the kinetics of electron migration and adsorption behavior, ultimately enhancing the efficacy of photo-redox catalysis.

3.2.2. Heteroatom doping

Semiconductor behavior within CTFs can be finely tuned through the introduction of heteroatoms, including but not limited to N, O, S, B, P, Fe, Pt, and others. This versatile doping strategy offers an effective and alternative means of modulating surface charge characteristics, altering energy level structures, enhancing light absorption capacities, and expediting charge transfer rates, all of which collectively serve as potent strategies to amplify the catalytic efficacy of heterogeneous CTF systems [63,64,123–133]. To date, extensive research has been conducted on the doping of nitrogen, phosphorus, sulfur, and boron [64,110,175–178]. The introduction of these dopants, whether possessing strong electronegativity (e.g., N, F) or weaker electronegativity (e.g., P, B), engenders efficacious heterointerfaces with the benzene and triazine rings intrinsic to the CTF structure. This phenomenon manifests in enhanced absorption of visible light, the modification of energy level potentials, and the improvement of photoluminescence properties concerning
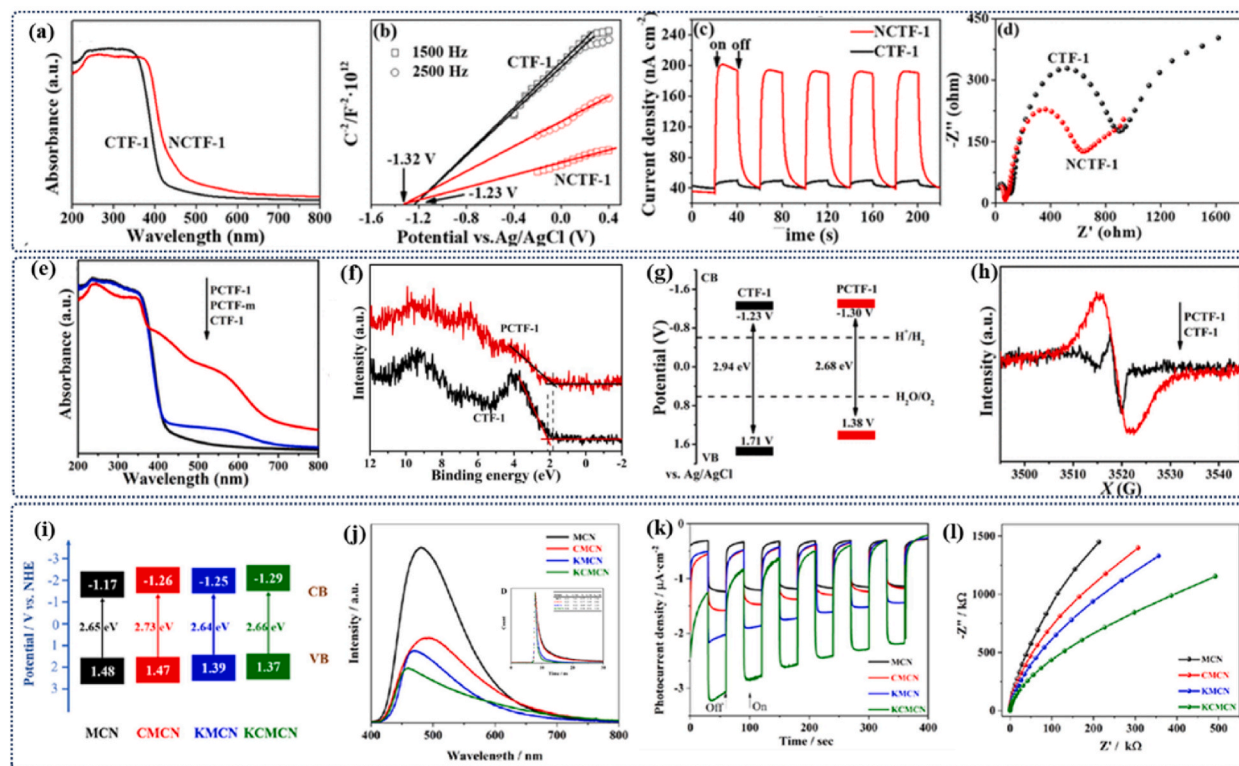
Fig. 5. (a) UV–vis DRS, (b) Mott–Schottky plots, (c) PL spectra, and (d) EIS plots of CTF-1 and NCTF-1. Reproduced with permission [115]. Copyright 2021, American Chemical Society. (e) UV–vis DRS, (f) Valence band XPS spectra, (g) band structures, and (h) room-temperature EPR spectra of CTF-1 and PCTF-1. Reproduced with permission [116]. Copyright 2018, American Chemical Society. (i) Band structures, (j) photo-luminescence (inset was time-resolved photoluminescence), (k) transient photocurrent response, and (l) electrochemical impedance spectra of different samples. Reproduced with permission [133]. Copyright 2022, Elsevier.

hole-electron pairs [115]. Among these doping atoms, nitrogen, in particular, has garnered significant attention due to its expansive optical adsorption range and favorable electronic properties. Furthermore, the catalytic activity can be finely regulated through careful modulation of nitrogen doping concentrations [179].

Huang et al. [115] employed a hydrothermal treatment involving hydrazine hydrate to introduce an excess of nitrogen, resulting in the synthesis of nitrogen self-doped conjugated triazine-based frameworks (NCTF-1). Comprehensive characterization following this process revealed noteworthy changes in the optical properties of NCTF-1 due to the incorporation of nitrogen. Upon nitrogen doping, a subtle redshift was observed in the absorption edge of NCTF-1, expanding the visible light absorption range from approximately 422 nm to around 448 nm (Fig. 5a). This shift corresponded to a reduction in the optical bandgap from 2.94 eV to 2.77 eV, effectively broadening the visible light responsiveness. Moreover, analysis using Mott-Schottky plots indicated an upward shift in the CB position of NCTF-1 (Fig. 5b), signifying an enhanced reduction capability following nitrogen doping. Furthermore, a more in-depth exploration of the electrochemical characteristics of the sample was undertaken through periodic on/off light irradiation, as depicted in Fig. 5c illustrating photocurrent responses. This analysis revealed a significant enhancement in the photocurrent density of NCTF-1, indicating that nitrogen doping accelerates charge separation and migration rates. Electrochemical impedance spectroscopy (EIS) (Fig. 5d) corroborated these findings, showcasing a reduction in the semicircular size of NCTF-1. This reduction is attributed to the heightened electron transfer efficiency resulting from nitrogen self-doping, primarily driven by the strong electron-withdrawing nature of nitrogen atoms within the conjugated C-plane. Consequently, these changes result in a broader visible light response range, improved electron transfer, enhanced charge carrier separation/transfer rates, and ultimately, augmented CO_2 adsorption capabilities.

Furthermore, Fang et al. [116]conducted a study involving the fabrication of red phosphorus-doped PCTF-1, which exhibited enhanced photocatalytic performance following a straightforward heat treatment process. Notably, upon characterizing the optical properties and electronic band structure of PCTF-1 using UV–vis diffuse reflectance spectroscopy (UV–vis DRS), it was observed that PCTF-1 exhibited a subtle redshift compared to the conventional CTF-1 (Fig. 5e). The Kubelka-Munk function analysis further revealed a reduction in the band gap energy from 2.94 eV to 2.68 eV. This shift was attributed to the optical transitions associated with phosphorus impurities within the band gap, resulting in enhanced light absorption across the entire visible spectrum for CTF-1. To elucidate the band gap modifications induced by the doping process, Mott-Schottky and XPS-VB analyses were conducted before and after modification (Fig. 5f). These analyses indicated that the CB potential of PCTF-1 became more negative (Fig. 5g), such an enhancement in photo-reductivity holds substantial promise for facilitating the photocatalytic generation of H_2. Furthermore, additional electronic properties of the sample were probed using room temperature electron paramagnetic resonance (EPR) (Fig. 5h). This analysis revealed a notable increase in the intensity of the Lorentz line with a g value of 2.0034, corresponding to unpaired electrons within the intrinsic π-conjugated aromatic ring of the material, particularly in the dark condition. This enhancement can be attributed to the delocalization of valence electrons from phosphorus into the CTF-1 conjugated system, potentially broadening the band distribution and facilitating electron transfer within the CTF-1 π-conjugated system. Consequently, these changes lead to improved charge migration, ultimately resulting in exceptional photocatalytic activity.

Notably, the modification of CTFs is not limited to non-metallic elements; the inclusion of metal elements can also yield improvements in photocatalytic performance. Ma et al. [133] successfully prepared potassium-intercalated CTF derivatives through a high-temperature mixing process, leading to a deliberate adjustment of the band structure and the formation of structured charge transfer pathways. The optical and electronic characteristics of samples were meticulously assessed using UV–vis DRS. Evidently, the introduction of potassium (K) doping gave rise to a novel absorption band associated with n-π* electron transitions in the 450–800 nm range. Simultaneously, there were notable shifts towards more negative potentials in the positions of the CB and VB (Fig. 5i). This sophisticated modulation of the band structure enhances the reduction capacity and augments visible light absorption capabilities. These enhancements bode well for elevating the driving force behind the oxygen reduction reaction. Furthermore, photoluminescence (PL) tests were conducted to evaluate the efficiency of photogenerated charge carrier migration, separation, and capture. The results (Fig. 5j) show a gradual quenching of the PL emission peak following K doping, suggesting a reduced likelihood of radiative recombination between photogenerated electrons and holes. Additionally, the significantly lowered τave values provide compelling evidence that K doping expedites the fastest non-radiative migration of effective charge separation within the framework. The maximal light response value and minimal radius, as ascertained through I-T response (Fig. 5k) and EIS (Fig. 5l), corroborate that the incorporation of potassium significantly reduces electron transfer resistance and enhances the mobility of photogenerated electrons. As a result, KCMCN exhibits a remarkable hydrogen peroxide (H_2O_2) yield of 317.9 μmol L^{-1} h^{-1}, surpassing bulk carbon nitride by a factor of 10.7.

As previously discussed, doping strategies provide an effective approach to engineering the electron band structure and charge transfer properties, simultaneously expanding the visible light optical absorption spectrum and enhancing its performance, which can further bolster photocatalytic efficacy significantly.

3.2.3. Defect engineering

An inherent advantage of organic polymers lies in their modifiable molecular structure. In recent developments, the deliberate introduction of structural irregularities into conjugated polymer planes has emerged as a viable tactic for hastening exciton electron capture. This approach minimizes exciton binding, augments charge separation, and effectively elevates photocatalytic activity under visible light exposure. Nonetheless, the introduction of such defects, often achieved through external conditions like infrared radiation, carries a substantial risk, primarily due to the uncontrollable nature of the process. In response to this challenge, certain researchers have adeptly pursued a precise molecular regulation strategy. They achieve this by selecting monomers with distinctive properties within their structure that are resistant to polymerization by terminal groups, all while meticulously adjusting their content ratios [44, 50,109–114].

Fan et al. [112] fabricate a layered CTF with an abundance of defect states, which was made possible through the utilization of sulfuric acid as an effective intercalator and ammonium persulfate as a mild oxidant. Characterization techniques and theoretical computations have jointly illustrated that the incorporation of defect states yields several beneficial effects in FL-CTF-X. This includes enhanced absorption of visible light, resulting in a narrower band gap and a lower CB position. These alterations collectively lead to a heightened absorption of photons and an intensified reducibility. Moreover, the utilization of nanosheets, precisely engineered to possess an optimal quantity of defect states, serves to increase the exposure of active sites. This orchestrated design facilitates the efficient migration of photogenerated charge carriers from their generation sites to the solid-liquid interface, resulting in a substantial enhancement of the HER performance.

In our prior research endeavors [44], we systematically engineered CTF-xTh materials with conspicuous disparities in terminal electronegativity by judiciously selecting monomers. This process enabled precise control over both the quantity and spatial distribution of defect sites within the material. Comprehensive experimental and theoretical investigations have substantiated that terminal defect configurations, characterized by substantial electronegative disparities, serve as conduits for intramolecular charge transfer transitions in D-A binary systems. This leads to the dispersion of photogenerated charges within the spatial vicinity of these terminal defect sites, thereby not only causing a significant reduction in the material's band gap and an extension of its range for absorbing visible light but also enhancing intramolecular charge separation and transfer processes (Fig. 6a–d). Moreover, these defect-rich sites function as high-energy adsorption sites for organic matter, thereby enhancing the likelihood of interactions with active substances and, consequently, expediting the rate of photocatalytic degradation.

In addition to selectively choosing monomers with defect groups, subjecting the original CTF to high-temperature treatment in a reducing atmosphere can also create terminal defects, resulting in a narrower band gap and improved photocatalytic performance. For instance, our previous research [178] demonstrated that a simple NaBH4 thermal cleavage strategy can be used to synthesize structurally defective CTF (CTF-SD) with exposed terminal cyanide (-CN) defect groups and boron (B) atom doping. Comprehensive studies and DFT calculations (Fig. 6e–h) indicate that the doughty electron-absorbing of –CN groups within terminal defect structure of the CTF-SD can as actively sites of charge accumulation, disrupting the equilibrium charge distribution and inducing effective delocalization of π conjugation in heterocycles. This, in turn, significantly promotes the separation-transfer of e^-/h^+. Furthermore, the enlargement of π delocalization resulting from the introduction of structural defects narrows the energy band gap and shifts the VB position downward, thereby perturbing the energy structure and offering adequate driving force for the process of oxidation reactions. Additionally, the synergistic effects of –CN defects and B dopants modulate the electronic structure of CTF-SD, creating adjacent electron-deficient regions that enhance affinity with oxidants, leading to the loosening of molecular bonds and, consequently, accelerating the rate of photocatalytic pollutant degradation.

It is indicated that defect engineering can not only control the intrinsic bandgap of CTFs derivatives to extend the visible absorption range, but also optimize the local charge density to speed the separation and transfer of photogenerated carriers.

3.2.4. Architecture of heterojunction

It is well-known that the design of heterostructure interfaces is a crucial factor in controlling the catalytic kinetics of mixed systems. This design can induce band bending and the formation of internal electric fields, significantly promoting effective spatial charge separation. Compared to their corresponding single-component counterparts, heterostructures are generated through the modulation

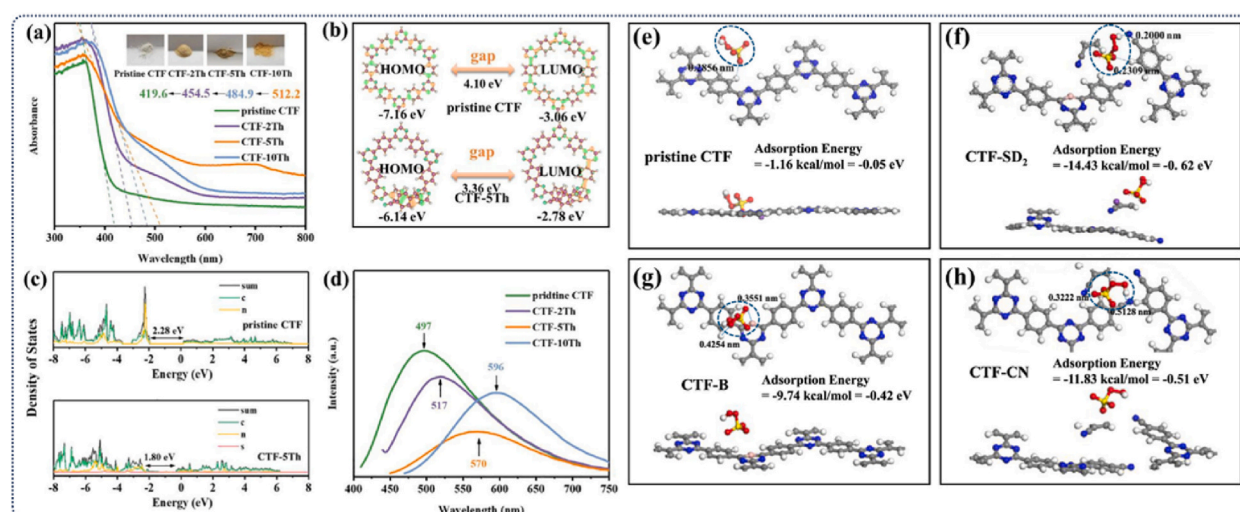**Fig. 6.** (a) UV–Vis DRS spectra of pristine CTF and CTF-xTh, (b) calculated HOMO/LUMO and (c) corresponding PDOS for pristine CTF and CTF-5Th, (d) photoluminescence spectra for pristine CTF and CTF-xTh. Reproduced with permission [44]. Copyright 2022, Elsevier. (e–h) Optimized calculated geometric structures of the PMS molecule on different samples. Reproduced with permission [109]. Copyright 2022, American Chemical Society.

of the catalyst's surface charge state. Heterostructures with higher catalytic capabilities can overcome the weak oxidative ability and reduced reductive ability of single-component CTFs, while also satisfying requirements for long-term stability, wide absorption spectra, strong redox ability, and high charge separation efficiency [37,180–191]. Therefore, the meticulous design and fabrication of heterogeneous structural materials with unique structures have become an important approach to enhance catalytic performance. Generally, CTF heterostructures can be classified into vertical [192] and lateral heterostructures (Fig. 7a and b) [193]. Former is produced through van der Waals forces via vertical layer stacking, and the latter is typically constructed by chemical bonding to seamlessly connect two-dimensional materials within the plane.

3.2.4.1. Vertical heterostructures. To ensure stronger oxidative/reductive capabilities while maintaining the appropriate band gap, researchers have extensively synthesized CTF heterostructure materials with van der Waals interfaces. This allows for the optimization of catalytic activity by regulating the charge displacement and flow direction of photoactive electrons along specific heterostructure interfaces. Experimental and theoretical researches of vertical heterostructures have matured over the years, and advanced products based on these structures have found applications in high-end optoelectronic devices and the field of catalysis.

Fan et al. [192] synthesized a novel 2D layered organic composite photocatalytic material, Triphenylphosphine-based COF (5 % P–COF-1/CTF), by employing tri(4-formylphenyl)phosphine and *p*-phenylenediamine as precursors through a solvent-thermal method. This material combines a 2D layered topology with a stacked solid spherical structure (Fig. 8a–f). Regarding the optical characteristics of the material, it is worth noting that the 5 % P–COF-1/CTF heterostructure displays a noticeable redshift in its absorption edge (Fig. 8g–i), accompanied by a minor improvement in absorption within the visible light spectrum. This indicates that the binding of P–COF-1 to CTF indeed broadens the visible light absorption range. The examination of the VB, CB, and Eg reveals that the 5 % P–COF-1/CTF exhibits a redshift in its absorption edge and a narrower bandgap (Fig. 8j), which is highly advantageous and holds great importance for the effective separation of electron-hole pairs. Furthermore, the smaller semicircular radius in the EIS Nyquist plot (Fig. 8k) and the stronger photocurrent response (Fig. 8l) of 5 % P–COF-1/CTF suggest that under illumination conditions, this hybrid material exhibits enhanced visible light responsiveness and greater photocurrent, H_2 production (Fig. 8m). This implies that the introduction of vertical heterostructures and interfacial connections can regulate the intrinsic band structure, thus photochemical performance, and accelerate the charge migration and separation of e^-/h^+ at the interface.

3.2.4.2. Lateral heterostructures. In contrast to vertical heterostructures, horizontal heterostructures are formed by extending covalent bonds in the in-plane structure. Due to their higher out-of-plane conjugation, they contribute to material stability and electron transfer
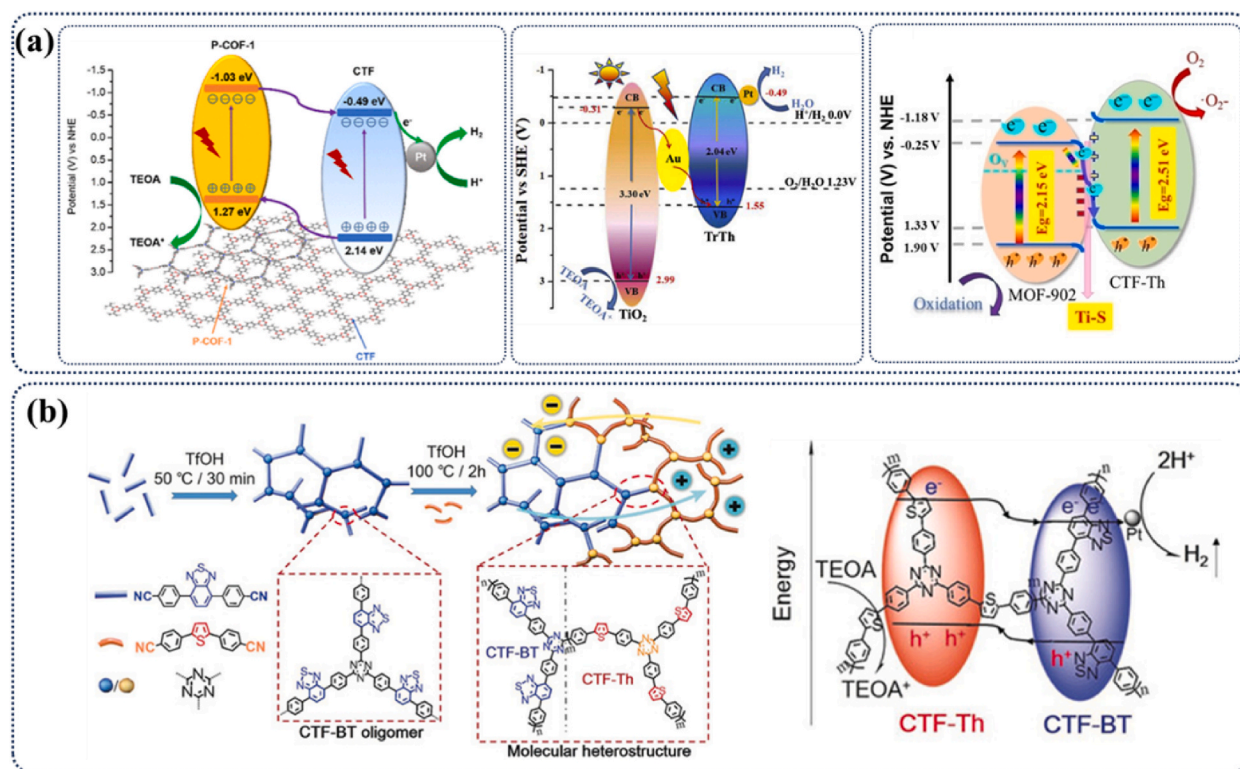
Fig. 7. Schematic illustrations of a) vertical heterostructures [37,194,192] and b) lateral heterostructures [193] of CTFs nanocomposites. Reproduced with permission [37]. Copyright 2023, Wiley. Reproduced with permission [194]. Copyright 2022, Elsevier. Reproduced with permission [192]. Copyright 2020, American Chemical Society. Reproduced with permission [193]. Copyright 2019, Wiley.
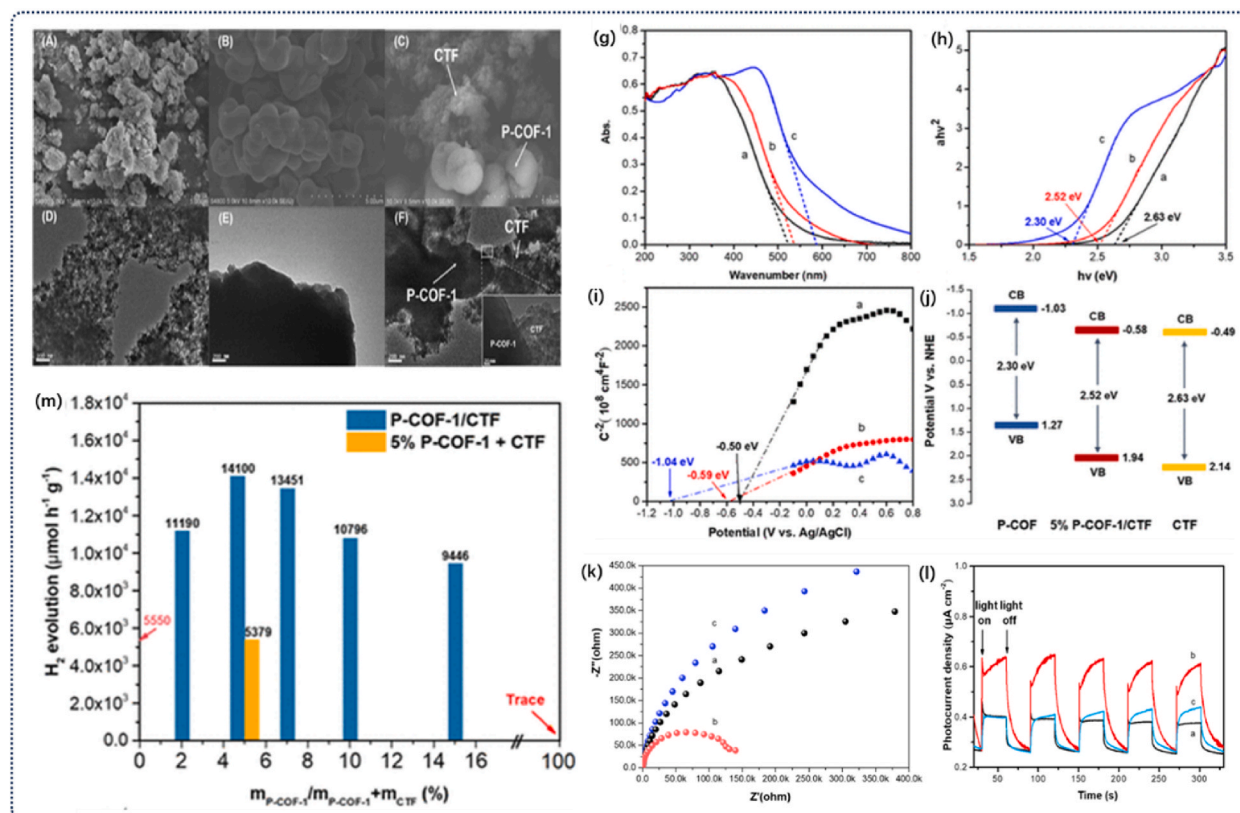
Fig. 8. (a–f) SEM and TEM images of P–COF-1/CTF samples. (g) UV–vis diffuse reflectance spectra, (h) Tauc plots, (i) Mott–Schottky plots, (j) band alignments, (k) EIS Nyquist plots, and (l) Transient photocurrent spectra of samples (m) Amount of H_2 evolution rate over P–COF-1/CTF with different amounts of P–COF-1. Reproduced with permission [192]. Copyright 2017, Elsevier.

[109,195,[196],197,198]. Moreover, electron transfer tends to occur in the horizontal direction within the plane, as opposed to the vertical direction. This implies that the potential barrier at the interface is significantly smaller compared to vertical heterostructures, indicating that electron migration is facilitated with the assistance of chemical bonds formed at the interface, thus serving as pathways for electron transport. Additionally, horizontal heterostructures can broaden the surface area of catalysts and expose more reactive
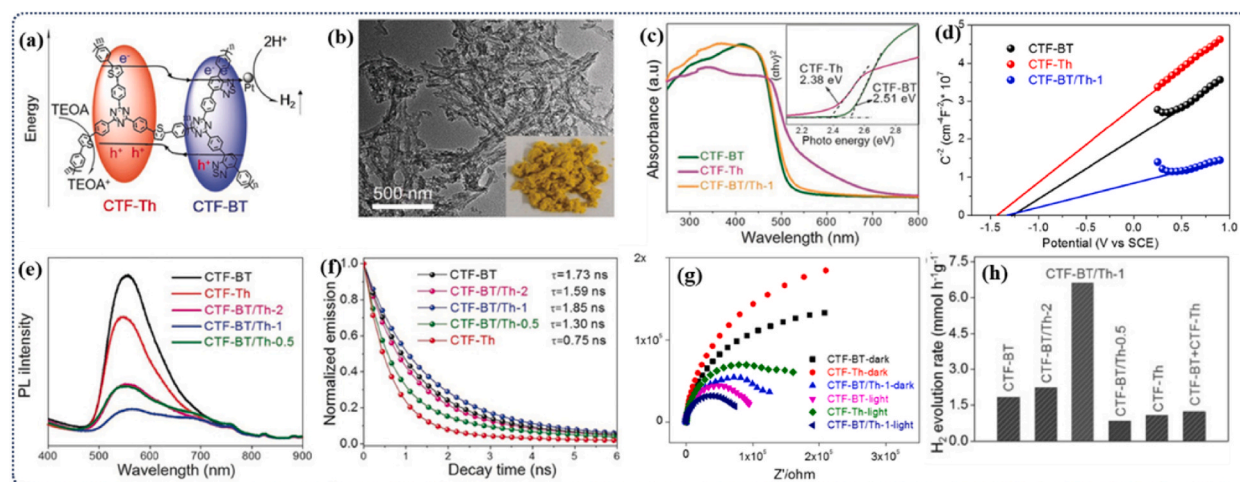
Fig. 9. (a) Illustration of the facilitated charge-carrier separation across the covalently interconnected molecular heterostructure. (b) TEM image and photograph of CTF-BT/Th-1. (c) UV/Vis DR spectra, (d) Mott-Schottky plots, (e) steady-state PL emission spectra, (f) time-resolved PL spectra, (g) EIS Nyquist plots, and (h) average H_2 production rates on different samples. Reproduced with permission [193]. Copyright 2019, Wiley.

sites, simultaneously, resulting in synergistic improvements in both active surface area exposure and enhanced charge transfer, ultimately leading to highly efficient photocatalytic activity.

Li et al. [193] achieved the assembly of fibrous horizontal heterostructure materials by introducing benzothiadiazole (BT) and thiophene (Th) functional groups as electron-withdrawing and electron-donating units, respectively (Fig. 9a and b). Optical property analysis revealed that hybrid CTF-BT/Th mainly inherits the optical characteristics of CTF-BT, with a slight redshift in the absorption edge as the Th content increases (Fig. 9c). Further inference using Mott-Schottky analysis indicated that CTF-BT/Th is capable of driving the opposite migration of photogenerated electrons and holes across the heterojunction (Fig. 9d), with a reduction potential highly conducive to H_2 production. Additionally, steady-state PL emission spectra (Fig. 9e) and time-resolved PL spectra (Fig. 9f) revealed that CTF-BT/Th exhibits the weakest intensity but the longest fluorescence lifetime. EIS Nyquist plots (Fig. 9g) results confirmed that the interfacial charge transfer resistance of CTF-BT/Th-1 is the smallest, clearly reflecting that this horizontal heterostructure effectively delays the radiative recombination of excitons within CTF. As a result, CTF-BT/Th-1 achieved a H_2 production rate of up to 6.6 mmol g^{-1} h^{-1} (Fig. 9h), which is 4–6 times higher than the single-component materials.

Moreover, the lateral heterostructures can be mostly divided into Type II, Z-scheme, and S-scheme, the development of them can accelerate the carrier separation and charge transfer effectively, and then enhance the photocatalytic performance significantly. Evidently, while Type II heterojunctions effectively facilitate charge carrier separation, the downward migration of electrons and holes to lower energy levels diminishes their redox capacity [49,192,199]. Z-scheme heterojunction emulates the charge transfer mechanism in photosynthesis stages, enhancing the redox capabilities of photocatalysts effectively, while the introduction of additional redox mediators may lead to unpredictable side reactions [200–202]. The S-scheme heterojunction is formed by the combination of two semiconductors with significant differences in band positions and work functions. Driven by the internal electric field, charge carriers in the photocatalytic process are effectively separated via S-scheme charge transfer pathways, and are retained in bands with higher redox potentials. Consequently, this enhances the efficiency of charge carrier separation and utilization in photocatalytic processes. However, the severe requirements for intrinsic energy band structure and Fermi energy levels have contributed to the challenges in semiconductor modification [37,203,204]. Thus, considering the characteristics of the three heterojunctions discussed above, we estimate that the S-scheme heterojunction owing the most promising avenue for development.

Also, most CTFs heterojunction materials exhibit remarkable structural stability after multiple cycles of photocatalytic reactions, with no significant changes observed in either the internal molecular layers or the physical morphology. Thus, the structural stability of CTF heterojunctions is well-maintained.

3.2.5. Templating modified

Beyond alterations in chemical composition, the collective influence of multiple factors exerts a pronounced impact on the catalytic
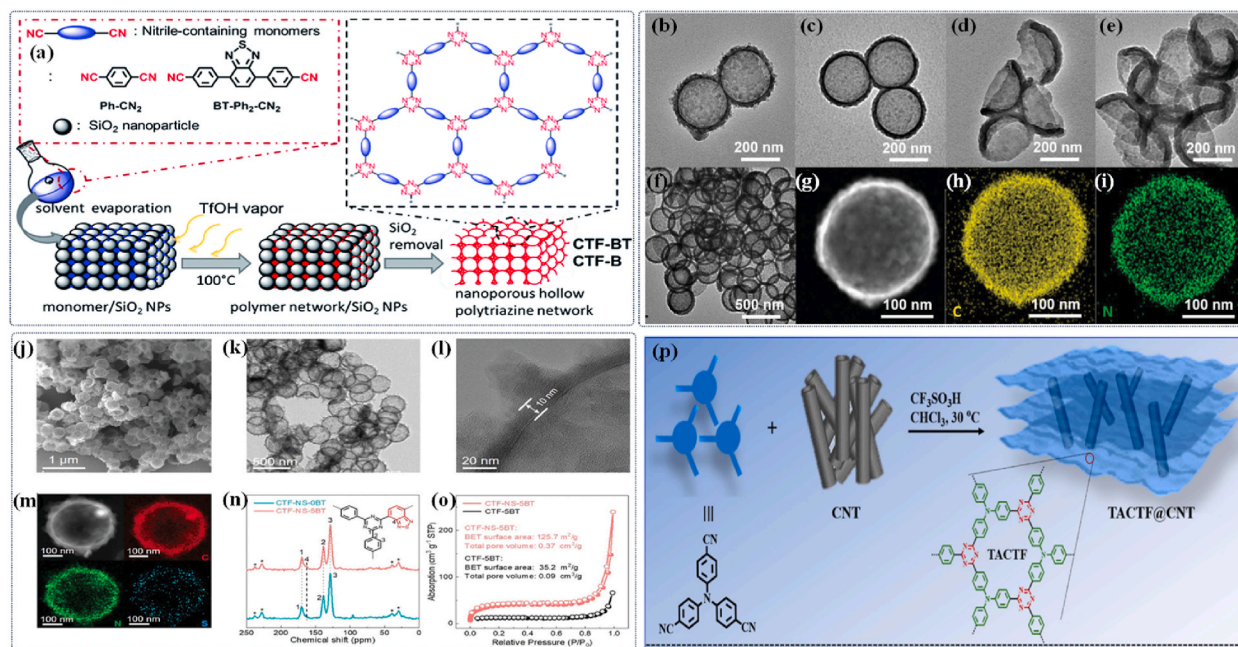
Fig. 10. (a) Schematic of solid vapor synthesis and idealized structures of the nanoporous hollow polytriazine networks. Reproduced with permission [81]. Copyright 2016, Royal Society of Chemistry. (b–e) TEM images of different etched samples, (f) large-scale TEM image of CTF-HS0.75-1, (g–i) Elemental mapping of CTF-HS0.75-1. Reproduced with permission [79]. Copyright 2019, Wiley. (j) SEM image, (k) TEM image, (l) HRTEM image, and (m) EDX mapping results of CTF–NS–5BT. (n) 13C CP-MAS NMR spectra of CTF–NS–0BT and CTF–NS–5BT. (o) Nitrogen sorption isotherm curves of CTF–NS–5BT and CTF-5BT. Reproduced with permission [52]. Copyright 2021, Wiley. (p) the schematic illustration for the synthesis of TACTF@CNT. Reproduced with permission [106]. Copyright 2023, Elsevier.

activity of materials, particularly concerning structural topology. The specific surface area of a photocatalyst constitutes a pivotal determinant of its photocatalytic efficacy. Consequently, the manipulation of morphology, structure, or the introduction of nanoscale modifications holds substantial sway over photocatalytic efficiency. Recent investigations have brought to light that CTF, when in its bulk form, lacks photoactivity [39,81,104–108]. This deficiency can be ascribed to its internal stratified configuration, comprising hexagonal ring structures with a pore size of approximately 1.2 nm [62,83,205]. The compact stacking of triazine rings within the π-π layers engenders structural symmetry, which, while stable, proves detrimental to charge transfer and conveyance to the surface [206, 207]. Photocatalytic responsiveness only manifests when CTF is exfoliated into well-dispersed nanosheets prior to utilization. Thus, the custom tailoring of materials with unique geometries stands poised to expedite the exposure of active interfaces to the reaction milieu, thus facilitating the rapid diffusion of charges along abbreviated pathways and consequent enhancement of photocatalytic activity. Among the myriad approaches to structural modification, the template method garners preference due to its potential to enhance photocatalytic efficacy, augment the specific surface area, and bolster light-capturing capabilities.

Zhang et al. [81] engineered a CTF featuring a meticulously structured network of hollow interconnected pores (Fig. 10a), each with an approximate diameter of 100 μm, under mild reaction conditions. Comprehensive experimental findings and thorough characterizations unequivocally demonstrated that the precisely ordered pore configuration played a pivotal role in broadening the spectrum of visible light absorption. Moreover, it facilitated the prompt separation, transfer, and subsequent reactivity of photo-generated electrons, thereby leading to a notable enhancement in the rate of H_2 production.

Bian et al. [79] delved into an efficacious approach aimed at fabricating morphologically adaptable CTF. The systematic reduction of shell thickness led to a discernible transition in shape, evolving from spherical to concave (Fig. 10b–i), or bowl-shaped structures. Comprehensive characterization and rigorous testing substantiated that the nanoscale size effect exerted a multifaceted influence. This effect not only significantly augmented the specific surface area, thereby exposing an increased number of active reaction sites but also facilitated enhanced light absorption via multiple reflections within the concavity. Consequently, these combined factors synergistically contributed to a marked enhancement in photocatalytic performance, resulting in a H_2 evolution rate approximately fourfold higher compared to bulk counterparts.

Huang et al. [52] have introduced an innovative approach featuring copolymeric monomer doping, employing silica nanoparticles as a template to fabricate a well-defined hollow shell structure with a shell thickness of approximately 10 nm (Fig. 10j–m). This method offers precise control over the electronic properties of CTFs nano shells. Extensive physicochemical characterization and spectral analyses reveal that the specific surface area of the modified material is quadrupled compared to its unmodified counterpart (Fig. 10o), which substantiates the effective exposure of a larger surface area facilitated by the thin-shell hollow structure of CTF-NS. Simultaneously, the material exhibits significantly enhanced visible light performance. In practical applications, when utilized as a photocatalyst in an aqueous environment, the optimized sample achieves an impressive H_2O_2 production rate of 1630 μmol g^{-1} h^{-1}. The exceptional performance outpaces undoped samples by a factor of approximately three and positions it as a leading contender when compared to the majority of both inorganic and organic competitors in the field.

Moreover, Wen et al. [106] introduced an innovative composite catalyst through the in-situ growth of two-dimensional tri-aniline-based covalent triazine skeleton (TACTF) semiconductors in conjunction with one-dimensional (1D) carbon nanotubes (CNT) acting as electron conduction mediators (Fig. 10p). The resulting TACTF@CNT complex showcases a minimal Schottky barrier, enhancing lateral charge transport and interlayer exciton dissociation by facilitating the interconnection between the TACTF layer and CNT. This arrangement ensures the efficient transfer of photogenerated charge from the TACTF semiconductor to the surface's active sites, thereby facilitating the subsequent photocatalytic reduction of Cr(VI).

3.2.6. CTFs films syntheses

Various methods have been developed for the preparation of CTFs films, which can be categorized into substrate-supported film formation and self-polymerized film formation. In the substrate-supported approach, monomers are dissolved in dimethyl sulfoxide (DMSO) to create a reaction solution. This solution is then applied to APTES-modified glass slides as templates, where different functional polymers are formed via Schiff base reactions [208]. The film thickness can be further modulated by incorporating additional monomers and solvents and adjusting the reaction temperature within the range of 120–150 °C. Furthermore, Xu et al. reported that uniform films can be achieved on substrates by first exfoliating the material into nanosheets using ultrasonication in DMF solution, followed by the drop-casting method [209]. The DMSO solution and a solution containing various monomers were placed in an oven to create the self-polymerized CTFs films by Professor Bian et al. [86]. After that, the imine precursor was evenly spread on top of the DMSO solution and heated until the n-hexane evaporated, producing a film with a thickness of roughly 500 nm that could be pipetted off or transferred to other substrates for photocatalytic or characterization purposes. What's more, Xu et al. [210] develop a convenient and general synthetic methodology to directly prepare a series of few-layer crystalline micrometer-size 2D-TPs with a high yield via cyclotrimerization reaction of aromatic aldoximes under solvent-free catalysis conditions.

All these studies provide versatile routes to synthesize 2D polymers with tailored structures and properties for various applications.

4. Environment applications of CTFs composite photocatalysts

As an environmentally sustainable photocatalyst that efficiently harnesses solar energy, CTFs exhibit significant promise for a wide range of applications in photocatalytic resource recycling and carbon reduction. They mainly introduce the applications in photocatalytic water splitting for H_2 [107,126,145,150,156,171,178] and H_2O_2 [52,53] evolution, reduction of CO_2 into hydrocarbon fuels [180,211–213], and degradation of pollutants [133,214,180,215], as well as the involved photocatalytic nitrogen fixation [121,122, 216] accordingly. Several papers have been evaluated and summarized based on the most recent findings to provide a quick knowledge

of CTF composites for various photochemistry applications.

4.1. Photocatalytic hydrogen evolution

Since the groundbreaking research conducted by Honda and Fujishima in 1972 [217], a diverse array of heterogeneous photocatalysts has found extensive application in the field of photocatalytic water splitting for H_2 generation. From both economic and ecological standpoints, the photocatalytic hydrolysis of H_2 offers significant advantages and higher value. Consequently, researchers are redoubling their efforts to advance the field of photocatalytic H_2 production [110,118,135,155,162,177,184,188,218–228].

Jin et al. [135] have presented a strategy that involves the construction of a donor (D) – acceptor1 (A_1) – acceptor2 (A_2) system within the framework of CTFs to suppress charge recombination and facilitate charge separation. Characterization and experimental results have indicated that, owing to the energy level gradient between the donor and acceptors, the copolymer forms an efficient photo-induced electron transfer system through HOMO to LUMO transitions (Fig. 11a), enabling electrons to flow directionally along a
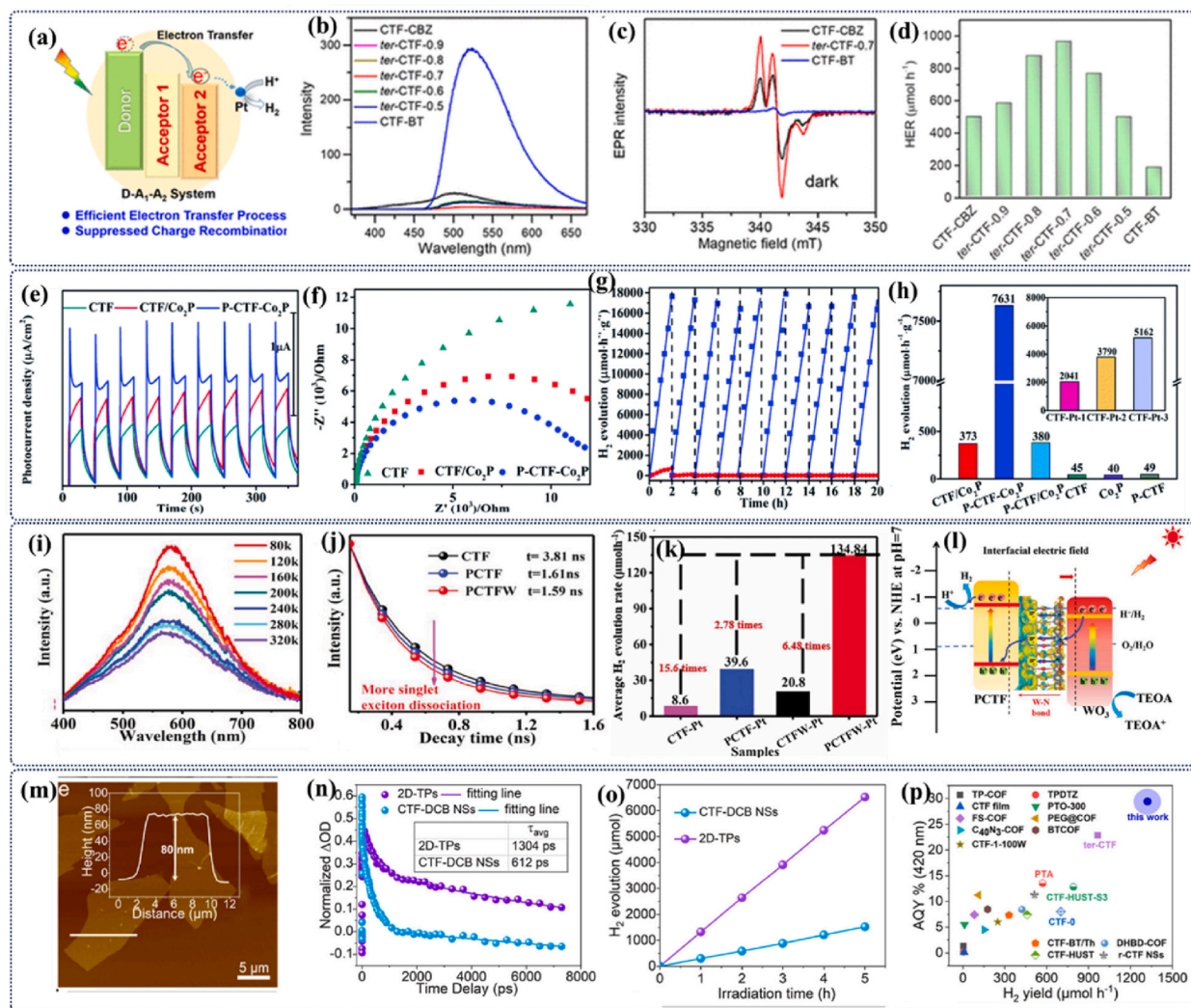
Fig. 11. (a) Comparison of D–A_1–A_2 system in the photoinduced electron-transfer process. (b) PL intensity excited by 365 nm. (c) Representative EPR in the dark. (d) HER of CTFs. Reproduced with permission [135]. Copyright 2019, American Chemical Society. (e) I–t curves of various and (f) EIS of various catalysts. (g) The cycling photocatalytic tests of P-CTF-Co$_2$P and the CTF/Co$_2$P composite. (h) comparative presentation of the H_2 evolution rates. Reproduced with permission [232]. Copyright 2022, Royal Society of Chemistry. (i) Temperature-dependent PL spectra with excitation wavelength at 380 nm and extracted exciton binding energies of PCTF, (j) time-resolved fluorescence kinetics, (k) average H_2 generation rate for all samples, and (l) Schematic illustration for the photocatalytic mechanism of PCTFW. Reproduced with permission [202]. Copyright 2023, Wiley (m) AFM image of CTF–DCB NSs with the inset showing height plot. (n) Time profiles of normalized transient absorption spectra and (o) Time course curves of the photocatalytic H_2 evolution reaction of 2D-TPs and CTF–DCB NSs. (p) H_2 evolution rates and apparent quantum yield (AQY) for 2D-TPs in this work compared with the recently reported representative CTFs and COF photocatalysts. Reproduced with permission [228]. Copyright 2023, American Chemical Society.

path from fragments with higher energy levels to those with lower energy levels. Moreover, the presence of larger delocalized systems and the longer distance between D and A_2 effectively mitigate the recombination of photo-generated electron-hole pairs, making it more challenging for separated charges to recombine, thereby enhancing the quantum efficiency. Furthermore, the lower PL intensity (Fig. 11b) evidences the reduction of charge recombination, EPR spectra (Fig. 11c) and theoretical calculations support the enhancement of charge separation. Additionally, the catalytic H_2 evolution rate of the polymer can be flexibly regulated by altering A_2, ultimately achieving a H_2 production rate of 19.3 mmol g^{-1} h^{-1} (420 nm) with an apparent quantum efficiency of 22.8 % (Fig. 11d). These results are comparable to certain metal polymers, highlighting their promising performance [229–231].

Huang et al. [232] have introduced a one-step phosphating strategy to firmly attach Co_2P nanocrystals onto CTFs. This innovative approach fundamentally alters the electron transfer dynamics within CTFs, shifting the direction from the triazine ring to the benzene ring, thanks to the introduction of an interfacial p bond and Co_2P anchoring. Remarkably, after bonding with the P atom and subsequent Co-anchoring, the carbon moiety of the benzene ring within CTFs significantly bolsters the photocurrent density (Fig. 11e) while concurrently reducing electron transport conductivity (Fig. 11f). This augmentation substantially enhances charge separation and transport capabilities. An in-depth analysis via in situ irradiation X-ray photoelectron spectroscopy clearly elucidates that charge transfer within CTFs occurs in the exact opposite direction, as photo-generated electrons efficiently migrate from the triazine ring to the p-bonded benzene ring. Notably, the Co_2P cocatalyst, through the interfacial P–C bond, adeptly attracts these electrons, facilitating efficient HER. Beyond the enhancement of catalytic activity, the interfacial P–C bond and Co_2P anchoring significantly bolster the stability of HER (Fig. 11g). Consequently, the H_2 evolution rate of the CTFs/Co_2P composite (Fig. 11h) reaches an impressive (7.6 mmol h^{-1} g^{-1}). This achievement positions it among the most active CTF-based photocatalysts, especially noteworthy as a non-platinum cocatalyst, representing a significant stride in the development of efficient and stable photocatalysts.

Li et al. [202] have successfully synthesized phosphorus-doped Z-scheme heterojunctions (PCTFW) through an in-situ hydrolysis method followed by high-temperature phosphorylation. Experimental and characterization results unequivocally demonstrate the multifaceted benefits of introducing phosphorus atoms into this structure. First and foremost, this incorporation optimizes the energy band structure, enhances the built-in electric field, and induces the dissociation of excitons into charge carriers within the CTFs. The high-quality interface N–W bonds play a pivotal role in improving the interfacial transfer of photogenerated electrons (Fig. 11i). This enhancement effectively promotes the efficient reduction and dissociation of photogenerated charge carriers, simultaneously restraining the recombination of electron-hole pairs and extending their lifetimes (Fig. 11j). Furthermore, it expedites the transfer of electrons within the built-in electric field. Consequently, PCTFW exhibits an impressive evolution rate of 67.42 mmol h^{-1} g^{-1} for photocatalytic H_2 production (Fig. 11k and l), with each surface area yielding 1.6 mmol h^{-1} m^2. Remarkably, these results signify a remarkable increase by a factor of 6.5 and 42.1 compared with pristine CTF. Moreover, the apparent quantum efficiency at 420 nm attains an astonishing figure of 37.63 %.

Xu et al. [228] have recently introduced an environmentally friendly and straightforward approach to the large-scale production of a series of atomic-thin 2D-TP (Fig. 11m) materials through a solvent-free salt-catalyzed 2D polymerization process. Experimental findings and theoretical calculations indicate that common salts like KCl not only serve as templates to facilitate the formation of nanosheets but also act as solid catalysts to promote cyanation polymerization, resulting in uniformly thick (~80 nm) kilogram-scale

Table 2

Performance comparison for H_2 production of CTFs.

Photocatalyst	Structure	Light source	H_2 evolution rate [μmol g^{-1} h^{-1}]	Refs.
5 % P–COF-1/CTF	2D layered topology stacked	Xe arc lamp, $\lambda \geq$ 420 nm	14100	[192]
P-CTF	nanosheets	300 W Xe lamp with an AM 1.5	6595	[110]
Ni-CAT-1/CTF-1 (1:19)	flaky accumulation state	300 W Xenon lamp, $\lambda \geq$ 420 nm	8030	[195]
CTF-HUST-A1	layered structure	300 W Xenon lamp, $\lambda \geq$ 420 nm	9200	[50]
r-CTF NSs	thin film	300 W Xenon lamp, $\lambda \geq$ 420 nm	512	[83]
P-CTF-Co_2P	lamellar/particles	300 W Xe lamp with an AM 1.5	7600	[232]
CTF-15	thick rods	300 W Xenon lamp, $\lambda \geq$ 420 nm	1909	[218]
BDT-CTF-1	layered structure	300 W Xenon lamp, $\lambda \geq$ 420 nm	4500	[162]
MoS_2/CTF-T1	layered structure	300 W Xenon lamp, $\lambda \geq$ 420 nm	1125	[233]
ter-CTF-0.7	tightly stacked irregular slices	300 W Xenon lamp, $\lambda \geq$ 420 nm	19300	[135]
Au@TiO_2-12%TrTh	flocculent morphology with irregular pores	300 W Xenon lamp, $\lambda \geq$ 420 nm	4289	[194]
CTF-NWU-1	bowl-shaped morphology	300 W Xenon lamp, $\lambda \geq$ 420 nm	17600	[234]
CTF-HUST-S_3	layered structure	300 W Xenon lamp, $\lambda \geq$ 420 nm	791	[215]
T_3N-CTF	orderly arranged fibrillar bundle structure	300 W Xenon lamp, $\lambda \geq$ 420 nm	6485	[235]
CTF-HC_2	lamellar morphology	300 W Xenon lamp, $\lambda \geq$ 420 nm	3472	[236]
TFA-COF	porous sponge-shape	300 W Xenon lamp, $\lambda \geq$ 420 nm	80	[177]
20%CdS-CTF-1	particles	300 W Xenon lamp, $\lambda \geq$ 420 nm	11430	[188]
C-GW_{15}	flower-like structure with a porous surface	300 W Xenon lamp, $\lambda \geq$ 420 nm	8740	[237]
PCTF-1	layered structure	300 W Xenon lamp, $\lambda \geq$ 420 nm	500	[221]
$C_{0.24}$/CTF	lamella	300 W Xenon lamp, $\lambda \geq$ 400 nm	102	[220]
CTF-TPA-Film-3	films	300 W Xenon lamp, $\lambda \geq$ 420 nm	77800	[208]
CTFs Film	film	300 W Xenon lamp, $\lambda \geq$ 420 nm	10200	[86]
CdS/CTF-1	layered stacking structure	300 W Xenon lamp, $\lambda \geq$ 420 nm	5400	[184]
CTF-0-M_2	layered stacking structure	300 W Xenon lamp, $\lambda \geq$ 420 nm	7010	[238]
Pd@CTF-HC_6	lamellar/particles	300 W Xenon lamp, $\lambda \geq$ 420 nm	10556	[239]
CTF–DCB NSs	wrinkled thin layer	300 W Xenon lamp, $\lambda \geq$ 420 nm	26412	[228]

crystalline nanosheets. The inclusion of KCl and the nanosheet morphology results in a more favorable bandgap for the material, and the robust interactions among distinct active groups significantly improve the separation and transfer of charge carriers (Fig. 11n), thereby extending their lifespans and manifesting remarkable photocatalytic capabilities. Impressively, the H_2 evolution rate achieves 26,412 µmol g^{-1} (Fig. 11o), accompanied by an AQY of 29.5 % at 420 nm. Furthermore, under standard one-sun illumination conditions, the solar-to-hydrogen (STH) efficiency for comprehensive photocatalytic water splitting attains 0.35 %. This performance surpasses that of previously reported CTF/COF-based materials and most non-metallic photocatalysts, highlighting the notable advancements in this study (Fig. 11p).

The aforementioned evidence strongly corroborates the suitability of optimized CTFs hybridization for photocatalytic water splitting. A performance comparison is provided in Table 2. Presently, these innovative heterogeneous semiconductors have experienced extensive development and garnered significant attention within the research community.

4.2. Photocatalytic H_2O_2 production

Solar photocatalysis offers an environmentally friendly pathway for the synthesis of H_2O_2 using O_2 and sunlight as the primary ingredients. Among the various categories of photocatalysts reported, metal-free polymeric photocatalysts have garnered substantial attention due to their modifiable structures and properties. This flexibility enables significant enhancements in the efficiency of photocatalytic H_2O_2 production. Table 3 provides an overview of the photocatalytic performance of CTFs-based photocatalysts for H_2O_2 generation under various conditions, which will be explored in detail to understand the pivotal role of catalysts in achieving highly efficient photocatalytic H_2O_2 evolution.

Han et al. [210] have developed a strategy for the production of H_2O_2 from water and O_2 through a two-electron oxygen reduction reaction (2e$^-$-ORR) using (thio)urea-functionalized CTFs, Bpt-CTF and Bpu-CTF. The research findings indicate that the incorporation of (thio)urea moieties enhance the polarization of CTFs, leading to strong absorption across a broad range of ultraviolet and visible light (Fig. 12a). Additionally, these functionalized CTFs exhibit enhanced oxidation capability and driving force, substantially suppressing radiative recombination (Fig. 12b) and prolonging the lifetime of charge carriers (Fig. 12c). Furthermore, the (thio)urea functional groups within Bpt-CTF demonstrate robust electronegative characteristics (Fig. 12d), which facilitate proton migration, enabling an efficient proton-coupled electron transfer process during the two-electron oxygen (2e$^-$-O$_2$) photocatalytic reduction process to produce H_2O_2. Consequently, this enhancement leads to a substantial increase in the rate of photocatalytic H_2O_2 production (Fig. 12e), reaching an impressive 3268.1 µmol h^{-1} g^{-1}, all achieved without the necessity for sacrificial agents or co-catalysts. This achievement represents an order of magnitude improvement over non-functionalized CTFs (Dc-CTF). Furthermore, the quantum efficiency at 400 nm reaches a noteworthy 8.6 %.

Chen et al. [55] employed a unified polymer incorporating s-heptazine and ethynyl constituents in their study, aiming to fabricate a polymer proficient in H_2O_2 production. Their comprehensive experimental and characterization investigations unveiled that ethylene-linked polymer, attributed to extended π-conjugation and spatial separation of oxidation centers, played a pivotal role in reducing binding energy of excitons. Additionally, it significantly bolstered charge transfer capability while concurrently suppressing charge recombination. Attributes like extended π-conjugation and spatial separation of oxidation centers proved paramount in ensuring efficient charge separation, thereby contributing to remarkable photocatalytic activity observed. Furthermore, electron-deficient heptazine segments, enriched with high nitrogen content, demonstrated pronounced electron affinity. Ethynyl groups functioned as conduits, effectively bridging electron donors and acceptors, thereby facilitating efficient transfer of photo-generated electrons. This synergistic interaction between heptazine and ethynyl units synergistically facilitated synthesis of H_2O_2 via 2e$^-$-ORR pathway, ultimately achieving commendable production rate of 1830 µmol h^{-1} g^{-1}. Notably, ethylene-linked polymer, featuring two distinct heptazine units and ethynyl-bearing connectors, displayed extraordinary chemical stability, even when exposed to rigorous conditions.

Zhang et al. [243] employed a multifaceted strategy to construct and develop sulfur-ether-modified triazine-based covalent organic framework (TDB-COF). In this framework, photocatalytic conversion of H_2O and O_2 to H_2O_2 was achieved without requiring sacrificial

Table 3
Performance comparison for H_2O_2 reduction of CTFs.

| Photocatalyst	Light source	apparent quantum efficiency [%]	H_2O_2 production rate [µmol g^{-1} h^{-1}]	Refs.
CTF-LTZ	300 W Xenon lamp, λ ≥ 420 nm	4.5 % at 400 nm	4068	[240]
CDs@CTFs	simulated sunlight (light intensity: 100 mWcm^{-2})	0.93 % at 505 nm	700	[241]
CsPbBr$_3$/CTF-2	300 W Xenon lamp, λ ≥ 420 nm	0.14 % at 420 nm		
CTF–NS–5BT	300 W Xenon lamp, λ ≥ 420 nm	6.6 % at 420 nm	1630	[52]
EBA-COF	50 W LED lamp, λ ≥ 420 nm	4.4 % at 420 nm	1830	[55]
TPT-3	300 W Xenon lamp, λ ≥ 400 nm	15 % at 425 nm	1351	[242]
TDB-COF	300 W Xenon lamp, AM 1.5 G filter	1.0 % at 400 nm	724	[243]
CTF-Ph	300 W Xenon lamp, AM 1.5 G filter	1.1 % under simulated sunlight	46900	[244]
TpAQ-COFs	300 W Xenon lamp, λ ≥ 420 nm	7.4 % at 420 nm	420	[245]
Bpt-CTF	300 W Xenon lamp, λ ≥ 420 nm	8.6 % at 400 nm	3268	[210]
COF-TAPB-BPDA	300 W Xenon lamp, λ ≥ 420 nm	–	1240	[246]
CTF-BDDBN	300 W Xenon lamp, λ ≥ 420 nm	–	90	[53]
CTF-1-G/WS$_2$	300 W Xenon lamp, λ ≥ 420 nm	–	8740	[237]
AQTT-COP	300 W Xenon lamp, λ ≥ 400 nm	–	3221	[247]
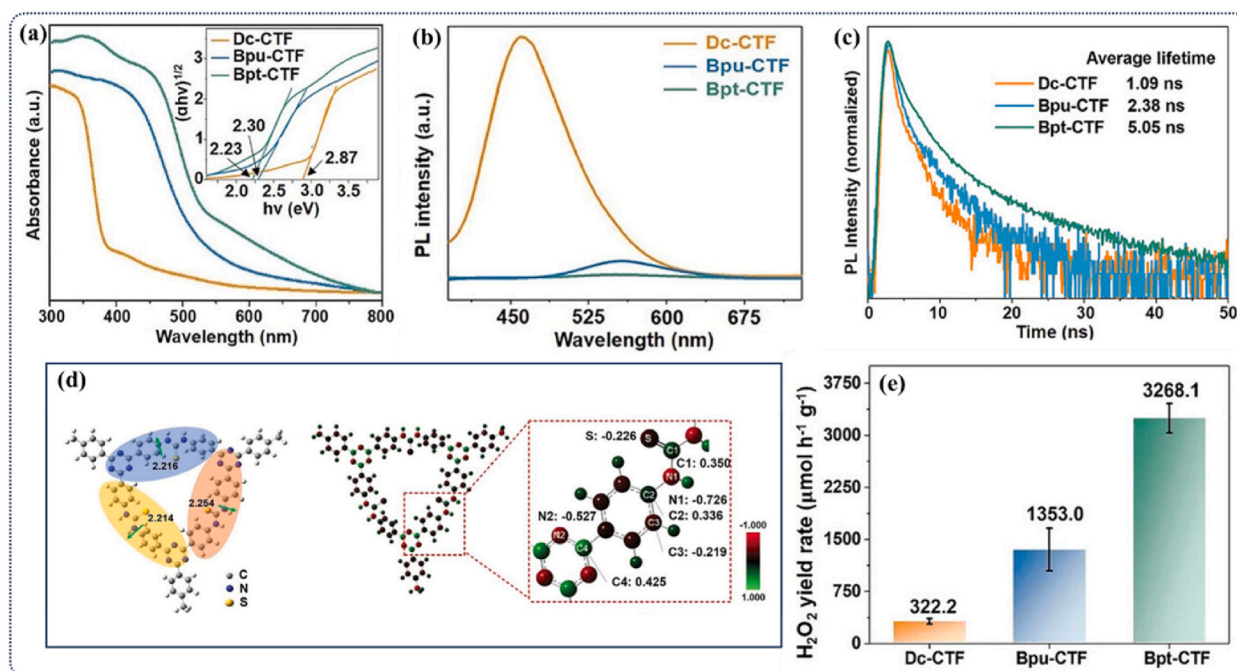
Fig. 12. (a) UV–vis spectra, (b) PL spectra, and (c) Time-resolved PL decay curves of all samples. (d) The dipole moments analysis for Bpt-CTF, illustration of the charge distribution near the surface of Bpt-CTF from TDDFT calculations. (e) Photocatalytic production of all samples. Reproduced with permission [210].Copyright 2022, Wiley.

Table 4
Performance comparison for CO_2 reduction of CTFs.

Photocatalyst	Structure	Light source	Selective products (activity) [μM h^{-1} g^{-1}]	Refs.
CN/CTF	lamella	300 W Xenon lamp in the full light region	151.1 (CO)	[180]
Re-CTF-py	lamella	300 W Xe lamp in the full light region	353.1 (CO)	[212]
Pd@Imine-CTF	loose particles of tiny sizes	300 W Xenon lamp, λ ≥ 420 nm	85.3 (CO) 21.1 (CH_4)	[63]
Pt-SA/CTF-1	graphene-like layered structure	300 W Xenon lamp, λ ≥ 420 nm	1.4 (CO) 4.7 (CH_4)	[256]
CTF-BP	layer structures	300 W Xe lamp in the full light region	4.6 (CO) 7.8 (CH_4)	[181]
NCTF-1	analogous layer structure	300 W Xenon lamp, λ ≥ 420 nm	1.6 (CO) 11.5 (CH_4)	[115]
Ru-CTF-2	irregularly stacked chunks and compact layer structure	300 W Xe lamp in the full light region	2090 (HCOOH)	[129]
α-Fe_2O_3@Por-CTF-10 × /Ru (bpy)$_3Cl_2$	plate-like particulate morphology	–	1.6 (CO) 11.5 (CH_4)	[257]
60-TiO_2@CTF-Py	particle sizes	300 W Xenon lamp, λ ≥ 320 nm	43.3 (CO)	[128]
CTF-TfOH-Co	agglomerated bulks	300 W Xenon lamp, λ ≥ 400 nm	2562.8(CO)	[74]
CTF-Bpy-Co	microfiber-like agglomerate morphology	300 W Xenon lamp, λ ≥ 420 nm	304 (HCOOH)	[258]
$Co_{0.10}$-SA/CTF	similar layered stacking structure	300 W Xenon lamp, λ ≥ 420 nm	1665.7(CO)	[255]
CABB/CTF-1	thin-layered NS morphology with a porous structure	300 W Xenon lamp, λ ≥ 420 nm	30.7 (CO) 8.6 (CH_4)	[259]
$Ni_{0.5}$-CTF-1	looser layered structure	300 W Xenon lamp, λ ≥ 420 nm	38.7 (CO)	[117]
CPB/CTF-1	superposition of the two counterparts	300 W Xenon lamp, λ ≥ 420 nm	86.5 (CO)	[90]
Re-bpy/PTF(Cu)	layer structures	300 W Xe lamp in the full light region	73.3 (C2H2) 164.2(CO) 16.9(CH4) 38.5(H2)	[254]
DQTP COF–Co	multi-layer overlapping nano-sheets	300 W Xenon lamp, λ ≥ 420 nm	152.5(CO)	[260]
2D CN–COF	thin nano-sheet	300 W Xe lamp in the full light region	7.1(CO) 2.4(CH4)	[61]

agents or co-catalysts. Experimental results and analysis revealed that ordered sulfur-ether groups introduced into the TDB-COF structure expanded its visible light absorption range and adjusted its energy band structure. This modification facilitated photo-generated charge carrier separation and charge transfer, enhancing photo responsiveness. TDB-COF became suitable for accelerating the $2e^-$-ORR, resulting in H_2O_2 production rate of 723.5 μmol g^{-1} h^{-1}, apparent quantum efficiency was 1.0 % at 400 nm [243].

Bayarkhuu et al. [244] not only utilized CTF as a photocatalyst but also devised an organic working solution (OWS) for the solar-assisted photocatalytic oxidation of aryl alcohols, leading to the production of H_2O_2. The meticulously crafted OWS achieved the highest solar-chemical conversion efficiency reported to date (1.1 %) along with a substantial H_2O_2 production rate of 46.9 mmol h^{-1} g^{-1}. This approach, which combines photocatalytic oxidation-reduction reactions and self-oxidation reactions, represents an efficient means of converting solar energy into valuable chemical compounds. The exceptional efficiency of this process can be attributed to the ingenious design of the photocatalyst.

4.3. Photocatalytic carbon dioxide reduction

For the past few years, there has been a persistent escalation in the emission of CO_2 as a consequence of fossil fuel combustion. This surge has engendered a grave greenhouse effect, casting a substantial menace to both human and animal existence. Encouragingly, the surplus CO_2 can be effectively transmuted into valuable fuels through the process of photocatalysis [248–252]. These methods enable the production of diverse high-value chemical fuels, including HCOOH, CO, HCHO, CH_3OH, CH_4, and others, by means of multi-electron transfer mechanisms (Table 4) [60,63,73,211–213,253]. This approach effectively amalgamates the realms of environmental conservation and energy rejuvenation, thereby making a significant contribution to the amelioration of human living standards. However, it is noteworthy that conventional catalysts frequently exhibit inadequacies in terms of their photocatalytic efficacy and durability, thus falling short of satisfying all the requisite prerequisites. In this context, derivatives stemming from CTFs present distinctive advantages attributable to their wide-ranging and potent light absorption capabilities, as well as their expeditious electron segregation and transfer proficiency [181,254,255].

Jiang et al. [63] have designed Pd nanoparticles confined within imine-linked CTF (Pd@Imine-CTF) for the purpose of photocatalytic CO_2 reduction. The interplay between palladium (Pd) and the nitrogenic domains enshrouded within the imine-linked CTF (imine-CTF) orchestrates an elegant choreography that artfully quells the burgeoning of nanoparticles. These Pd nanoparticles
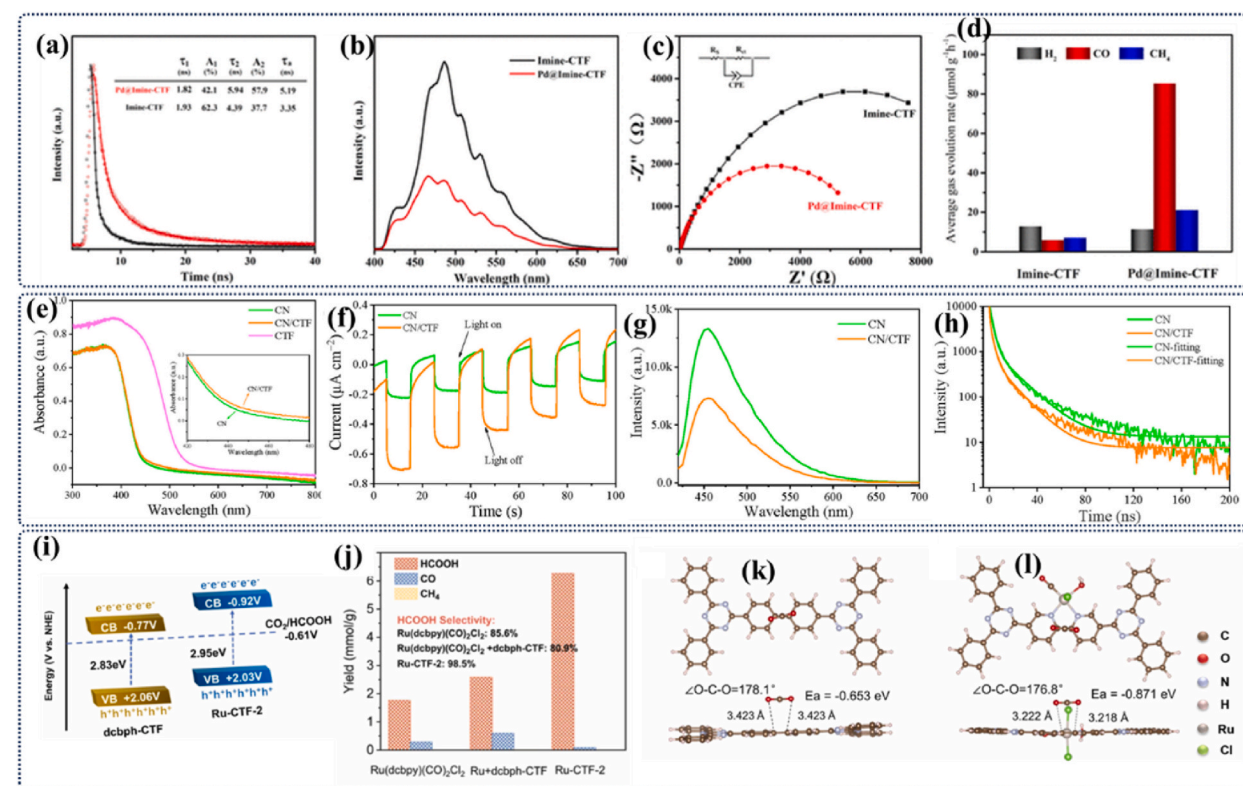
Fig. 13. (a) Time-resolved transient photoluminescence decay spectra, (b) steady-state photoluminescence spectra, (c) EIS Nyquist plots, (d) average gas production rates of Imine-CTF and Pd@Imine-CTF. Reproduced with permission [63]. Copyright 2021, American Chemical Society. (e) UV–Vis DRS, (b) Instantaneous photocurrent, (c) PL and (d) TR-PL decay curve of CN and CN/CTF. Reproduced with permission [180]. Copyright 2022, Elsevier. (i) The band diagram of different samples. (j) The selectivity of HCOO- and the yield distribution of different photoreduction products in 3 h. Adsorption energy of CO_2 on (k) dcbph-CTF and (l) Ru-CTF surface. Reproduced with permission [129]. Copyright 2022, Elsevier.

proficiently capture and accumulate photoelectrons on their surfaces, mitigating the recombination of electron-hole pairs and facilitating CO_2 conversion. Furthermore, the highly porous structure of Pd@Imine-CTF provides an increased number of sites for CO_2 adsorption, expediting the completion of the reduction reaction. Consequently, Pd@Imine-CTF demonstrates a remarkable enhancement in performance and exceptional stability for CO_2 photoreduction when exposed to visible light irradiation. Importantly, both the short and long lifetimes of Pd@Imine-CTF are significantly extended in comparison to Imine-CTF (Fig. 13a), signifying that Pd fixation serves as a substantial deterrent to electron-hole pair recombination. And the PL intensity of Pd@Imine-CTF (Fig. 13b) is conspicuously quenched compared to that of Imine-CTF, indicative of Pd nanoparticles effectively trapping electrons from Imine-CTF to accelerate charge carrier separation. Besides, the smaller semicircular radius of Pd@Imine-CTF (Fig. 13c) attributed to the formation of a functional Schottky junction between Pd nanoparticles and Imine-CTF, a feature that significantly promotes electron-hole pair separation. Furthermore, Schottky junctions facilitate efficient charge transfer through closely interfacing regions and the high electrical conductivity of metallic Pd nanoparticles. As a result, Pd@Imine-CTF exhibits a remarkable CO_2 photoreduction efficiency of 98 %, with a CO evolution rate of 85.3 μmol g^{-1} h^{-1}, and a CH_4 generation rate of 21.1 μmol g^{-1} h^{-1} (Fig. 13d).

Zhu et al. [180] utilized a straightforward and convenient self-assembly technique to amalgamate the two-dimensional (2D) CTF and carbon nitride (CN), engendering a non-metallic CN/CTF heterostructure. Empirical observations and comprehensive characterizations elucidate that the incorporation of CTF augments the capacity of CN for visible light absorption (Fig. 13e). In the doped CN/CTF heterostructure, there is evident amplification in photocurrent response and a notable increase in photocurrent density post-doping, indicating an enhanced ability of the photogenerated charge carriers in the heterostructure to expedite their transfer and separation (Fig. 13f). The diminished electrochemical impedance values signify that in semiconductor materials, a lower charge carrier mobility impedance translates into swifter charge transfer rates. Additionally, the CN/CTF heterostructure effectively curtails the recombination of electron-hole pairs under various shallow trap conditions (Fig. 13g and h), thereby prolonging the lifespan of charge carriers. Consequently, the CN/CTF (2.5 %) attains an impressive optimal photo-reduction yield of 453.4 μmol g^{-1}.

Wang et al. [129] have introduced a pioneering covalent bonding strategy, heretofore unprecedented, wherein they interlace a precisely defined Ru–N_2 unit within conjugated CTFs to realize an exceedingly discriminating photoreduction of CO_2. The resultant Ru-CTF structure not only elevates charge separation to unprecedented levels but also bestows remarkable stability upon the molecular catalyst. This ground-breaking achievement yields a solar-driven conversion to formate at a rate of 2090 μmol g^{-1} h^{-1}, unaided by

Table 5
Performance comparison for pollutant degradation of CTFs.

Photocatalyst	Pollutant	Light source	Main active species	Degradation rate (min^{-1})	Degradation efficiency (%)	Ref.
DA-CTF	Rh B	Visible light (380–750 nm, 7 W)	$^{\bullet}O_2^-$, $^{\bullet}OH$, h^+	0.041	92.3	[56]
DA-CTF	MB	Visible light (380–750 nm, 7 W)	$^{\bullet}O_2^-$, $^{\bullet}OH$, h^+	0.048	99.2	[56]
Co/CTF-1	MB	Visible light	$^{\bullet}O_2^-$, h^+	0.081	99.9	[121]
5 % CTF-Bi$_2$WO$_6$	TC	300 W Xl, $\lambda \geq 420$ nm	$^{\bullet}O_2^-$, h^+	0.021	92.2	[214]
CTF	CBZ	Xenon lamp, $\lambda \geq 420$ nm	$SO_4^{\bullet-}$, $^{\bullet}OH$, $^1O_2$	–	95	[57]
GO/PB@CTF-3	TC	Sunlight/Visible light/Near-infrared light	$^{\bullet}O_2^-$, $^{\bullet}OH$	0.140	95	[265]
Fe$_3$O$_4$@TpMa	phenol	Xenon lamp, $\lambda \geq 420$ nm	$SO_4^{\bullet-}$, $^{\bullet}OH$, $^{\bullet}O_2^-$, h^+, $^1O_2$	0.059	100	[183]
CTF-Cu$_{50-50}$	MB	250 W halogen lamp	$^{\bullet}OH$, $^{\bullet}O_2^-$	0.017	91.1	[126]
Ni-CAT-1/CTF-1	TC	300 W Xenon lamp, $\lambda \geq 420$ nm	$^{\bullet}O_2^-$, h^+, e^-	0.066	98	[266]
CTF-1-NR/GO	MB	AM 1.5G spectrum	$^{\bullet}OH$, $^{\bullet}O_2^-$, h^+	–	99.9	[158]
CdS–P-ACTF-5%	TC	300 W Xenon lamp	$^{\bullet}O_2^-$	0.050	99.7	[267]
COFs-Ph@CdS-3	TC	300 W Xenon lamp	$^{\bullet}OH$, $^{\bullet}O_2^-$, h^+	–	87.2	[104]
COFs-Ph@CdS-3	2,4-DCP	300 W Xenon lamp	$^{\bullet}OH$, $^{\bullet}O_2^-$, h^+	–	95.4	[104]
COFs-Ph@CdS-3	RhB	300 W Xenon lamp	$^{\bullet}OH$, $^{\bullet}O_2^-$, h^+	–	82.6	[104]
TACTF@CNT	Cr(VI)	300 W Xenon lamp, $\lambda \geq 400$ nm	e^-	0.003	100	[106]
H-CTF-Na	CBZ	300 W Xenon lamp, $\lambda \geq 400$ nm	$^{\bullet}OH$, $^{\bullet}O_2^-$	0.030	96.8	[39]
ZnONPs/CTFs	Congo red	72W LED lamps	$^{\bullet}OH$, $^{\bullet}O_2^-$	–	99.97	[268]
JOU-7	Cr(VI)	300 W Xenon lamp	$^{\bullet}OH$, $^{\bullet}O_2^-$, $^1O_2$	0.032	95.2	[137]
SEP@Th-CTF2:1	PRO	300 W Xenon lamp, $\lambda \geq 420$ nm	$^{\bullet}OH$, $^{\bullet}O_2^-$	0.094	99	[269]
CTF-SD$_2$	BPA	300 W Xenon lamp, $\lambda \geq 420$ nm	$^1O_2$	0.043	100	[178]
BiOBr@TpPa-1	BPA	500 W Xenon lamp, $\lambda \geq 420$ nm	$^{\bullet}OH$, $^{\bullet}O_2^-$	–	60	[270]
CT-2	TC	300 W Xenon lamp, $\lambda \geq 420$ nm	$^{\bullet}OH$, $^{\bullet}O_2^-$, h^+	0.080	100	[189]
COFs-Br	TC	300 W Xenon lamp, $\lambda \geq 420$ nm	$^{\bullet}OH$, $^{\bullet}O_2^-$	0.111	90	[271]
COFs-OMe	Cr(VI)	300 W Xenon lamp, $\lambda \geq 420$ nm	$^{\bullet}O_2^-$	0.022	100	[271]
MS@TpTt	TC	visible light, AM-1.5 spectrum	$^{\bullet}OH$, $^{\bullet}O_2^-$	0.027	97.3	[272]
Tp-Mela COF	RhB	300 W Xenon lamp, $\lambda \geq 420$ nm	$^{\bullet}OH$, $^{\bullet}O_2^-$	0.206	98	[263]
CTF-5Th	BPA	300 W Xenon lamp, $\lambda \geq 420$ nm	$SO_4^{\bullet-}$, $^{\bullet}OH$, h^+	0.086	100	[44]
CdS/PANI/MWCNTs	SBX	mercury lamp (125 W)	$^{\bullet}OH$, $^{\bullet}O_2^-$	–	99.2	[273]
BTDC	RhB	300 W Xenon lamp, $\lambda \geq 400$ nm	$^{\bullet}OH$, $^{\bullet}O_2^-$, h^+	0.178	97	[190]
COF-DBT	TC	300 W Xenon lamp, $\lambda \geq 420$ nm	$^{\bullet}O_2^-$, e^-	0.122	98.7	[274]

MB: Methylene blue, TC: Tetracycline, Rh B: Rhodamine B, PRO: Propranolol Hydrochloride, BPA Bisphenol A, SBX: Sodium Butyl Xanthate, 2,4-DCP: 2,4-Dichlorophenol, CBZ: Carbamazepine.

supplementary photosensitizers, and showcases an impressive selectivity of up to 98.5 %. Experimental investigations, complemented by DFT computations, elucidate the swift activation of CO_2 by a lone Ru–N_2 nucleus, thereby emphasizing its effectiveness as a pivotal photocatalytic core, notably surpassing alternative catalysts. This monumental endeavor has ushered in novel pathways, enriched foundational insights, and bequeathed profound comprehension in the quest for tailoring bespoke CTFs photocatalysts for the exceptionally discriminating task of CO_2 photoreduction.

Cao et al. [254] have pioneered an efficacious tandem photocatalysis strategy, ingeniously crafting synergistic dual sites within the copper-porphyrinic triazine framework [PTF(Cu)] and rhenium-(I) bipyridine fac-[Re^I(bpy)(CO)$_3$Cl] (Re-bpy) systems. This innovative approach enables the conversion of CO_2 into ethylene, a process previously unattainable with either individual Re-bpy or PTF(Cu) catalysts alone. Under visible light irradiation, this tandem system yields a substantial ethylene production rate of 73.2 μmol g^{-1} h^{-1}. Intriguingly, when utilizing a single catalyst, the outcome is restricted to the formation of monocarbon product CO, even under identical conditions. The tandem photocatalytic mechanism unfolds as follows: CO, generated at the Re-bpy sites, undergoes adsorption by neighboring Cu single sites within PTF(Cu). Subsequently, a synergistic C–C coupling process ensues, culminating in the production of ethylene. This study unveils a novel avenue for engineering highly efficient photocatalysts capable of converting CO_2 into valuable C_2 products through a tandem process, propelled by the gentle touch of visible light under mild conditions.

4.4. Photocatalytic degradation of pollutants

Amidst the burgeoning global population and the rapid evolution of society, various sources of pollution, including domestic waste and industrial contaminants, notably from pharmaceutical and pigment manufacturing enterprises, have led to a grave concern of water pollution in contemporary times. Photocatalysis emerges as a viable and environmentally friendly technology, providing an efficient solution to treat wastewater, especially when conventional methods struggle to completely eliminate recalcitrant pollutants [106,126,137,138,189,190,261,262]. In this context, CTFs have garnered attention as a metal-free and sustainable photocatalyst, harnessing the power of visible light to effectively degrade organic pollutants (Table 5) [137,263,264]. Here, some seminal works that explore the photocatalytic degradation of pollutants using CTFs, elucidating the diverse mechanisms and classifications that underlie their remarkable performance.

Xi et al. [263] have pioneered the development of a metal-free photocatalytic system centered around the Tp-Mela COF/H_2O_2 platform, tailored for Fenton-like reactions. Leveraging its vast porosity, augmented by a high concentration of photoactive triazine
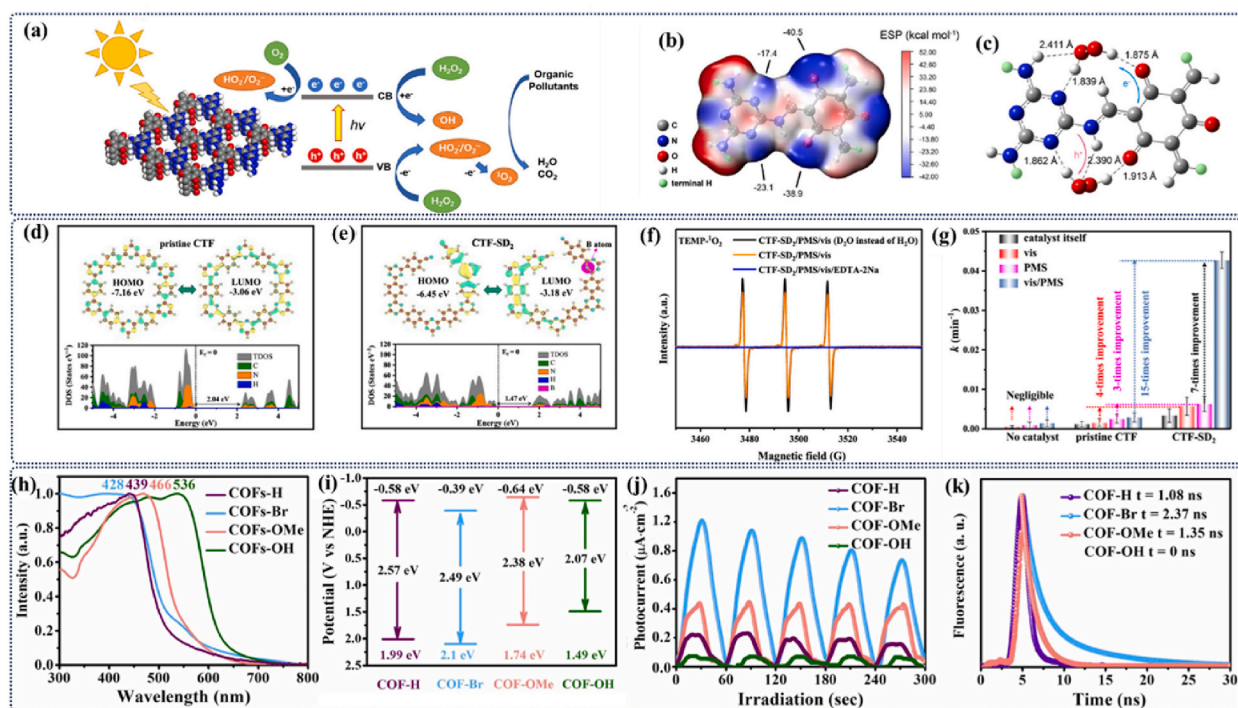

Fig. 14. (a) Proposed mechanism of Fenton-like reaction with Tp-Mela COF/H_2O_2 photocatalytic system. (b) Distribution of ESP for Tp-Mela COF fragment via the DFT calculations. (c) The calculated model for the hydrogen-bonding interactions between two H_2O_2 molecules and the Tp-Mela COF unit. Reproduced with permission [263]. Copyright 2021, Elsevier. Calculated HOMO/LUMO and total density of states/projected density of states for (d) pristine CTF and (e) CTF-SD$_2$. (f) TEMP-$^1O_2$ signals in different systems. (g) BPA degradation rate constants in various processes. Reproduced with permission [178]. Copyright 2022, American Chemical Society. (h) UV–vis spectra, (i) band alignment, (j) photocurrent responses (λ ≥ 420 nm) and (k) transient fluorescence spectra of COFs-Rs. Reproduced with permission [271]. Copyright 2023, Elsevier.

moieties, a bandgap fine-tuned through the partial interruption of π-conjugation, as well as the effectiveness of charge separation and transfer facilitated by AA stacking, this unique standalone photocatalyst, Tp-Mela COF, has manifested remarkable prowess in the degradation of organic pollutants (Fig. 14a–c). Furthermore, the Tp-Mela COF/H_2O_2 photocatalytic system has demonstrated commendable reusability and a remarkable versatility in the degradation of diverse organic pollutants. Mechanistic insights suggest that visible light excitation generates electrons and holes, which are subsequently directed through hydrogen bonds to engage with H_2O_2 molecules, thereby engendering a profusion of reactive oxygen species (ROSs), encompassing HO_2/O_2^-, ·OH, and $^1O_2$. These ROSs are the chief architects of the impressive efficiency achieved in the Fenton-like reaction. Thus, this work not only presents an efficient metal-free photocatalyst but also unfurls new horizons in the domain of Fenton-like reactions.

Our previous research [178] unveiled the synthesis and characterization of structural defect CTFs (CTF-SDs), which exhibit a remarkable juxtaposition of structural attributes, featuring the concurrent the strategic introduction of boron (B) atoms and terminal presence of cyano (-CN) groups. The electron-withdrawing cyano (-CN) groups located at the structural terminations of CTF-SDs have the potential to serve as sites for charge accumulation, thereby energetically promoting the separation and transfer of photo-carriers. (Fig. 14d and e), according to the findings of extensive investigations and DFT calculations. Additionally, the reduced band gap and downshifted VB location generated by the inclusion of structural flaws disrupted the energy structure and provided a strong enough driving force for photocatalytic oxidation processes. And the interaction between the B dopant and the CN defect changes the electronic structure of CTF-SDs to create nearby electron-deficient regions. This promotes a high affinity for PMS and loosens the links between its molecules. It is imperative to emphasize that quenching experiments and detailed EPR characterization unequivocally
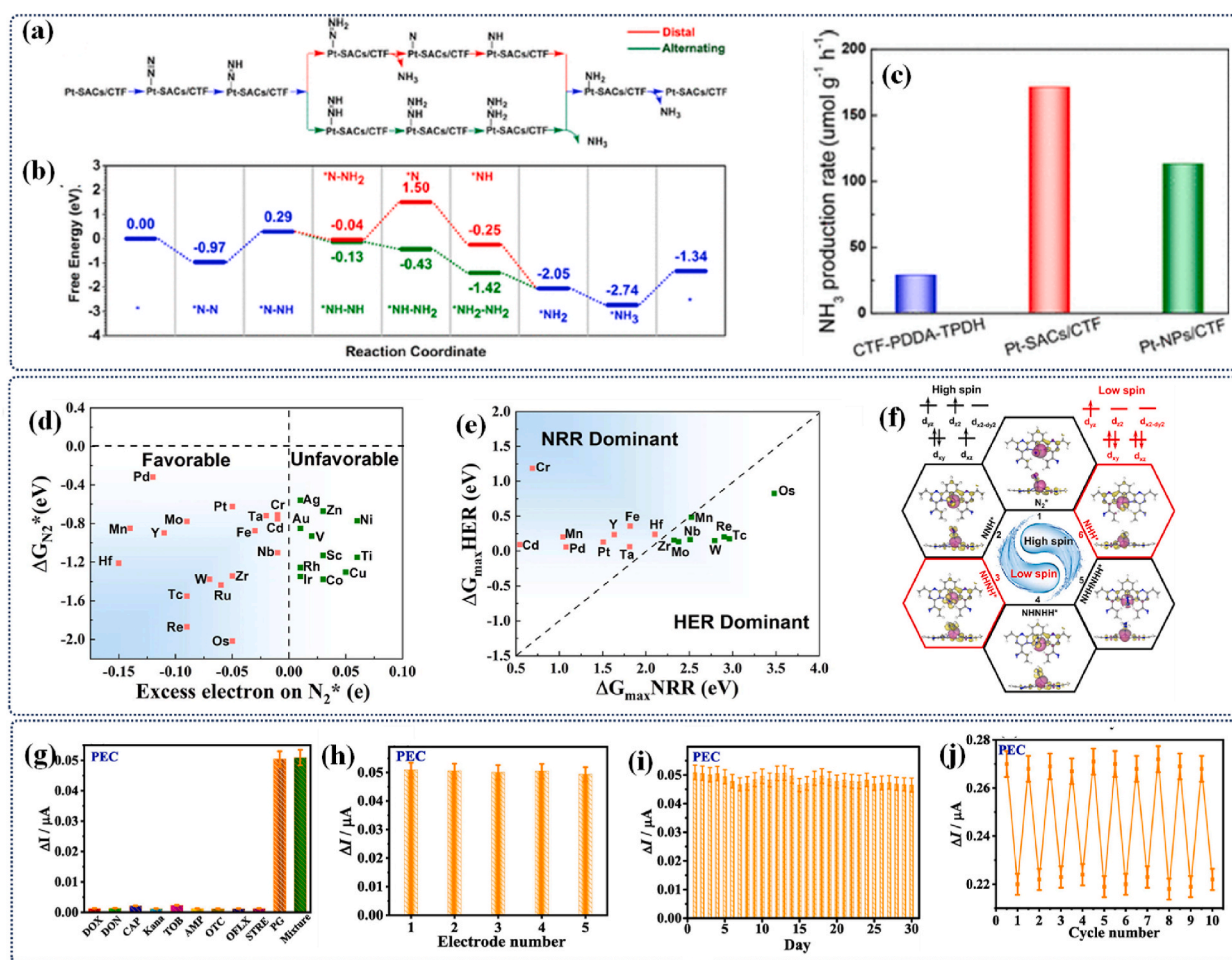

Fig. 15. Schematic of the distal and the alternating mechanisms for the nitrogen reduction process on the Pt-SACs/CTF catalyst. (b) Free energy profiles of the distal and the alternating mechanisms for nitrogen reduction process on the Pt-SACs/CTF catalyst. (c) the normalized NH_3 production rate of all samples. Reproduced with permission [120]. Copyright 2020, American Chemical Society. (d) Free energy changes of N_2^* (ΔGN_2^*) as a function of the excess electron on N_2^*. (e) $\Delta GmaxHER$ vs $\Delta GmaxNRR$. (f) Top view and front view of the spin densities of the intermediates adsorbed on Cr/CTF. Reproduced with permission [64]. Copyright 2022, Elsevier. (g) Photocurrent responses for the detection of PG and different varieties of interferents. (h) Photocurrent responses of the five independent Fe-MA-Dha-CTFs aptasensor for detecting PG. (i) Photocurrent responses of the same aptasensor for the detection of PG per day for 30 days. (j) The regenerability of the developed aptasensor evaluated by (h) PEC methods. Reproduced with permission [119]. Copyright 2023, Elsevier.

identify $^1O_2$ as the principal active species in this context (Fig. 14f). Benefiting from these advantages, CTF-SDs with moderate structural defects demonstrated significantly improved photocatalytic performance in the metal-free solar-driven activation of PMS for organic removal when compared to pristine CTFs. (Fig. 14g).

Zhu et al. [271] have undertaken a transformative endeavor by functionalizing the structural units with electron-donating and electron-withdrawing substituents, denoted as –R (where R encompasses H, Br, OMe, OH). This pioneering work has led to the creation of a comprehensive series of triazine-CoFS-R materials that exhibit responsiveness to visible light. Through meticulous theoretical and experimental studies, it has been unequivocally demonstrated that the incorporation of electron-donor substituents serves to abbreviate the band gap of materials (Fig. 14h), which leading to a lower energy associated with photoinduced excitation and charge carrier generation, thus rendering these materials conducive to efficient visible light utilization. Furthermore, the introduction of diverse halogens into the material has the remarkable effect of either reducing the VB or elevating the CB (Fig. 14i). Notably, the materials exhibit an augmented photocurrent response following the introduction of electron-OMe and electron-BR substituents, signifying enhanced carrier separation, mobility, prolonged carrier lifetime (Fig. 14j and k), and reduced recombination efficiency. These attributes are highly advantageous in the utilization of electron-hole pairs for photocatalytic degradation processes. Additionally, the decrease in Stokes displacement observed in COFs-OMe and COFs-Br indicates reduced energy loss during excitation, ultimately enhancing the energy utilization efficiency of the photocatalytic process. This innovative modification approach opens new vistas for the precise regulation of COF materials, enabling highly efficient visible-driven degradation of organic pollutants and the removal of heavy metal ions.

4.5. Multifunctional applications

It is preferred that the photocatalyst integrates dual or more functions into a single reaction system while simultaneously taking the environment and energy into account [134,142,153,182,265,267,275–278]. The establishment of suitable energy structures is essential to initiate the dual reactive process required for photocatalysis [120,158,182]. In recent years, the field of photocatalytic nitrogen fixation has emerged as a prominent area of research, holding substantial promise for widespread practical applications [121, 216]. Mei et al. [120] achieved the precise anchoring of a solitary Pt atom onto the well-defined –N_3 site within an enduring ultra-thin CTF nanosheet (referred to as PT-SACS/CTF).

It has been observed that the introduction of ultrathin CTF-PDDA-TPDH nanosheets and single-atom Pt into stable enhances the separation of photogenerated electron-hole pairs [120]. The electrons residing in the CB of CTF-PDDA-TPDH migrate to the single Pt atoms, facilitating the reduction of adsorbed nitrogen molecules to produce NH_3 (Fig. 15a and b). Hence, when exposed to visible light, the Pt-SACs/CTF catalyst achieved a NH_4^+ yield of 7.71 mg L^{-1} following 5 h of photo illumination, boasting an average NH_4^+ production rate of 171.40 μmol g^{-1} h^{-1} (Fig. 15c), which significantly surpasses the majority of previously reported photocatalytic ammonia production rates utilizing various catalysts. Meanwhile, Li et al. [64] harnessed the versatility of CTFs as a multifunctional platform to synthesize M/CTFs (M = transition metal) distinguished by robust coordination capabilities. Among them, Cr/CTF emerged as an exceptional nitrogen fixation material, displaying the remarkable attributes of substantial HER suppression (Fig. 15d–f), outstanding thermodynamic stability ($E_b = -4.40$ eV), a moderate adsorption energy ($E_a = -0.84$ eV), narrow band gap ($E_g = 0.03$ eV), considerable activation energy ($\Delta GN_2^* = -0.71$ eV), and a theoretical Faradaic efficiency of 100 %.

Furthermore, Wang et al. [119] harnessed the distinctive electrochemical and photoelectric attributes of CTFs to engineer a novel CTF-based dual-mode EC-PEC aptamer sensor, tailored for the ultrasensitive detection of penicillin G (PG). This innovative approach not only inherited the inherent advantages of CTFs, including its rich functionality rooted in triazine, high porosity, and enhanced electrochemical activity induced by doped β-FeOOH, as well as the superior photoabsorption performance of MA-Dha-CTF but also demonstrated improved electrochemical activity (Fig. 15g). Consequently, it facilitated amplified sensing signals, obviating the necessity for any EC or PEC indicators in PG detection. The proposed label-free Fe-MA-Dha-CTFs dual-modal EC–PEC aptasensor exhibited a substantially lower detection limit (0.08 and 0.7 fg mL^{-1} as deduced by the PEC and EC techniques, respectively) compared to previously reported PG biosensors (Fig. 15h). This superior performance was attributed to its abundant aptamer strands and remarkable stability, stemming from the stable chemical structure of Fe-MA-Dha-CTF (Fig. 15i and j). Furthermore, Kamiya et al. [275] devised a Cu-doped CTF–TiO_2 hybrid that demonstrated photocatalytic reduction of HNO_2 without the need for an external bias, utilizing both artificial light and natural sunlight. Interestingly, variations in light intensity led to a transformation in the primary reaction product, shifting from N_2O to NH_4^+. This phenomenon was attributed to alterations in the operating potentials induced by changes in light intensity. Recently, Fang et al. [182] pioneered the development of a novel composite membrane, featuring a [0D + 2D] structure, which combines CTF-1 nanosheets with integrated CdS quantum dots (QDs). The CdS/CTF-1 composite membrane exhibits remarkable water permeability (>170 L m^{-2} h^{-1}, 0.1 MPa) and exceptional dye rejection (>94 %), achieved through precise control of transport pathways. Of particular significance, the embedded [0D+2D]-heterojunction significantly enhances the in-situ photocatalytic cleaning and disinfection capabilities of the CdS/CTF-1 membrane. This innovation allows for the restoration of permeability (>95 %) with the aid of H_2O_2 during multiple operational cycles.

5. Conclusions and future prospects

In the domain of metal-free CTFs for photocatalysis, we embark on a comprehensive exploration. Firstly, different synthesis methods of CTFs were studied in depth, which leverage inherent synergistic effects such as π–π interactions, electrostatic attraction, and chemical bonding. The focus then shifts to strategies for enhancing performance, encompassing compositional optimization, dopant incorporation, heterostructure engineering, morphological control, and more. These approaches collectively contribute to four

pivotal facets: heightened optical absorption abilities, expanded surface active sites, augmented separation of e^- and h^+, and modified energy level structures, holding paramount significance in the realm of photocatalysis. Heterogeneous CTFs have demonstrated remarkable prowess in various applications, including H_2 evolution, H_2O_2 Production, CO_2 reduction into "green" fuels, contaminant degradation and N_2 Fixation, which is powerful countermeasure in energy- and environmental-related subjects.

Despite plenty of state-of-the-art achievements are grabbed rapidly, the development of CTFs is still in its infancy. In light of this, the following pivotal issues are elaborated upon.

1. Efforts must continue to be devoted to the development of environmentally friendly and streamlined synthesis routes to enhance the performance of hybrid catalysts. For instance, the meticulous design of molecular-level structures to finely adjust band structures and optimize factors such as charge separation and transfer efficiency remains pivotal in influencing the characteristics of CTFs semiconductors. Furthermore, the regulation of morphology and porosity holds paramount significance within the realm of photocatalytic applications.
2. The production of well-organized, stable crystal structures and precisely defined CTFs remains a huge challenge, which may hinder further in-depth study of structure-activity relationships, hence the need for further development of advanced CTFs.
3. To date, CTFs has not fully harnessed the potential of visible and near-infrared light, primarily due to its dependence on intrinsic properties and supplementary components. Consequently, there is a pressing imperative to engineer materials that possess the requisite energy range and light responsiveness when strategically integrated.
4. Currently, CTFs find predominant application in HER through water splitting, CO_2 reduction, and the degradation of organic pollutants. However, there is a growing necessity to shift focus towards methane oxidation and the selective conversion of foundational chemicals or biomass into valuable high-grade compounds. Addressing this challenge will require a comprehensive understanding of the underlying principles driving photocatalytic enhancements in these contexts.
5. The fusion of theoretical research and experimental practice must be further intensified in order to address the challenges associated with CTFs. Achieving a substantial enhancement in the catalytic efficiency of CTFs demands in-depth and comprehensive investigations, aimed at unraveling the intricacies of their mechanistic actions. Such insights will play a pivotal role in steering the design and construction of artificial optical systems tailored for multifunctional applications. Additionally, the economic upscaling, mass production, and exploration of potential industrial uses of CTFs stand as critical imperatives in this field.

Moreover, the potential applications of CTFs in membrane energy storage, photoelectrochemical cells, and flexible energy storage devices may emerge as promising avenues for future research. Such endeavors hold promise for meeting the demands of clean energy and sustainability, aligning with the emphasis on universally accessible, reliable, and essential energy outlined in the United Nations Sustainable Development Goals.

CRediT authorship contribution statement

Shuqi Li: Writing – original draft. **Yintian Mao:** Data curation. **Jian Yang:** Data curation. **Yin Li:** Data curation. **Jun Dong:** Data curation. **Zhen Wang:** Supervision. **Lixian Jiang:** Validation, Software. **Shilong He:** Visualization.

Declaration of competing interest

The authors declare that they have no known competing financial interests or personal relationships that could have appeared to influence the work reported in this paper.

Acknowledgements

References

[1] H. Liao, H. Ding, B. Li, X. Ai, C. Wang, Covalent-organic frameworks: potential host materials for sulfur impregnation in lithium-sulfur batteries, J. Mater. Chem. A 2 (2014) 8854–8858, https://doi.org/10.1039/c4ta00523f.
[2] R.Z. Wang, D.L. Huang, Y.G. Liu, C. Zhang, C. Lai, G.M. Zeng, M. Cheng, X.M. Gong, J. Wan, H. Luo, Investigating the adsorption behavior and the relative distribution of Cd^{2+} sorption mechanisms on biochars by different feedstock, Bioresour. Technol. 261 (2018) 265–271, https://doi.org/10.1016/j.biortech.2018.04.032.
[3] W. Xue, Z. Peng, D. Huang, G. Zeng, J. Wan, R. Xu, M. Cheng, C. Zhang, D. Jiang, Z. Hu, Nanoremediation of cadmium contaminated river sediments: Microbial response and organic carbon changes, J. Hazard Mater. 359 (2018) 290–299, https://doi.org/10.1016/j.jhazmat.2018.07.062.
[4] G.H. Jeong, S.P. Sasikala, T. Yun, G.Y. Lee, W.J. Lee, S.O. Kim, Nanoscale assembly of 2D materials for energy and environmental applications, Adv. Mater. 32 (2020) 1907006, https://doi.org/10.1002/adma.201907006.
[5] S. De, J. Zhang, R. Luque, N. Yan, Ni-based bimetallic heterogeneous catalysts for energy and environmental applications, Energy Environ. Sci. 9 (2016) 3314–3347, https://doi.org/10.1039/c6ee02002j.
[6] J.S.M. Lee, A.I. Cooper, Advances in conjugated microporous polymers, Chem. Rev. 120 (2020) 2171–2214, https://doi.org/10.1021/acs.chemrev.9b00399.
[7] Y. Sun, L. Han, P. Strasser, A comparative perspective of electrochemical and photochemical approaches for catalytic H_2O_2 production, Chem. Soc. Rev. 49 (2020) 6605–6631, https://doi.org/10.1039/d0cs00458h.

[8] T. Xiong, W. Cen, Y. Zhang, F. Dong, Bridging the g-C₃N₄ interlayers for enhanced photocatalysis, ACS Catal. 6 (2016) 2462–2472, https://doi.org/10.1021/acscatal.5b02922.

[9] X. Wang, K. Maeda, A. Thomas, K. Takanabe, G. Xin, J.M. Carlsson, K. Domen, M. Antonietti, A metal-free polymeric photocatalyst for hydrogen production from water under visible light, Nat. Mater. 8 (2009) 76–80, https://doi.org/10.1038/nmat2317.

[10] D. Huang, X. Wang, C. Zhang, G. Zeng, Z. Peng, J. Zhou, M. Cheng, R. Wang, Z. Hu, X. Qin, Sorptive removal of ionizable antibiotic sulfamethazine from aqueous solution by graphene oxide-coated biochar nanocomposites: influencing factors and mechanism, Chemosphere 186 (2017) 414–421, https://doi.org/10.1016/j.chemosphere.2017.07.154.

[11] J. Zhang, X. Chen, K. Takanabe, K. Maeda, K. Domen, J.D. Epping, X. Fu, M. Antonieta, X. Wang, Synthesis of a carbon nitride structure for visible-light catalysis by copolymerization, Angew. Chemie - Int. Ed. 49 (2010) 441–444, https://doi.org/10.1002/anie.200903886.

[12] V. Etacheri, C. Di Valentin, J. Schneider, D. Bahnemann, S.C. Pillai, Visible-light activation of TiO₂ photocatalysts: advances in theory and experiments, J. Photochem. Photobiol. C Photochem. Rev. 25 (2015) 1–29, https://doi.org/10.1016/j.jphotochemrev.2015.08.003.

[13] F. Zhao, Y. Liu, S. Ben Hammouda, B. Doshi, N. Guijarro, X. Min, C.J. Tang, M. Sillanpää, K. Sivula, S. Wang, MIL-101(Fe)/g-C₃N₄ for enhanced visible-light-driven photocatalysis toward simultaneous reduction of Cr(VI) and oxidation of bisphenol A in aqueous media, Appl. Catal. B Environ. 272 (2020) 119033, https://doi.org/10.1016/j.apcatb.2020.119033.

[14] Q. Yang, M. Luo, K. Liu, H. Cao, H. Yan, Covalent organic frameworks for photocatalytic applications, Appl. Catal. B Environ. 276 (2020) 119174, https://doi.org/10.1016/j.apcatb.2020.119174.

[15] X. Xu, C. Wu, A. Guo, B. Qin, Y. Sun, C. Zhao, F. Zhang, A. Cai, Visible-light photocatalysis of organic contaminants and disinfection using biomimetic-synthesized TiO₂-Ag-AgCl composite, Appl. Surf. Sci. 588 (2022) 152886, https://doi.org/10.1016/j.apsusc.2022.152886.

[16] Z. Fang, Q. Li, L. Su, J. Chen, K.C. Chou, X. Hou, Efficient synergy of photocatalysis and adsorption of hexavalent chromium and rhodamine B over Al₄SiC₄/rGO hybrid photocatalyst under visible-light irradiation, Appl. Catal. B Environ. 241 (2019) 548–560, https://doi.org/10.1016/j.apcatb.2018.09.074.

[17] V.R. Battula, S. Kumar, D.K. Chauhan, S. Samanta, K. Kailasam, A true oxygen-linked heptazine based polymer for efficient hydrogen evolution, Appl. Catal. B Environ. 244 (2019) 313–319, https://doi.org/10.1016/j.apcatb.2018.11.027.

[18] J.M. Dangwang Dikdim, Y. Gong, G.B. Noumi, J.M. Sieliechi, X. Zhao, N. Ma, M. Yang, J.B. Tchatchueng, Peroxymonosulfate improved photocatalytic degradation of atrazine by activated carbon/graphitic carbon nitride composite under visible light irradiation, Chemosphere 217 (2019) 833–842, https://doi.org/10.1016/j.chemosphere.2018.10.177.

[19] Y. Zhu, Y. Wang, Q. Ling, Y. Zhu, Enhancement of full-spectrum photocatalytic activity over BiPO₄/Bi₂WO₆ composites, Appl. Catal. B Environ. 200 (2017) 222–229, https://doi.org/10.1016/j.apcatb.2016.07.002.

[20] C. Liu, H. Dai, C. Tan, Q. Pan, F. Hu, X. Peng, Applied Catalysis B : environmental Photo-Fenton degradation of tetracycline over Z-scheme Fe-g-C₃N₄/Bi₂WO₆ heterojunctions : mechanism insight, degradation pathways and DFT calculation, Appl. Catal. B Environ. 310 (2022) 121326, https://doi.org/10.1016/j.apcatb.2022.121326.

[21] S. Ma, Z. Li, J. Jia, Z. Zhang, H. Xia, H. Li, X. Chen, Y. Xu, X. Liu, Amide-linked covalent organic frameworks as efficient heterogeneous photocatalysts in water, Chinese J. Catal. 42 (2021) 2010–2019, https://doi.org/10.1016/S1872-2067(21)63836-6.

[22] Y. Chen, M. Bhati, B.W. Walls, B. Wang, M.S. Wong, T.P. Senftle, Mechanistic insight into the photo-oxidation of perfluorocarboxylic acid over boron nitride, Environ. Sci. Technol. 56 (2022) 8942–8952, https://doi.org/10.1021/acs.est.2c01637.

[23] K. Wang, L.M. Yang, X. Wang, L. Guo, G. Cheng, C. Zhang, S. Jin, B. Tan, A. Cooper, Covalent triazine frameworks via a low-temperature polycondensation approach, Angew. Chemie - Int. Ed. 56 (2017) 14149–14153, https://doi.org/10.1002/anie.201708548.

[24] P. Kuhn, M. Antonietti, A. Thomas, Ionothermalsynthese von porösen kovalenten triazin- polymernetzwerken, Angew. Chem. 120 (2008) 3499–3502, https://doi.org/10.1002/ange.200705710.

[25] S. Ren, M.J. Bojdys, R. Dawson, A. Laybourn, Y.Z. Khimyak, D.J. Adams, A.I. Cooper, Porous, fluorescent, covalent triazine-based frameworks via room-temperature and microwave-assisted synthesis, Adv. Mater. 24 (2012) 2357–2361, https://doi.org/10.1002/adma.201200751.

[26] M. Zhu, Y. Osakada, S. Kim, M. Fujitsuka, T. Majima, Black phosphorus : a promising two dimensional visible and near-infrared-activated photocatalyst for hydrogen evolution, Appl. Catal. B Environ. 217 (2017) 285–292, https://doi.org/10.1016/j.apcatb.2017.06.002.

[27] W. Gao, Y. Zhou, X. Wu, Q. Shen, J. Ye, Z. Zou, State-of-the-Art progress in diverse black phosphorus-based structures : basic properties, synthesis, stability, photo- and electrocatalysis-driven energy conversion, Adv. Funct. Mater. 18 (2021) 2005197, https://doi.org/10.1002/adfm.202005197.

[28] S. Zang, G. Zhang, Z.A. Lan, D. Zheng, X. Wang, Enhancement of photocatalytic H₂ evolution on pyrene-based polymer promoted by MoS₂ and visible light, Appl. Catal. B Environ. 251 (2019) 102–111, https://doi.org/10.1016/j.apcatb.2019.03.061.

[29] D. Zhang, Y. Guo, Z. Zhao, Porous defect-modified graphitic carbon nitride via a facile one-step approach with significantly enhanced photocatalytic hydrogen evolution under visible light irradiation, Appl. Catal. B Environ. 226 (2018) 1–9, https://doi.org/10.1016/j.apcatb.2017.12.044.

[30] J. Sun, J. Xu, A. Grafmueller, X. Huang, C. Liedel, G. Algara-Siller, M. Willinger, C. Yang, Y. Fu, X. Wang, M. Shalom, Self-assembled carbon nitride for photocatalytic hydrogen evolution and degradation of p-nitrophenol, Appl. Catal. B Environ. 205 (2017) 1–10, https://doi.org/10.1016/j.apcatb.2016.12.030.

[31] R. Feng, W. Lei, G. Liu, M. Liu, Visible- and NIR-light responsive black-phosphorus-based nanostructures in solar fuel production and environmental remediation, Adv. Mater. 30 (2018) 1804770, https://doi.org/10.1002/adma.201804770.

[32] S. Wang, L. Li, Z. Zhu, M. Zhao, L. Zhang, N. Zhang, Q. Wu, X. Wang, G. Li, Remarkable improvement in photocatalytic performance for tannery wastewater processing via SnS₂ modified with N-doped carbon quantum dots: synthesis, Characterization, and 4-nitrophenol-aided Cr(VI) photoreduction, Small 15 (2019) 1804515, https://doi.org/10.1002/smll.201804515.

[33] S.N. Habisreutinger, L. Schmidt-Mende, J.K. Stolarczyk, Photocatalytic reduction of CO₂ on TiO₂ and other semiconductors, Angew. Chemie - Int. Ed. 52 (2013) 7372–7408, https://doi.org/10.1002/anie.201207199.

[34] Y. Wang, J. Chen, G. Wang, Y. Li, Z. Wen, Perfluorinated covalent triazine framework derived hybrids for the highly selective electroconversion of carbon dioxide into methane, Angew. Chemie - Int. Ed. 57 (2018) 13120–13124, https://doi.org/10.1002/anie.201807173.

[35] B. Chon, S. Choi, Y. Seo, H.S. Lee, C.H. Kim, H. Son, InP-quantum dot surface-modified TiO₂ catalysts for sustainable photochemical carbon dioxide reduction, ACS Sustain. Chem. Eng. 10 (2022) 6033–6044, https://doi.org/10.1021/acssuschemeng.2c00938.

[36] Q. Zhou, S. Ma, S. Zhan, Superior photocatalytic disinfection effect of Ag-3D ordered mesoporous CeO₂ under visible light, Appl. Catal. B Environ. 224 (2018) 27–37, https://doi.org/10.1016/j.apcatb.2017.10.032.

[37] Z. Gao, Y. Jian, S. Yang, Q. Xie, C.J. Ross Mcfadzean, B. Wei, J. Tang, J. Yuan, C. Pan, G. Yu, Interfacial Ti−S bond modulated S-scheme MOF/covalent triazine framework nanosheet heterojunctions for photocatalytic C−H functionalization, Angew. Chemie - Int. Ed. 62 (2023) e202304173, https://doi.org/10.1002/anie.202304173.

[38] X. Zhu, C. Tian, S.M. Mahurin, S.H. Chai, C. Wang, S. Brown, G.M. Veith, H. Luo, H. Liu, S. Dai, A superacid-catalyzed synthesis of porous membranes based on triazine frameworks for CO₂ separation, J. Am. Chem. Soc. 134 (2012) 10478–10484, https://doi.org/10.1021/ja304879c.

[39] T. Zeng, S. Li, Y. Shen, H. Zhang, H. Feng, X. Zhang, L. Li, Z. Cai, S. Song, Sodium doping and 3D honeycomb nanoarchitecture: key features of covalent triazine-based frameworks (CTF) organocatalyst for enhanced solar-driven advanced oxidation processes, Appl. Catal. B Environ. 257 (2019) 117915, https://doi.org/10.1016/j.apcatb.2019.117915.

[40] D. Li, C. Li, L. Zhang, H. Li, L. Zhu, D. Yang, Q. Fang, S. Qiu, X. Yao, Metal-free thiophene-sulfur covalent organic frameworks: precise and controllable synthesis of catalytic active sites for oxygen reduction, J. Am. Chem. Soc. 142 (2020) 8104–8108, https://doi.org/10.1021/jacs.0c02225.

[41] W. Huang, B.C. Ma, H. Lu, R. Li, L. Wang, K. Landfester, K.A.I. Zhang, Visible-light-promoted selective oxidation of alcohols using a covalent triazine framework, ACS Catal. 7 (2017) 5438–5442, https://doi.org/10.1021/acscatal.7b01719.

[42] S. Li, Z. Jin, W. Lai, H. Zhang, D. Wang, S. Song, T. Zeng, Alkali and donor-acceptor bridged three-dimensional interpenetrating polymer networks boost photocatalytic performance by efficient electron delocalization and charge transfer, Appl. Catal. B Environ. 292 (2021) 120153, https://doi.org/10.1016/j.apcatb.2021.120153.

[43] K. Schwinghammer, S. Hug, M.B. Mesch, J. Senker, B.V. Lotsch, Phenyl-triazine oligomers for light-driven hydrogen evolution, Energy Environ. Sci. 8 (2015) 3345–3353, https://doi.org/10.1039/c5ee02574e.

[44] S. Li, Z. Jin, X. Jiang, J. Yu, J. Wang, Y. Wang, S. Jin, H. Zhang, S. Song, T. Zeng, Thiophene-incorporated CTFs with boosted intramolecular charge transfer and defect-abundant networks for potent photosensitized oxidation of organics, Chem. Eng. J. 431 (2022) 133900, https://doi.org/10.1016/j.cej.2021.133900.

[45] T. Sun, S. Li, L. Zhang, Y. Xu, Aqueous processable Two-dimensional triazine polymers with superior photocatalytic properties, Angew. Chem. 62 (2023) e202301865, https://doi.org/10.1002/anie.202301865.

[46] L. Yang, R. Gong, G.I.N. Waterhouse, J. Dong, J. Xu, A novel covalent triazine framework developed for efficient determination of 1-naphthol in water, Environ. Sci. Pollut. Res. 28 (2021) 31185–31194.

[47] F. Paper, C.O. Frameworks, A. Karmakar, A. Kumar, A.K. Chaudhari, P. Samanta, A. V Desai, R. Krishna, S.K. Ghosh, Bimodal functionality in a porous covalent triazine framework by rational integration of an electron-rich and -deficient pore, Chem. Eur J. 22 (2016) 4931–4937, https://doi.org/10.1002/chem.201600109.

[48] J. Low, J. Yu, M. Jaroniec, S. Wageh, A.A. Al-Ghamdi, Heterojunction photocatalysts, Adv. Mater. 29 (2017) 1601694, https://doi.org/10.1002/adma.201601694.

[49] W. Huang, Q. He, Y. Hu, Y. Li, Molecular heterostructures of covalent triazine frameworks for enhanced photocatalytic hydrogen production, Angew. Chemie - Int. Ed. 58 (2019) 8676–8680, https://doi.org/10.1002/anie.201900046.

[50] S. Zhang, G. Cheng, L. Guo, N. Wang, B. Tan, S. Jin, Strong-base-assisted synthesis of a crystalline covalent triazine framework with high hydrophilicity via benzylamine monomer for photocatalytic water splitting, Angew. Chemie - Int. Ed. 59 (2020) 6007–6014, https://doi.org/10.1002/anie.201914424.

[51] A.M. Elewa, A.F.M. EL-Mahdy, M.H. Elsayed, M.G. Mohamed, S.W. Kuo, H.H. Chou, Sulfur-doped triazine-conjugated microporous polymers for achieving the robust visible-light-driven hydrogen evolution, Chem. Eng. J. 421 (2021) 129825, https://doi.org/10.1016/j.cej.2021.129825.

[52] X. Yu, B. Viengkeo, Q. He, X. Zhao, Q. Huang, P. Li, W. Huang, Y. Li, Electronic tuning of covalent triazine framework nanoshells for highly efficient photocatalytic H2O2 production, Adv. Sustain. Syst. 5 (2021) 2100184, https://doi.org/10.1002/adsu.202100184.

[53] L. Chen, L. Wang, Y. Wan, Y. Zhang, Z. Qi, X. Wu, H. Xu, Acetylene and diacetylene functionalized covalent triazine frameworks as metal-free photocatalysts for hydrogen peroxide Production: a new two-electron water oxidation pathway, Adv. Mater. 32 (2020) 1904433, https://doi.org/10.1002/adma.201904433.

[54] C. Ayed, J. Yin, K. Landfester, K.A.I. Zhang, Visible-light-promoted switchable selective oxidations of styrene over covalent triazine frameworks in water, Angew. Chemie - Int. Ed. 62 (2023) e202216159, https://doi.org/10.1002/anie.202216159.

[55] L. Zhai, Z. Xie, C.X. Cui, X. Yang, Q. Xu, X. Ke, M. Liu, L.B. Qu, X. Chen, L. Mi, Constructing synergistic triazine and acetylene cores in fully conjugated covalent organic frameworks for cascade photocatalytic H2O2 production, Chem. Mater. 34 (2022) 5232–5240, https://doi.org/10.1021/acs.chemmater.2c00910.

[56] Y. Zhuang, Q. Zhu, G. Li, Z. Wang, P. Zhan, C. Ren, Z. Si, S. Li, D. Cai, P. Qin, Photocatalytic degradation of organic dyes using covalent triazine-based framework, Mater. Res. Bull. 146 (2022) 111619, https://doi.org/10.1016/j.materresbull.2021.111619.

[57] R. Yin, Y. Chen, J. Hu, S. Jin, W. Guo, M. Zhu, Peroxydisulfate bridged photocatalysis of covalent triazine framework for carbamazepine degradation, Chem. Eng. J. 427 (2022) 131613, https://doi.org/10.1016/j.cej.2021.131613.

[58] E. Saputra, B. Aditya, P. Muhammad, W. Nugraha, N. Soraya, Fabrication of hybrid covalent triazine framework-zinc ferrite spinel to uplift visible light-driven photocatalytic organic pollutant degradation, Environ. Sci. Pollut. Res. 30 (2023) 39961–39977, https://doi.org/10.1007/s11356-022-25021-1.

[59] C. Zhu, L. Lu, Q. Fang, S. Song, B. Chen, Y. Shen, Unveiling spin state-dependent micropollutant removal using single-atom covalent triazine framework, Adv. Funct. Mater. 33 (2023) 2210905, https://doi.org/10.1002/adfm.202210905.

[60] S.Y. Yu, J. Mahmood, H.J. Noh, J.M. Seo, S.M. Jung, S.H. Shin, Y.K. Im, I.Y. Jeon, J.B. Baek, Direct synthesis of a covalent triazine-based framework from aromatic amides, Angew. Chemie - Int. Ed. 57 (2018) 8438–8442, https://doi.org/10.1002/anie.201801128.

[61] X. Song, Y. Wu, X. Zhang, X. Li, Z. Zhu, C. Ma, Boosting charge carriers separation and migration efficiency via fabricating all organic van der waals heterojunction for efficient photoreduction, Chem. Eng. J. 408 (2021) 127292, https://doi.org/10.1016/j.cej.2020.127292.

[62] H. Zhong, Z. Hong, C. Yang, L. Li, Y. Xu, X. Wang, R. Wang, A covalent triazine-based framework consisting of donor–acceptor dyads for visible-light-driven photocatalytic CO2 reduction, ChemSusChem 12 (2019) 4493–4499, https://doi.org/10.1002/cssc.201901997.

[63] S. Guo, Y. Xiao, B. Jiang, Encapsulation of Pd nanoparticles in covalent triazine frameworks for enhanced photocatalytic CO2 conversion, ACS Sustain. Chem. Eng. 9 (2021) 12646–12654, https://doi.org/10.1021/acssuschemeng.1c04176.

[64] L. Fang, G. Gou, J. Shang, M. Liu, Q. Gu, L. Li, Regulating the spin state of single-atom doped covalent triazine frameworks for efficient nitrogen fixation, J. Colloid Interface Sci. 627 (2022) 931–941, https://doi.org/10.1016/j.jcis.2022.07.090.

[65] I.H. Chowdhury, S. Gupta, V.G. Rao, Covalent organic framework: an emerging catalyst for renewable ammonia production, ChemCatChem 15 (2023) e202300243, https://doi.org/10.1002/cctc.202300243.

[66] P. Kuhn, M. Antonietti, A. Thomas, Porous, covalent triazine-based frameworks prepared by ionothermal synthesis, Angew. Chemie - Int. Ed. 47 (2008) 3450–3453, https://doi.org/10.1002/anie.200705710.

[67] Z.-A. Lan, Y. Fang, Y. Zhang, X. Wang, Photocatalytic oxygen evolution from functional triazine-based polymers with tunable band structures, Angew. Chem. 130 (2018) 479–483, https://doi.org/10.1002/anie.201711155.

[68] K. Wang, L.M. Yang, X. Wang, L. Guo, G. Cheng, C. Zhang, S. Jin, B. Tan, A. Cooper, Covalent triazine frameworks via a low-temperature polycondensation approach, Angew. Chemie - Int. Ed. 56 (2017) 14149–14153, https://doi.org/10.1002/anie.201708548.

[69] P. Chem, S. Ren, R. Dawson, A. Laybourn, J. Jiang, Y. Khimyak, D.J. Adams, A.I. Cooper, Functional conjugated microporous polymers : from 1,3,5-benzene to, Polym. Chem. 3 (2012) 928–934, https://doi.org/10.1039/c2py00585a.

[70] L. Ma, W. Hu, B. Mei, H. Liu, B. Yuan, J. Zang, T. Chen, L. Zou, Z. Zou, B. Yang, Y. Yu, J. Ma, Z. Jiang, K. Wen, H. Yang, Covalent triazine framework confined copper catalysts for selective electrochemical CO2 reduction: operando diagnosis of active sites, ACS Catal. 10 (2020) 4534–4542, https://doi.org/10.1021/acscatal.0c00243.

[71] Y. Zheng, N.A. Khan, X. Ni, K.A.I. Zhang, Y. Shen, N. Huang, X.Y. Kong, L. Ye, Emerging covalent triazine framework-based nanomaterials for electrochemical energy storage and conversion, Chem. Commun. 59 (2023) 6314–6334, https://doi.org/10.1039/d3cc00712j.

[72] C. Lu, J. Yang, S. Wei, S. Bi, Y. Xia, M. Chen, Y. Hou, M. Qiu, C. Yuan, Y. Su, F. Zhang, H. Liang, X. Zhuang, Atomic Ni anchored covalent triazine framework as high efficient electrocatalyst for carbon dioxide conversion, Adv. Funct. Mater. 29 (2019) 1806884, https://doi.org/10.1002/adfm.201806884.

[73] P. Katekomol, J. Roeser, M. Bojdys, J. Weber, A. Thomas, Covalent triazine frameworks prepared from 1,3,5-tricyanobenzene, Chem. Mater. 25 (2013) 1542–1548, https://doi.org/10.1021/cm303751n.

[74] K. Ma, J. Li, J. Liu, C. Li, X.B. Chen, Z. Li, L. Wang, Z. Shi, S. Feng, Covalent triazine framework featuring single electron Co2+ centered in intact porphyrin units for efficient CO2 photoreduction, Appl. Surf. Sci. 629 (2023) 157453, https://doi.org/10.1016/j.apsusc.2023.157453.

[75] J. Jia, Z. Chen, Y. Belmabkhout, K. Adil, P.M. Bhatt, V.A. Solovyeva, O. Shekhah, M. Eddaoudi, Carbonization of covalent triazine-based frameworks: via ionic liquid induction, J. Mater. Chem. A 6 (2018) 15564, https://doi.org/10.1039/c8ta05583a.

[76] G. Wang, K. Leus, S. Zhao, P. Van Der Voort, Newly designed covalent triazine framework based on novel N-heteroaromatic building blocks for efficient CO2 and H2 capture and storage, ACS Appl. Mater. Interfaces 10 (2018) 1244–1249, https://doi.org/10.1021/acsami.7b16239.

[77] Z.A. Lan, M. Wu, Z. Fang, Y. Zhang, X. Chen, G. Zhang, X. Wang, Ionothermal synthesis of covalent triazine frameworks in a NaCl-KCl-ZnCl2 eutectic salt for the hydrogen evolution reaction, Angew. Chemie - Int. Ed. 61 (2022) e202201482, https://doi.org/10.1002/anie.202201482.

[78] C. Covalent, T. Frameworks, A general strategy for kilogram-scale preparation of highly crystalline covalent triazine frameworks, Angew. Chemie - Int. Ed. 61 (2022) e202203327, https://doi.org/10.1002/ange.202203327.

[79] N. Wang, G. Cheng, L. Guo, B. Tan, S. Jin, Hollow covalent triazine frameworks with variable shell thickness and morphology, Adv. Funct. Mater. 29 (2019) 1904781, https://doi.org/10.1002/adfm.201904781.

[80] Y. Zheng, S. Chen, K.A.I. Zhang, J. Guan, X. Yu, W. Peng, H. Song, J. Zhu, J. Xu, X. Fan, C. Zhang, T. Liu, Template-free construction of hollow mesoporous carbon spheres from a covalent triazine framework for enhanced oxygen electroreduction, J. Colloid Interface Sci. 608 (2022) 3168–3177, https://doi.org/10.1016/j.jcis.2021.11.048.

[81] W. Huang, Z.J. Wang, B.C. Ma, S. Ghasimi, D. Gehrig, F. Laquai, K. Landfester, K.A.I. Zhang, Hollow nanoporous covalent triazine frameworks: via acid vapor-assisted solid phase synthesis for enhanced visible light photoactivity, J. Mater. Chem. A 4 (2016) 7555–7559, https://doi.org/10.1039/c6ta01828a.

[82] J. Liu, M. Liu, X. Wang, K. Wang, S. Jin, B. Tan, The exfoliation of crystalline covalent triazine frameworks by glycerol intercalation, Adv. Mater. Interfaces. 8 (2021) 2100374, https://doi.org/10.1002/admi.202100374.

[83] C. Wang, H. Zhang, W. Luo, T. Sun, Y. Xu, Ultrathin crystalline covalent-triazine-framework nanosheets with electron donor groups for synergistically enhanced photocatalytic water splitting, Angew. Chemie - Int. Ed. 60 (2021) 25381–25390, https://doi.org/10.1002/anie.202109851.

[84] J. Li, P. Liu, Y. Tang, H. Huang, H. Cui, D. Mei, C. Zhong, Single-atom Pt−N₃ sites on the stable covalent triazine framework nanosheets for photocatalytic N₂ fixation, ACS Catal. 10 (2020) 2395–2881, https://doi.org/10.1021/acscatal.9b04925.

[85] X. Lan, C. Du, L. Cao, T. She, Y. Li, G. Bai, Ultrafine Ag nanoparticles encapsulated by covalent triazine framework nanosheets for CO₂ conversion, ACS Appl. Mater. Interface. 10 (2018) 38659–39410, https://doi.org/10.1021/acsami.8b14743.

[86] X. Hu, Z. Zhan, J. Zhang, I. Hussain, B. Tan, Immobilized covalent triazine frameworks films as effective photocatalysts for hydrogen evolution reaction, Nat. Commun. 12 (2021) 6596, https://doi.org/10.1038/s41467-021-26817-4.

[87] P. Xiong, S. Zhang, R. Wang, L. Zhang, Q. Ma, X. Ren, Y. Gao, Z. Wang, Z. Guo, C. Zhang, Covalent triazine frameworks for advanced energy storage: challenges and new opportunities, Energy Environ. Sci. 16 (2023) 3181–3213, https://doi.org/10.1039/d3ee01360j.

[88] Z. Xiang, D. Cao, Synthesis of luminescent covalent–organic polymers for detecting nitroaromatic explosives and small organic molecules, Macromol. Rapid Commun. 33 (2012) 1184–1190.

[89] V. Sadhasivam, R. Balasaravanan, C. Chithiraikumar, Palladium nanoparticles supported on nitrogen-rich containing melamine-based microporous covalent triazine polymers as efficient heterogeneous catalyst for C-Se coupling reactions, ChemCatChem 10 (2018) 3833–3844, https://doi.org/10.1002/cctc.201800400.

[90] Q. Wang, J. Wang, J.C. Wang, X. Hu, Y. Bai, X. Zhong, Z. Li, Coupling CsPbBr₃ quantum dots with covalent triazine frameworks for visible-light-driven CO₂ reduction, ChemSusChem 14 (2021) 1131–1139, https://doi.org/10.1002/cssc.202002847.

[91] P. Puthiaraj, S. Cho, Y. Lee, W. Ahn, Microporous covalent triazine polymers: efficient friedel–crafts synthesis and adsorption/storage of CO₂ and CH₄, J. Mater. Chem. A 3 (2015) 6792, https://doi.org/10.1039/c5ta00665a.

[92] T. Geng, X. Fang, F. Wang, F. Zhu, The synthesis of covalent triazine-based frameworks via friedel–crafts reactions of cyanuric chloride with thienyl and carbazolyl derivatives for fluorescence sensing to picric acid , iodine and capturing iodine, Macromol. Mater. Eng. 306 (2021) 2100461, https://doi.org/10.1002/mame.202100461.

[93] P. Puthiaraj, W. Ahn, Synthesis of copper nanoparticles supported on a microporous covalent triazine polymer : an efficient and reusable catalyst for O-arylation, Catal. Sci. Technol. 6 (2016) 1701, https://doi.org/10.1039/c5cy01590a.

[94] E. Troschke, S. Gr, L. Tilo, L. Borchardt, Microporous materials mechanochemical friedel-crafts alkylation-a sustainable pathway towards porous organic polymers, Angew. Chemie Int. Ed. 56 (2017) 6859–6863, https://doi.org/10.1002/anie.201702303.

[95] J. Yan, G. Yu, Sulfur-rich covalent triazine polymer nanospheres for environmental mercury removal and detection, Polym. Chem. 9 (2018) 4125–4131, https://doi.org/10.1039/c8py00419f.

[96] T. Geng, W. Zhang, Z. Zhu, G. Chen, L. Ma, S. Ye, Q. Niu, A covalent triazine-based framework from, Polym. Chem. 9 (2018) 777–784, https://doi.org/10.1039/c7py01834g.

[97] X. Li, J. Yu, Hierarchical photocatalysts, Chem. Soc. Rev. 45 (2016) 2603–2636, https://doi.org/10.1039/x0xx00000x.

[98] M.D. Ward, J.R. White, A.J. Bard, Electrochemical investigation of the energetics of particulate titanium dioxide photocatalysts. The methyl viologen-acetate system, J. Am. Chem. Soc. 105 (1983) 27–31.

[99] M. Long, W. Cai, H. Kisch, Visible light induced photoelectrochemical properties of n-BiVO₄ and n-BiVO₄/p-Co₃O₄, J. Phys. Chem. 112 (2008) 548–554.

[100] Y. Duan, A double Z-scheme catalyst BiOI/g-C₃N₄/Bi₂WO₆ for enhanced photocatalytic activity, J. Chem. Technol. Biotechnol. 98 (2022) 247–256, https://doi.org/10.1002/jctb.7243.

[101] R. Shen, G. Liang, L. Hao, P. Zhang, X. Li, In Situ synthesis of chemically bonded 2D/2D covalent organic frameworks/O-vacancy WO₃ Z-scheme heterostructure for photocatalytic overall water splitting, Adv. Mater. 35 (2023) 2303649, https://doi.org/10.1002/adma.202303649.

[102] X. Li, J. Yu, J. Low, Y. Fang, J. Xiao, X. Chen, Engineering heterogeneous semiconductors for solar water splitting, J. Mater. Chem. A 3 (2015) 2485–2534, https://doi.org/10.1039/C4TA04461D.

[103] L. Li, W. Fang, P. Zhang, J. Bi, Y. He, J. Wang, W. Su, Sulfur-doped covalent triazine-based frameworks for enhanced photocatalytic hydrogen evolution from water under visible light, J. Mater. Chem. A 4 (2016) 12402, https://doi.org/10.1039/c6ta04711d.

[104] D. You, Z. Pan, Q. Cheng, COFs-Ph@CdS S-scheme heterojunctions with photocatalytic hydrogen evolution and efficient degradation properties, J. Alloys Compd. 930 (2023) 167069, https://doi.org/10.1016/j.jallcom.2022.167069.

[105] M.M. Vadiyar, J.Y. Kim, J.H. Bae, K.W. Nam, Imidazole linker-induced covalent triazine framework–ZIF hybrids for confined hollow carbon super-heterostructures toward a long-life supercapacitor, Carbon Energy (2023) e344, https://doi.org/10.1002/cey2.344.

[106] X. Xu, W. Huang, X. Li, Y. Sui, W. Chen, Y. Li, H. Ye, C. Pan, H. Zhong, M. Wen, Triphenylamine-based covalent triazine framework@ carbon nanotube complex : efficient photogenerated charges migration for metal free photocatalytic Cr(VI) reduction, J. Environ. Chem. Eng. 11 (2023) 109331, https://doi.org/10.1016/j.jece.2023.109331.

[107] Z. Li, T. Deng, S. Ma, Z. Zhang, G. Wu, J. Wang, Q. Li, H. Xia, S.W. Yang, X. Liu, Three-component donor-π-acceptor covalent-organic frameworks for boosting photocatalytic hydrogen evolution, J. Am. Chem. Soc. 145 (2023) 8364–8374, https://doi.org/10.1021/jacs.2c11893.

[108] L. Guo, J. Gong, C. Song, Y. Zhao, B. Tan, Q. Zhao, S. Jin, Donor-acceptor charge migration system of superhydrophilic covalent triazine framework and carbon nanotube toward high performance solar thermal conversion, ACS Energy Lett. 5 (2020) 1300–1306, https://doi.org/10.1021/acsenergylett.0c00394.

[109] Z. Gao, Y. Jian, S. Yang, Q. Xie, C.J. Ross Mcfadzean, B. Wei, J. Tang, J. Yuan, C. Pan, G. Yu, Interfacial Ti−S bond modulated S-scheme MOF/covalent triazine framework nanosheet heterojunctions for photocatalytic C−H functionalization, Angew. Chemie - Int. Ed. 62 (2023) e202304173, https://doi.org/10.1002/anie.202304173.

[110] H. Ye, N. Gong, Y. Cao, X. Fan, X. Song, H. Li, C. Wang, Y. Mei, Y. Zhu, Insights into the role of protonation in covalent triazine framework-based photocatalytic hydrogen evolution, Chem. Mater. 134 (2022) 1481–1490, https://doi.org/10.1021/acs.chemmater.1c02697.

[111] Y. Shen, C. Zhu, S. Song, T. Zeng, L. Li, Z. Cai, Defect-abundant covalent triazine frameworks as sunlight-driven self-cleaning adsorbents for volatile aromatic pollutants in water, Environ. Sci. Technol. 53 (2019) 9091–9101, https://doi.org/10.1021/acs.est.9b02222.

[112] L. Li, Y. Zhu, N. Gong, W. Zhang, W. Peng, Y. Li, F. Zhang, X. Fan, Band-gap engineering of layered covalent organic frameworks via controllable exfoliation for enhanced visible-light-driven hydrogen evolution, Int. J. Hydrogen Energy 45 (2020) 2689–2698, https://doi.org/10.1016/j.ijhydene.2019.11.049.

[113] T. Zeng, Z. Jin, S. Li, J. Bao, Z. Huang, Y. Shen, H. Zhang, D. Wang, S. Song, Blocking polymerization of CTFs induces plentiful structural terminations for synchronous removal of organics and Cr(VI), Chem. Commun. 57 (2021) 4946–4949, https://doi.org/10.1039/d1cc00780g.

[114] Z. Jin, S. Jin, R. Zou, D. Wang, F. Dong, M. Liu, S. Song, T. Zeng, Intramolecular engineering of defective terminations within triazine-based conjugated polymers for augmented photocatalytic H₂ production and Cr(VI) reduction, J. Clean. Prod. 422 (2023) 138556, https://doi.org/10.1016/j.jclepro.2023.138556.

[115] Q. Niu, Z. Cheng, Q. Chen, G. Huang, J. Lin, J. Bi, L. Wu, Constructing nitrogen self-doped covalent triazine-based frameworks for visible-light-driven photocatalytic conversion of CO₂ into CH₄, ACS Sustain. Chem. Eng. 9 (2021) 1333–1340, https://doi.org/10.1021/acssuschemeng.0c07930.

[116] Z. Cheng, W. Fang, T. Zhao, S. Fang, J. Bi, S. Liang, L. Li, Y. Yu, L. Wu, Efficient visible-light-driven photocatalytic hydrogen evolution on phosphorus-doped covalent triazine-based frameworks, ACS Appl. Mater. Interfaces 10 (2018) 41415–41421, https://doi.org/10.1021/acsami.8b16013.

[117] T. Zhao, Q. Niu, G. Huang, Q. Chen, Y. Gao, J. Bi, L. Wu, Rational construction of Ni(OH)₂ nanoparticles on covalent triazine-based framework for artificial CO₂ reduction, J. Colloid Interface Sci. 602 (2021) 23–31, https://doi.org/10.1016/j.jcis.2021.05.131.

[118] N. Nouruzi, M. Dinari, B. Gholipour, M. Afshari, S. Rostamnia, In situ organized Pd and Au nanoparticles in a naphthalene-based imine-linked covalent triazine framework for catalytic suzuki reactions and H_2 generation from formic acid, ACS Appl. Nano Mater. 5 (2022) 6241–6248, https://doi.org/10.1021/acsanm.2c00285.

[119] M. Xu, H. Dang, M. Wang, S. Zhang, Q. Jia, J. Tian, M. Wang, M. Du, New dual-modal electrochemical and photoelectrochemical aptasensing strategy for the sensitive detection of penicillin G based on an iron-doped covalent triazine framework, Microchem. J. 194 (2023) 109242, https://doi.org/10.1016/j.microc.2023.109242.

[120] J. Li, P. Liu, Y. Tang, H. Huang, H. Cui, D. Mei, C. Zhong, Single-atom Pt−N_3 sites on the stable covalent triazine framework nanosheets for photocatalytic N_2 fixation, ACS Catal. 10 (2020) 2431–2442, https://doi.org/10.1021/acscatal.9b04925.

[121] J. Chen, G. Li, N. Lu, H. Lin, S. Zhou, F. Liu, Anchoring cobalt single atoms on 2D covalent triazine framework with charge nanospatial separation for enhanced photocatalytic pollution degradation, Mater. Chem. 24 (2022) 100832, https://doi.org/10.1016/j.mtchem.2022.100832.

[122] Z. Zhou, C. Liu, C. Cai, N. Wang, X. Yu, Co-immobilization of laccase and PEG modified COFs into Cu doped gel beads to achieve synergistic effect of photocatalysis and enzymatic catalysis for pollutants removal, Colloids Surfaces A Physicochem. Eng. Asp. 656 (2023) 130201, https://doi.org/10.1016/j.colsurfa.2022.130201.

[123] A. Manuscript, Construction of cerium-based oxide catalysts with abundant defects/vacancies and their application to catalytic elimination of air pollutants, J. Mater. Chem. A 9 (2021) 3555–3566, https://doi.org/10.1039/D0TA10875H.Volume.

[124] R. He, K. Xue, J. Wang, T. Yang, R. Sun, L. Wang, X. Yu, U. Omeoga, W. Wang, T. Yang, Y. Hu, S. Pi, Design and synthesis of La^{3+}-, Sb^{3+}-doped MOF-In_2S_3 @ FcDc-TAPT COFs hybrid materials with enhanced photocatalytic activity, J. Mater. Sci. 54 (2019) 14690–14706, https://doi.org/10.1007/s10853-019-03914-w.

[125] J. Wang, Y. Yu, W. Xu, H. Yu, W. Zhang, H. Huang, Á. Pd, Covalent triazine framework encapsulated Pd nanoclusters for efficient hydrogen production via ammonia borane hydrolysis, J. Catal. 411 (2022) 72–83, https://doi.org/10.1016/j.jcat.2022.05.009.

[126] E. Saputra, M. Wahyu Nugraha, B. Aditya Prawiranegara, N. Soraya Sambudi, W. Da Oh, W. Peng, H. Sugesti, P. Setia Utama, Synergistic copper-modified covalent triazine framework for visible-light-driven photocatalytic degradation of organic pollutant, Environ. Nanotechnol. Monit. Manag. 19 (2023) 100774, https://doi.org/10.1016/j.enmm.2022.100774.

[127] S.P. Deshmukh, A.G. Dhodamani, S.M. Patil, S.B. Mullani, K.V. More, S.D. Delekar, Interfacially interactive ternary silver-supported polyaniline/multiwalled carbon nanotube nanocomposites for catalytic and antibacterial activity, ACS Omega 5 (2020) 219–227, https://doi.org/10.1021/acsomega.9b02526.

[128] Z. Xu, Y. Cui, D.J. Young, J. Wang, H.Y. Li, G.Q. Bian, H.X. Li, Combination of Co^{2+}-immobilized covalent triazine framework and TiO_2 by covalent bonds to enhance photoreduction of CO_2 to CO with H_2O, J. CO_2 Util. 49 (2021) 101561, https://doi.org/10.1016/j.jcou.2021.101561.

[129] L. Wang, L. Wang, S. Yuan, L. Song, H. Ren, Y. Xu, M. He, Y. Zhang, H. Wang, Y. Huang, T. Wei, J. Zhang, Y. Himeda, Z. Fan, Covalently-bonded single-site Ru-N_2 knitted into covalent triazine frameworks for boosting photocatalytic CO_2 reduction, Appl. Catal. B Environ. 322 (2023) 122097, https://doi.org/10.1016/j.apcatb.2022.122097.

[130] D. Kong, X. Han, S.A. Shevlin, C. Windle, J.H. Warner, Z. Guo, A Metal-free oxygenated covalent triazine 2-D photocatalyst works effectively from the ultraviolet to near-infrared spectrum for water oxidation apart from water reduction, ACS Appl. Energy Mater. 3 (2020) 8960–8968, https://doi.org/10.1021/acsaem.0c01153.

[131] H. Zhuang, W. Chen, W. Xu, X. Liu, Facile synthesis of MoS_2 QDs/TiO_2 nanosheets via a self-assembly strategy for enhanced photocatalytic hydrogen production, Int. J. Energy Res. 44 (2020) 3224–3230, https://doi.org/10.1002/er.5153.

[132] A. Manuscript, Covalent triazine frameworks: synthesis and applications, J. Mater. Chem. A 7 (2019) 5153–5172, https://doi.org/10.1039/C8TA12442F.

[133] Q. Cao, X. Wu, Y. Zhang, B. Yang, X. Ma, J. Song, J. Zhang, Potassium-doped carbon nitride : highly efficient photoredox catalyst for selective oxygen reduction and arylboronic acid hydroxylation, J. Catal. 414 (2022) 64–75, https://doi.org/10.1016/j.jcat.2022.08.030.

[134] X. Lan, X. Liu, Y. Zhang, Q. Li, J. Wang, Q. Zhang, G. Bai, Unveiling charge dynamics in acetylene-bridged donor-π-acceptor covalent triazine framework for enhanced photoredox catalysis, ACS Catal. 11 (2021) 7429–7441, https://doi.org/10.1021/acscatal.1c01794.

[135] L. Guo, Y. Niu, S. Razzaque, B. Tan, S. Jin, Design of D−A1−A2 covalent triazine frameworks via copolymerization for photocatalytic hydrogen evolution, ACS Catal. 9 (2019) 9438–9445, https://doi.org/10.1021/acscatal.9b01951.

[136] D. Wang, W. Wang, R. Wang, S. Xi, B. Dong, A fluorescent covalent triazine framework consisting of donor–acceptor structure for selective and sensitive sensing of Fe^{3+}, Eur. Polym. J. 147 (2021) 110297 https://doi.org/10.1016/j.eurpolymj.2021.110297.

[137] W. Geng, X. Lu, H. Zhang, Y. Luo, Z. Wang, S. Guo, Z. Zhou, D. Zhang, Effective design and synthesis of donor-acceptor covalent triazine polymers with boosted photocatalytic performance for Cr(VI) reduction, Sep. Purif. Technol. 290 (2022) 120829, https://doi.org/10.1016/j.seppur.2022.120829.

[138] Y. Shen, S. Liu, L. Lu, C. Zhu, Q. Fang, R. Liu, Y. Shen, Pyridine-linked covalent triazine frameworks with bidirectional electron donor-acceptor for efficient organic pollution removal, J. Hazard Mater. 444 (2023) 130428, https://doi.org/10.1016/j.jhazmat.2022.130428.

[139] W. Huang, J. Byun, I. Rçrich, C. Ramanan, P.W.M. Blom, H. Lu, D. Wang, L. Caire, R. Li, L. Wang, K. Landfester, K.A.I. Zhang, Asymmetric covalent triazine framework for enhanced visible-light photoredox catalysis via energy transfer cascade, Angew. Chem. Int. Ed. 57 (2018) 8316–8320, https://doi.org/10.1002/anie.201801112.

[140] S. Chaubey, R.K. Yadav, S.K. Tripathi, B.C. Yadav, S.N. Singh, T.W. Kim, Covalent triazine framework as an efficient photocatalyst for regeneration of NAD(P)H and selective oxidation of organic sulfide, Photochem. Photobiol. 98 (2022) 150–159, https://doi.org/10.1111/php.13504.

[141] Z. Li, T. Li, J. Miao, C. Zhao, Y. Jing, F. Han, K. Zhang, X. Yang, Amide-functionalized covalent triazine framework for enhanced photocatalytic hydrogen evolution, Sci. China Mater. 66 (2023) 2290–2298, https://doi.org/10.1007/s40843-022-2394-6.

[142] M.A. Fávaro, J. Yang, D. Ditz, H. Küçükkeçeci, M.H. Alkhurisi, S. Bergwinkl, A. Thomas, E.A. Quadrelli, R. Palkovits, J. Canivet, F.M. Wisser, Pyrene- and bipyridine-based covalent triazine framework as versatile platform for photocatalytic solar fuels production, ChemCatChem 15 (2023) e202300197, https://doi.org/10.1002/cctc.202300197.

[143] L. Guo, Y. Niu, H. Xu, Q. Li, S. Razzaque, Q. Huang, S. Jin, B. Tan, Engineering heteroatoms with atomic precision in donor-acceptor covalent triazine frameworks to boost photocatalytic hydrogen production, J. Mater. Chem. A 6 (2018) 19775–19781, https://doi.org/10.1039/c8ta07391k.

[144] Z. Li, H. Fang, Z. Chen, W. Zou, C. Zhao, X. Yang, Regulating donor-acceptor interactions in triazine-based conjugated polymers for boosted photocatalytic hydrogen production, Appl. Catal. B Environ. 312 (2022) 121374, https://doi.org/10.1016/j.apcatb.2022.121374.

[145] F. Yi, Q. Yang, X. Li, Y. Yuan, H. Cao, K. Liu, H. Yan, A 1,3,5-triazine and benzodithiophene based donor-acceptor type semiconducting conjugated polymer for photocatalytic overall water splitting, J. Solid State Chem. 318 (2023) 123769, https://doi.org/10.1016/j.jssc.2022.123769.

[146] C. Li, J. Liu, H. Li, K. Wu, J. Wang, Q. Yang, Covalent organic frameworks with high quantum efficiency in sacrificial photocatalytic hydrogen evolution, Nat. Commun. 13 (2022) 2357, https://doi.org/10.1038/s41467-022-30035-x.

[147] X. Lan, Q. Li, Y. Zhang, Q. Li, L. Ricardez-Sandoval, G. Bai, Engineering donor-acceptor conjugated organic polymers with boron nitride to enhance photocatalytic performance towards visible-light-driven metal-free selective oxidation of sulfides, Appl. Catal. B Environ. 277 (2020) 119274, https://doi.org/10.1016/j.apcatb.2020.119274.

[148] S. Vijayakrishnan, J.W. Ward, A.I. Cooper, Discovery of a covalent triazine framework photocatalyst for visible-light-driven chemical synthesis using high-throughput screening, ACS Catal. 12 (2022) 10057–10064, https://doi.org/10.1021/acscatal.2c02743.

[149] D. Chen, K. Kannan, H. Tan, Z. Zheng, Y.L. Feng, Y. Wu, M. Widelka, Bisphenol analogues other than BPA: environmental occurrence, human exposure, and toxicity-a review, Environ. Sci. Technol. 50 (2016) 5438–5453, https://doi.org/10.1021/acs.est.5b05387.

[150] S. Li, L. Li, Y. Li, L. Dai, C. Liu, Y. Liu, J. Li, J. Lv, P. Li, B. Wang, Fully conjugated donor-acceptor covalent organic frameworks for photocatalytic oxidative amine coupling and thioamide cyclization, ACS Catal. 10 (2020) 8717–8726, https://doi.org/10.1021/acscatal.0c01242.

[151] W.Y. Geng, F.Y. Chen, Y.H. Luo, Z.Y. Liu, S.F. Guo, Y.Y. Zhang, D.E. Zhang, X.Y. Yu, Boosting photocatalytic Cr(VI) reduction activities of layered COF through regulating donor-acceptor units and the orientation of imine bonds, Microporous Mesoporous Mater. 351 (2023) 112479, https://doi.org/10.1016/j.micromeso.2023.112479.

[152] W. Qiu, Y. He, L. Li, Z. Liu, S. Zhong, Y. Yu, Donor-acceptor pairs in covalent organic frameworks promoting electron transfer for metal-free photocatalytic organic synthesis, Langmuir 37 (2021) 11535–11543, https://doi.org/10.1021/acs.langmuir.1c01801.

[153] S. Li, L. Hu, Z. Qian, J. Yin, J. Tang, C. Pan, G. Yu, K.A.I. Zhang, Covalent triazine frameworks with unidirectional electron transfer for enhanced photocatalytic oxidation reactions, ACS Catal. 13 (2023) 12041–12047, https://doi.org/10.1021/acscatal.3c02122.

[154] Y. Hu, Y. Ji, Z. Qiao, L. Tong, Phenothiazine-linked covalent triazine frameworks for enhanced photocatalytic aerobic oxidation reactions, Microporous Mesoporous Mater. 362 (2023) 2070, https://doi.org/10.1016/j.micromeso.2023.112767.

[155] G. Zhang, W. Ou, J. Wang, Y. Xu, D. Xu, T. Sun, S. Xiao, M. Wang, H. Li, W. Chen, C. Su, Stable, carrier separation tailorable conjugated microporous polymers as a platform for highly efficient photocatalytic H$_2$ evolution, Appl. Catal. B Environ. 245 (2019) 114–121, https://doi.org/10.1016/j.apcatb.2018.12.007.

[156] C. Lin, X. Liu, B. Yu, C. Han, L. Gong, C. Wang, Y. Gao, Y. Bian, J. Jiang, Rational modification of two-dimensional donor-acceptor covalent organic frameworks for enhanced visible light photocatalytic activity, ACS Appl. Mater. Interfaces 13 (2021) 27041–27048, https://doi.org/10.1021/acsami.1c04880.

[157] Y. Zou, S. Abednatanzi, P. Gohari Derakhshandeh, S. Mazzanti, C.M. Schüßlbauer, D. Cruz, P. Van Der Voort, J.W. Shi, M. Antonietti, D.M. Guldi, A. Savateev, Red edge effect and chromoselective photocatalysis with amorphous covalent triazine-based frameworks, Nat. Commun. 13 (2022) 2171, https://doi.org/10.1038/s41467-022-29781-9.

[158] J. Chen, G. Li, H. Lin, F. Liu, Covalent triazine framework nanoribbons via polar solvent-induced fragmentation for ultrafast and solar-cleaning membrane separation, Chem. Eng. J. 429 (2022) 132401, https://doi.org/10.1016/j.cej.2021.132401.

[159] W. Zhang, B. Wang, H. Cui, Q. Wan, B. Yi, H. Yang, Unveiling the exciton dissociation dynamics steered by built-in electric fields in conjugated microporous polymers for photoreduction of uranium (VI) from seawater, J. Colloid Interface Sci. 662 (2024) 377–390, https://doi.org/10.1016/j.jcis.2024.02.073.

[160] W. Zhang, P. Sun, B. Wang, S. Li, B. Yi, Q. Liu, H. Yang, Polarization engineering of conjugated microporous polymers to boost exciton dissociation by dielectric constant regulation for photocatalytic degradation of antibiotics, Sep. Purif. Technol. 332 (2024) 125776, https://doi.org/10.1016/j.seppur.2023.125776.

[161] W. Zhang, Z. Deng, J. Deng, C.T. Au, Y. Liao, H. Yang, Q. Liu, Regulating the exciton binding energy of covalent triazine frameworks for enhancing photocatalysis, J. Mater. Chem. A 10 (2022) 22419–22427, https://doi.org/10.1039/d2ta06479k.

[162] B. Cai, L. Cao, R. Zhang, N. Xu, J. Tang, K. Wang, Q. Li, B. Xu, Y. Liu, Y. Fan, Construction of benzodithiophene-based donor-acceptor-type covalent triazine frameworks with tunable structure for photocatalytic hydrogen evolution, ACS Appl. Energy Mater. 6 (2023) 930–938, https://doi.org/10.1021/acsaem.2c03322.

[163] S.J. Hong, S. Lee, J.S. Jang, J.S. Lee, Heterojunction BiVO$_4$/WO$_3$ electrodes for enhanced photoactivity of water oxidation, Energy Environ. Sci. 4 (2011) 1781–1787, https://doi.org/10.1039/c0ee00743a.

[164] X. Kong, F. Yang, X. Li, M. Fu, T. Zeng, S. Song, Z. He, Y. Yu, Covalent triazine frameworks decorated with pyridine-type carbonitride moieties: enhanced photocatalytic hydrogen evolution by improved charge separation, Polymers 15 (2023) 1781, https://doi.org/10.3390/polym15071781.

[165] K. Wu, X.Y. Liu, M. Xie, P.W. Cheng, J. Zheng, W. Lu, D. Li, Rational design of D−π−A−π−D porous organic polymer with polarized π for photocatalytic aerobic oxidation, Appl. Catal. B Environ. 334 (2023) 122847, https://doi.org/10.1016/j.apcatb.2023.122847.

[166] J. Wang, W. Zhu, Y. Zhang, X. Yang, G. Bai, Q. Zhang, Y. Chen, X. Lan, Structural engineering of donor-π-acceptor conjugated polymers for facilitating charge separation: a dual-functional photocatalysis, Macromolecules 55 (2022) 10842–10853, https://doi.org/10.1021/acs.macromol.2c02014.

[167] J. Xiao, Z. Xiao, J. Hu, X. Gao, M. Asim, L. Pan, C. Shi, X. Zhang, J.J. Zou, Rational design of alkynyl-based linear donor-π-acceptor conjugated polymers with accelerated exciton dissociation for photocatalysis, Macromolecules 55 (2022) 5412–5421, https://doi.org/10.1021/acs.macromol.2c00885.

[168] X. Liu, R.X. Bi, F.T. Yu, C.R. Zhang, Q.X. Luo, R.P. Liang, J.D. Qiu, D-π-A array structure of Bi$_4$Ti$_3$O$_{12}$-triazine-aldehyde group benzene skeleton for enhanced photocatalytic uranium (VI) reduction, J. Hazard Mater. 451 (2023) 131189, https://doi.org/10.1016/j.jhazmat.2023.131189.

[169] H. Zhang, W. Wei, K.A.I. Zhang, Emerging conjugated polymers for heterogeneous photocatalytic chemical transformation, Chem. Commun. 59 (2023) 9167–9181, https://doi.org/10.1039/d3cc02081a.

[170] M.G. Kotp, A.M. Elewa, A.F.M. El-Mahdy, H.H. Chou, S.W. Kuo, Tunable pyridyl-based conjugated microporous polymers for visible light-driven hydrogen evolution, ACS Appl. Energy Mater. 4 (2021) 13140–13151, https://doi.org/10.1021/acsaem.1c02772.

[171] V.M. Vidya, S. Pola, P. Chetti, Synthesis and optical properties of mono- and di-substituted 1,3,5-triazines functionalized with thiophene and furan, J. Mol. Struct. 1254 (2022) 132408, https://doi.org/10.1016/j.molstruc.2022.132408.

[172] W.C. Lin, J. Jayakumar, C.L. Chang, L.Y. Ting, M.H. Elsayed, M. Abdellah, K. Zheng, A.M. Elewa, Y.T. Lin, J.J. Liu, W.S. Wang, C.Y. Lu, H.H. Chou, Effect of energy bandgap and sacrificial agents of cyclopentadithiophene-based polymers for enhanced photocatalytic hydrogen evolution, Appl. Catal. B Environ. 298 (2021) 120577, https://doi.org/10.1016/j.apcatb.2021.120577.

[173] P. Xie, C. Han, S. Xiang, S. Jin, M. Ge, C. Zhang, J.X. Jiang, Toward high-performance dibenzo[g,p]chrysene-based conjugated polymer photocatalysts for photocatalytic hydrogen production through donor-acceptor-acceptor structure design, Chem. Eng. J. 459 (2023) 141553, https://doi.org/10.1016/j.cej.2023.141553.

[174] T.X. Wang, H.P. Liang, D.A. Anito, X. Ding, B.H. Han, Emerging applications of porous organic polymers in visible-light photocatalysis, J. Mater. Chem. A 8 (2020) 7003–7034, https://doi.org/10.1039/d0ta00364f.

[175] H.S. Jena, C. Krishnaraj, S. Parwaiz, F. Lecoeuvre, J. Schmidt, D. Pradhan, P. Van Der Voort, Illustrating the role of quaternary-N of BINOL covalent triazine-based frameworks in oxygen reduction and hydrogen evolution reactions, ACS Appl. Mater. Interfaces 12 (2020) 44689–44699, https://doi.org/10.1021/acsami.0c11381.

[176] A. Manuscript, Covalent triazine frameworks–a sustainable perspective, Green Chem. 22 (2020) 1038–1071, https://doi.org/10.1039/C9GC03482J.

[177] C. Liu, Y. Xiao, Q. Yang, Y. Wang, R. Lu, Y. Chen, C. Wang, H. Yan, A highly fluorine-functionalized 2D covalent organic framework for promoting photocatalytic hydrogen evolution, Appl. Surf. Sci. 537 (2021) 148082, https://doi.org/10.1016/j.apsusc.2020.148082.

[178] T. Zeng, S. Jin, S. Li, J. Bao, Z. Jin, F. Dong, H. Zhang, S. Song, Covalent triazine frameworks with defective accumulation sites: exceptionally modulated electronic structure for solar-driven oxidative activation of peroxymonosulfate, Environ. Sci. Technol. 56 (2022) 9474–9485, https://doi.org/10.1021/acs.est.2c00126.

[179] T. Review, Metal nanoparticles at mesoporous N-doped carbons and carbon nitrides: functional Mott–Schottky heterojunctions for catalysis, Chem. Soc. Rev. 42 (2013) 6593–6604, https://doi.org/10.1039/c3cs60067j.

[180] J. He, X. Wang, S. Jin, Z.Q. Liu, M. Zhu, 2D metal-free heterostructure of covalent triazine framework/g-C$_3$N$_4$ for enhanced photocatalytic CO$_2$ reduction with high selectivity, Chinese J. Catal. 43 (2022) 1306–1315, https://doi.org/10.1016/S1872-2067(21)63936-0.

[181] J. Li, P. Liu, H. Huang, Y. Li, Y. Tang, D. Mei, C. Zhong, Metal-free 2D/2D black phosphorus and covalent triazine framework heterostructure for CO$_2$ photoreduction, ACS Sustain. Chem. Eng. 8 (2020) 5175–5183, https://doi.org/10.1021/acssuschemeng.9b07591.

[182] G. Li, J. Ye, Y. Shen, Q. Fang, F. Liu, Covalent triazine frameworks composite membrane (CdS/CTF-1) with enhanced photocatalytic in-situ cleaning and disinfection properties for sustainable separation, Chem. Eng. J. 421 (2021) 127784, https://doi.org/10.1016/j.cej.2020.127784.

[183] L. Ai, Q. Wang, F. Cui, G. Jiang, Peroxymonosulfate-assisted phenol degradation via a magnetic covalent-triazine-framework-based photocatalyst, ChemCatChem 15 (2023) e202300313, https://doi.org/10.1002/cctc.202300313.

[184] H. Huang, B. Xu, Z. Tan, Q. Jiang, S. Fang, L. Li, J. Bi, L. Wu, A facile in situ growth of CdS quantum dots on covalent triazine-based frameworks for photocatalytic H$_2$ production, J. Alloys Compd. 833 (2020) 155057, https://doi.org/10.1016/j.jallcom.2020.155057.

[185] X. Liu, R.X. Bi, C.R. Zhang, Q.X. Luo, R.P. Liang, J.D. Qiu, SnS$_2$-covalent organic framework Z-scheme van der waals heterojunction for enhanced photocatalytic reduction of uranium (VI) in rare earth tailings wastewater, Chem. Eng. J. 460 (2023) 141756, https://doi.org/10.1016/j.cej.2023.141756.

[186] Y. Yu, Y. Sun, B. Ge, J. Yan, K. Zhang, H. Chen, J. Hu, J. Tang, S. Song, T. Zeng, Synergistic removal of organic pollutants from water by CTF/BiVO$_4$ heterojunction photocatalysts, Environ. Sci. Pollut. Res. 30 (2023) 27570–27582, https://doi.org/10.1007/s11356-022-24184-1.

[187] C. Chen, J. Hu, X. Yang, T. Yang, J. Qu, C. Guo, C.M. Li, Ambient-stable black phosphorus-based 2D/2D S-scheme heterojunction for efficient photocatalytic CO$_2$ reduction to syngas, ACS Appl. Mater. Interfaces 13 (2021) 20162–20173, https://doi.org/10.1021/acsami.1c03482.

[188] D. Wang, H. Zeng, X. Xiong, M. Wu, M. Xia, M. Xie, J. Zou, S. Luo, Highly efficient charge transfer in CdS-covalent organic framework nanocomposites for stable photocatalytic hydrogen evolution under visible light, Sci. Bull. 65 (2020) 113–122, https://doi.org/10.1016/j.scib.2019.10.015.

[189] Y. Zhang, W. Xue, J. Liu, J. Yang, H. Song, X. Zhu, 2D/2D Covalent triazine-based heterostructure membrane for highly enhanced photoactivity and anti-fouling ability, Chem. Eng. J. 424 (2021) 129829, https://doi.org/10.1016/j.cej.2021.129829.

[190] Y. Zhang, Z. Chen, Z. Shi, T. Lu, D. Chen, Q. Wang, Z. Zhan, A direct Z-scheme BiOBr/TzDa COF heterojunction photocatalyst with enhanced performance on visible-light driven removal of organic dye and Cr(VI), Sep. Purif. Technol. 275 (2021) 119216, https://doi.org/10.1016/j.seppur.2021.119216.

[191] Q. Niu, S. Dong, J. Tian, G. Huang, J. Bi, L. Wu, Rational design of novel COF/MOF S-scheme heterojunction photocatalyst for boosting CO$_2$ reduction at gas−solid interface, ACS Appl. Mater. Interfaces 14 (2022) 24299–24308, https://doi.org/10.1021/acsami.2c02439.

[192] N. Xu, Y. Liu, W. Yang, J. Tang, B. Cai, Q. Li, J. Sun, K. Wang, B. Xu, Q. Zhang, Y. Fan, 2D-2D Heterojunctions of a covalent triazine framework with a triphenylphosphine-based covalent organic framework for efficient photocatalytic hydrogen evolution, ACS Appl. Energy Mater. 3 (2020) 11939–11946, https://doi.org/10.1021/acsaem.0c02102.

[193] W. Huang, Q. He, Y. Hu, Y. Li, Molecular heterostructures of covalent triazine frameworks for enhanced photocatalytic hydrogen production, Angew. Chem. 131 (2019) 8768–8772, https://doi.org/10.1002/ange.201900046.

[194] X. Han, Y.Y. Dong, J. Zhao, S. Ming, Y. Xie, Construction of ternary Z-scheme covalent triazine framework@Au@TiO$_2$ for enhanced visible-light-driven hydrogen evolution activity, Int. J. Hydrogen Energy 47 (2022) 18334–18346, https://doi.org/10.1016/j.ijhydene.2022.04.054.

[195] L.H. Shao, A.X. Huang, X.C. Yan, Y.H. Liu, Y. Wang, X. Jin, F.M. Zhang, Constructing tightly integrated conductive metal-organic framework/covalent triazine framework heterostructure by coordination bonds for photocatalytic hydrogen evolution, J. Colloid Interface Sci. 633 (2023) 233–242, https://doi.org/10.1016/j.jcis.2022.11.094.

[196] J. Chen, C.L. Dong, D. Zhao, Y.C. Huang, X. Wang, L. Samad, L. Dang, M. Shearer, S. Shen, L. Guo, Molecular design of polymer heterojunctions for efficient solar–hydrogen conversion, Adv. Mater. 29 (2017) 1606198, https://doi.org/10.1002/adma.201606198.

[197] W. Huang, Q. He, Y. Hu, Y. Li, Molecular heterostructures of covalent triazine frameworks for enhanced photocatalytic hydrogen production, Angew. Chemie - Int. Ed. 58 (2019) 8676–8680, https://doi.org/10.1002/anie.201900046.

[198] S. Cao, Y. Zhang, N. He, J. Wang, H. Chen, F. Jiang, Metal-free 2D/2D heterojunction of covalent triazine-based frameworks/graphitic carbon nitride with enhanced interfacial charge separation for highly efficient photocatalytic elimination of antibiotic pollutants, J. Hazard Mater. 391 (2020) 122204, https://doi.org/10.1016/j.jhazmat.2020.122204.

[199] Y. Zhang, H. Lv, Z. Zhang, L. Wang, X. Wu, H. Xu, Stable unbiased photo-electrochemical overall water splitting exceeding 3% efficiency via covalent triazine framework/metal oxide hybrid photoelectrodes, Adv. Mater. 33 (2021) 2008264, https://doi.org/10.1002/adma.202008264.

[200] Z. Wang, H. Wang, P. Shi, J. Qiu, R. Guo, J. You, H. Zhang, Hybrid organic frameworks: synthesis strategies and applications in photocatalytic wastewater treatment - a review, Chemosphere 350 (2024) 141143, https://doi.org/10.1016/j.chemosphere.2024.141143.

[201] H. Yan, Y.H. Liu, Y. Yang, H.Y. Zhang, X.R. Liu, J.Z. Wei, L.L. Bai, Y. Wang, F.M. Zhang, Covalent organic framework based WO$_3$@COF/rGO for efficient visible-light-driven H$_2$ evolution by two-step separation mode, Chem. Eng. J. 431 (2022) 133404, https://doi.org/10.1016/j.cej.2021.133404.

[202] R. Shen, N. Li, C. Qin, X. Li, P. Zhang, X. Li, J. Tang, Heteroatom- and bonded Z-scheme channels-modulated ultrafast carrier dynamics and exciton dissociation in covalent triazine frameworks for efficient photocatalytic hydrogen evolution, Adv. Funct. Mater. 33 (2023) 2301463, https://doi.org/10.1002/adfm.202301463.

[203] X. Qin, L. Ji, A. Zhu, Colloids and Surfaces A : physicochemical and engineering aspects construction of Ti$_3$C$_2$/ZnTCPP/CTFs ohmic/S-scheme hybrid heterojunction with robust built-in electric field for boosting photocatalytic hydrogen evolution, Colloids Surfaces A Physicochem. Eng. Asp. 676 (2023) 132198, https://doi.org/10.1016/j.colsurfa.2023.132198.

[204] G. Zhang, X. Li, D. Chen, N. Li, Q. Xu, H. Li, J. Lu, Internal electric field and adsorption effect synergistically boost carbon dioxide conversion on cadmium sulfide, covalent triazine frameworks core–shell photocatalyst, Adv. Funct. Mater. 33 (2023) 2308553, https://doi.org/10.1002/adfm.202308553.

[205] M. Liu, K. Jiang, X. Ding, S. Wang, C. Zhang, J. Liu, Z. Zhan, G. Cheng, B. Li, H. Chen, S. Jin, B. Tan, Controlling monomer feeding rate to achieve highly crystalline covalent triazine frameworks, Adv. Mater. 31 (2019) 1807865, https://doi.org/10.1002/adma.201807865.

[206] W. Huang, N. Huber, S. Jiang, K. Landfester, K.A.I. Zhang, Covalent triazine framework nanoparticles via size-controllable confinement synthesis for enhanced visible-light photoredox catalysis, Angew. Chem. Int. Ed. 59 (2020) 18368–18373, https://doi.org/10.1002/anie.202007358.

[207] J. Liu, C. Feng, Y. Li, Y. Zhang, Q. Liang, S. Xu, Z. Li, S. Wang, Photocatalytic detoxification of hazardous pymetrozine pesticide over two-dimensional covalent-organic frameworks coupling with Ag$_3$PO$_4$ nanospheres, Sep. Purif. Technol. 288 (2022) 120644, https://doi.org/10.1016/j.seppur.2022.120644.

[208] Y. Guo, X. Hu, R. Sun, X. Wang, B. Tan, Covalent triazine framework films through in-situ growth for photocatalytic hydrogen evolution, ChemSusChem 16 (2023) e202300759, https://doi.org/10.1002/cssc.202300759.

[209] C. Wang, H. Zhang, W. Luo, T. Sun, Y. Xu, Ultrathin crystalline covalent-triazine-framework nanosheets with electron donor groups for synergistically enhanced photocatalytic water splitting, Angew. Chemie - Int. Ed. 60 (2021) 25381–25390, https://doi.org/10.1002/anie.202109851.

[210] J. Zhen, J. Shen, T. Sun, C. Wang, P. Lyu, Y. Xu, Direct synthesis of ultrathin crystalline two-dimensional triazine polymers from aldoximes, CCS Chem. 6 (2024) 932–940, https://doi.org/10.31635/ccschem.023.202303111.

[211] J. Roeser, K. Kailasam, A. Thomas, Covalent triazine frameworks as heterogeneous catalysts for the synthesis of cyclic and linear carbonates from carbon dioxide and epoxides, ChemSusChem 5 (2012) 1793–1799, https://doi.org/10.1002/cssc.201200091.

[212] R. Xu, X.S. Wang, H. Zhao, H. Lin, Y.B. Huang, R. Cao, Rhenium-modified porous covalent triazine framework for highly efficient photocatalytic carbon dioxide reduction in a solid-gas system, Catal. Sci. Technol. 8 (2018) 2224–2230, https://doi.org/10.1039/c8cy00176f.

[213] S.Y. Yu, J. Mahmood, H.J. Noh, J.M. Seo, S.M. Jung, S.H. Shin, Y.K. Im, I.Y. Jeon, J.B. Baek, Direct synthesis of a covalent triazine-based framework from aromatic amides, Angew. Chemie - Int. Ed. 57 (2018) 8438–8442, https://doi.org/10.1002/anie.201801128.

[214] S. Deng, Z. Li, T. Zhao, G. Huang, J. Wang, J. Bi, Direct Z-scheme covalent triazine-based framework/Bi$_2$WO$_6$ heterostructure for efficient photocatalytic degradation of tetracycline: kinetics, mechanism and toxicity, J. Water Process Eng. 49 (2022) 103021, https://doi.org/10.1016/j.jwpe.2022.103021.

[215] L. Guo, X. Wang, Z. Zhan, Y. Zhao, L. Chen, T. Liu, B. Tan, S. Jin, Crystallization of covalent triazine frameworks via a heterogeneous nucleation approach for efficient photocatalytic applications, Chem. Mater. 33 (2021) 1994–2003, https://doi.org/10.1021/acs.chemmater.0c03716.

[216] Y. Wei, W. Jiang, Y. Liu, X. Bai, D. Hao, B.J. Ni, Recent advances in photocatalytic nitrogen fixation and beyond, Nanoscale 14 (2022) 2990–2997, https://doi.org/10.1039/d2nr00198e.

[217] F. Akira, H. Kenichi, Electrochemical photolysis of water at a semiconductor electrode, Nature 238 (1972) 37–38.

[218] C.B. Meier, R. Clowes, E. Berardo, K.E. Jelfs, M.A. Zwijnenburg, R.S. Sprick, A.I. Cooper, Structurally diverse covalent triazine-based framework materials for photocatalytic hydrogen evolution from water, Chem. Mater. 31 (2019) 8830–8838, https://doi.org/10.1021/acs.chemmater.9b02825.

[219] C.B. Meier, R.S. Sprick, A. Monti, P. Guiglion, J.S.M. Lee, M.A. Zwijnenburg, A.I. Cooper, Structure-property relationships for covalent triazine-based frameworks: the effect of spacer length on photocatalytic hydrogen evolution from water, Polymer 126 (2017) 283–290, https://doi.org/10.1016/j.polymer.2017.04.017.

[220] Y. Chen, G. Huang, Y. Gao, Q. Chen, J. Bi, Up-conversion fluorescent carbon quantum dots decorated covalent triazine frameworks as efficient metal-free photocatalyst for hydrogen evolution, Int. J. Hydrogen Energy 47 (2022) 8739–8748, https://doi.org/10.1016/j.ijhydene.2021.12.220.

[221] Z. Cheng, W. Fang, T. Zhao, S. Fang, J. Bi, S. Liang, L. Li, Y. Yu, L. Wu, Efficient visible-light-driven photocatalytic hydrogen evolution on phosphorus-doped covalent triazine-based frameworks, ACS Appl. Mater. Interfaces 10 (2018) 41415–41421, https://doi.org/10.1021/acsami.8b16013.

[222] D. Wang, X. Li, L.L. Zheng, L.M. Qin, S. Li, P. Ye, Y. Li, J.P. Zou, Size-controlled synthesis of CdS nanoparticles confined on covalent triazine-based frameworks for durable photocatalytic hydrogen evolution under visible light, Nanoscale 10 (2018) 19509–19516, https://doi.org/10.1039/c8nr06691d.

[223] F. Li, D. Wang, Q.J. Xing, G. Zhou, S.S. Liu, Y. Li, L.L. Zheng, P. Ye, J.P. Zou, Design and syntheses of MOF/COF hybrid materials via postsynthetic covalent modification: an efficient strategy to boost the visible-light-driven photocatalytic performance, Appl. Catal. B Environ. 243 (2019) 621–628, https://doi.org/10.1016/j.apcatb.2018.10.043.

[224] L.-L. Zheng, D. Wang, S.-L. Wu, X.-H. Jiang, J. Zhang, Q.-J. Xing, J.-P. Zou, S.-L. Luo, Unveiling localized Pt–P–N bonding states constructed on covalent triazine-based frameworks for boosting photocatalytic hydrogen evolution, J. Mater. Chem. A 28 (2023) 25425–25430, https://doi.org/10.1039/D0TA10165F.

[225] S. Li, M.F. Wu, T. Guo, L.L. Zheng, D. Wang, Y. Mu, Q.J. Xing, J.P. Zou, Chlorine-mediated photocatalytic hydrogen production based on triazine covalent organic framework, Appl. Catal. B Environ. 272 (2020) 118989, https://doi.org/10.1016/j.apcatb.2020.118989.

[226] G. Zhou, L.L. Zheng, D. Wang, Q.J. Xing, F. Li, P. Ye, X. Xiao, Y. Li, J.P. Zou, A general strategy: via chemically covalent combination for constructing heterostructured catalysts with enhanced photocatalytic hydrogen evolution, Chem. Commun. 55 (2019) 4150–4153, https://doi.org/10.1039/c9cc01161g.

[227] M. Chen, J. Xiong, Q. Shi, T. Li, X. Li, Y. Feng, B. Zhang, How the π bridge in donor-π-acceptor type covalent triazine frameworks influenced their photocatalytic hydrogen evolution performance, Chem. Eng. J. 475 (2023) 146099, https://doi.org/10.1016/j.cej.2023.146099.

[228] C. Wang, P. Lyu, Z. Chen, Y. Xu, Green and scalable synthesis of atomic-thin crystalline two-dimensional triazine polymers with ultrahigh photocatalytic properties, J. Am. Chem. Soc. 145 (2023) 12745–12754, https://doi.org/10.1021/jacs.3c02874.

[229] F. Yu, Z. Wang, S. Zhang, H. Ye, K. Kong, X. Gong, J. Hua, H. Tian, Molecular engineering of donor–acceptor conjugated polymer/g-C$_3$N$_4$ heterostructures for significantly enhanced hydrogen evolution under visible-light irradiation, Adv. Funct. Mater. 28 (2018) 1804512, https://doi.org/10.1002/adfm.201804512.

[230] S. Kampouri, T.N. Nguyen, C.P. Ireland, B. Valizadeh, F.M. Ebrahim, G. Capano, D. Ongari, A. Mace, N. Guijarro, K. Sivula, A. Sienkiewicz, L. Forró, B. Smit, K. C. Stylianou, Photocatalytic hydrogen generation from a visible-light responsive metal-organic framework system: the impact of nickel phosphide nanoparticles, J. Mater. Chem. A 6 (2018) 2476–2481, https://doi.org/10.1039/c7ta10225a.

[231] X. Hu, Q. Yin, C. Shu, X.F. Jiang, J. Zhang, Y. Zhang, J.X. Jiang, F. Huang, Y. Cao, Water-soluble conjugated molecule for solar-driven hydrogen evolution from salt water, Adv. Funct. Mater. 29 (2019) 1808156, https://doi.org/10.1002/adfm.201808156.

[232] L. Zhang, Y. Zhang, X. Huang, Y. Bi, Reversing electron transfer in a covalent triazine framework for efficient photocatalytic hydrogen evolution, Chem. Sci. 13 (2022) 8074–8079, https://doi.org/10.1039/d2sc02638d.

[233] Q. Jiang, L. Sun, J. Bi, S. Liang, L. Li, Y. Yu, L. Wu, MoS$_2$ quantum dots-modified covalent triazine-based frameworks for enhanced photocatalytic hydrogen evolution, ChemSusChem 11 (2018) 1108–1113, https://doi.org/10.1002/cssc.201702220.

[234] H. Wang, L. Guan, J. Liu, T. Lei, Y. Xue, Z. Qu, S. Jin, H. Ma, Z. Guo, A thiazolo[5,4-d]thiazole functionalized covalent triazine framework showing superior photocatalytic activity for hydrogen production and dye degradation, J. Mater. Chem. A 10 (2022) 16328, https://doi.org/10.1039/d2ta04177d.

[235] X. Han, F. Zhao, Q. Shang, Z. Zhao, X. Zhong, J. Zhang, Effect of nitrogen atom introduction on the photocatalytic hydrogen evolution activity of covalent triazine frameworks: experimental and theoretical study, ChemSusChem 15 (2022) e202200828, https://doi.org/10.1002/cssc.202200828.

[236] Z. Xu, Y. Cui, B. Guo, H.Y. Li, H.X. Li, Boosting visible-light-driven H$_2$ evolution of covalent triazine framework from water by modifying Ni(II) Pyrimidine-2-thiolate cocatalyst, ChemCatChem 13 (2021) 958–965, https://doi.org/10.1002/cctc.202001631.

[237] Y. Shao, D. You, Y. Wan, Q. Cheng, Z. Pan, A novel molecularly expanded covalent triazine framework heterojunction with significantly enhanced molecular oxygen activation and photocatalysis performance under visible light, Dalton Trans. 52 (2023) 11272, https://doi.org/10.1039/d3dt01726e.

[238] D. Kong, X. Han, J. Xie, Q. Ruan, C.D. Windle, S. Gadipelli, K. Shen, Z. Bai, Z. Guo, J. Tang, Tunable covalent triazine-based frameworks (CTF-0) for visible-light-driven hydrogen and oxygen generation from water splitting, ACS Catal. 9 (2019) 7697–7707, https://doi.org/10.1021/acscatal.9b02195.

[239] M. Liu, X. Wang, J. Liu, K. Wang, S. Jin, B. Tan, Palladium as a superior cocatalyst to platinum for hydrogen evolution using covalent triazine frameworks as a support, ACS Appl. Mater. Interfaces 12 (2020) 12774–12782, https://doi.org/10.1021/acsami.9b21903.

[240] P. Gao, C. Wu, S. Wang, G. Zheng, Q. Han, Efficient photosynthesis of hydrogen peroxide by triazole-modified covalent triazine framework nanosheets, J. Colloid Interface Sci. 650 (2023) 40–46, https://doi.org/10.1016/j.jcis.2023.06.186.

[241] W. Ren, Q. Chang, N. Li, J. Yang, S. Hu, Carbon dots-modulated covalent triazine frameworks with exceptionally rapid hydrogen peroxide production in water, Chem. Eng. J. 451 (2023) 139035, https://doi.org/10.1016/j.cej.2022.139035.

[242] H. Yan, Y. Deng, M. Shen, Y.X. Ye, F. Zhu, X. Yang, G. Ouyang, Regulation the reactive oxygen species on conjugated polymers for highly efficient photocatalysis, Appl. Catal. B Environ. 314 (2022) 121488, https://doi.org/10.1016/j.apcatb.2022.121488.

[243] Z. Zhou, M. Sun, Y. Zhu, P. Li, Y. Zhang, M. Wang, Y. Shen, A thioether-decorated triazine-based covalent organic framework towards overall H$_2$O$_2$ photosynthesis without sacrificial agents, Appl. Catal. B Environ. 334 (2023) 122862, https://doi.org/10.1016/j.apcatb.2023.122862.

[244] B.C. Moon, B. Bayarkhuu, K.A.I. Zhang, D.K. Lee, J. Byun, Solar-driven H$_2$O$_2$ production via cooperative auto- and photocatalytic oxidation in fine-tuned reaction media, Energy Environ. Sci. 15 (2022) 5082–5092, https://doi.org/10.1039/d2ee02504c.

[245] X. Zhang, J. Zhang, J. Miao, X. Wen, C. Chen, B. Zhou, M. Long, Keto-enamine-based covalent organic framework with controllable anthraquinone moieties for superior H$_2$O$_2$ photosynthesis from O$_2$ and water, Chem. Eng. J. 466 (2023) 143085, https://doi.org/10.1016/j.cej.2023.143085.

[246] T. Yang, Y. Chen, Y. Wang, X. Peng, A. Kong, Weakly hydrophilic imine-linked covalent benzene-acetylene frameworks for photocatalytic H$_2$O$_2$ production in the two-phase system, ACS Appl. Mater. Interfaces 15 (2023) 8066–8075, https://doi.org/10.1021/acsami.2c20506.

[247] X. Xu, Y. Sui, W. Chen, G. Zhou, Y. Li, H. Zhong, H.R. Wen, Anthraquinone-based conjugated organic polymers containing dual oxidation centers for photocatalytic H$_2$O$_2$ production from H$_2$O and O$_2$ under visible-light irradiation, ACS Appl. Polym. Mater. 5 (2023) 7571–7580, https://doi.org/10.1021/acsapm.3c01455.

[248] K. Li, B. Peng, T. Peng, Recent advances in heterogeneous photocatalytic CO$_2$ Conversion to solar fuels, ACS Catal. 6 (2016) 7485–7527, https://doi.org/10.1021/acscatal.6b02089.

[249] J. Ran, M. Jaroniec, S. Qiao, Cocatalysts in semiconductor-based photocatalytic CO$_2$ reduction: achievements, challenges, and opportunities, Adv. Mater. 30 (2018) 1704649, https://doi.org/10.1002/adma.201704649.

[250] U. Ulmer, T. Dingle, P.N. Duchesne, R.H. Morris, A. Tavasoli, T. Wood, G.A. Ozin, Fundamentals and applications of photocatalytic, Nat. Commun. 10 (2019) 3169, https://doi.org/10.1038/s41467-019-10996-2.

[251] Y. Zhang, B. Xia, J. Ran, K. Davey, S.Z. Qiao, Atomic-level reactive sites for semiconductor-based photocatalytic CO$_2$ reduction, Adv. Energy Mater. 10 (2020) 1903879, https://doi.org/10.1002/aenm.201903879.

[252] Y. Wang, E. Chen, J. Tang, Insight on reaction pathways of photocatalytic CO$_2$ conversion, ACS Catal. 12 (2022) 7300–7316, https://doi.org/10.1021/acscatal.2c01012.

[253] L. Guo, S. Jin, Stable covalent organic frameworks for photochemical applications, ChemPhotoChem 3 (2019) 973–983, https://doi.org/10.1002/cptc.201900089.

[254] R. Xu, D.H. Si, S.S. Zhao, Q.J. Wu, X.S. Wang, T.F. Liu, H. Zhao, R. Cao, Y.B. Huang, Tandem photocatalysis of CO$_2$ to C$_2$H$_4$ via a synergistic rhenium-(I) bipyridine/copper-porphyrinic triazine framework, J. Am. Chem. Soc. 145 (2023) 8261–8270, https://doi.org/10.1021/jacs.3c02370.

[255] G. Huang, G. Lin, Q. Niu, J. Bi, L. Wu, Covalent triazine-based frameworks confining cobalt single atoms for photocatalytic CO$_2$ reduction and hydrogen production, J. Mater. Sci. Technol. 116 (2022) 41–49, https://doi.org/10.1016/j.jmst.2021.11.035.

[256] G. Huang, Q. Niu, J. Zhang, H. Huang, Q. Chen, J. Bi, L. Wu, Platinum single-atoms anchored covalent triazine framework for efficient photoreduction of CO$_2$ to CH$_4$, Chem. Eng. J. 427 (2022) 131018, https://doi.org/10.1016/j.cej.2021.131018.

[257] S. Zhang, S. Wang, L. Guo, H. Chen, B. Tan, S. Jin, An artificial photosynthesis system comprising a covalent triazine framework as an electron relay facilitator for photochemical carbon dioxide reduction, J. Mater. Chem. C 8 (2019) 192–200, https://doi.org/10.1039/c9tc05297f.

[258] X. Hu, L. Zheng, S. Wang, X. Wang, B. Tan, Integrating single Co sites into crystalline covalent triazine frameworks for photoreduction of CO$_2$, Chem. Commun. 58 (2022) 8121–8124, https://doi.org/10.1039/d2cc02481k.

[259] Z. Zhang, Y. Jiang, Z. Dong, Y. Chu, J. Xu, 2D/2D Inorganic/organic hybrid of lead-free Cs$_2$AgBiBr$_6$ double perovskite/covalent triazine frameworks with boosted charge separation and efficient CO$_2$ photoreduction, Inorg. Chem. 61 (2022) 16028–16037, https://doi.org/10.1021/acs.inorgchem.2c02440.

[260] M. Lu, Q. Li, J. Liu, F.M. Zhang, L. Zhang, J.L. Wang, Z.H. Kang, Y.Q. Lan, Installing earth-abundant metal active centers to covalent organic frameworks for efficient heterogeneous photocatalytic CO$_2$ reduction, Appl. Catal. B Environ. 254 (2019) 624–633, https://doi.org/10.1016/j.apcatb.2019.05.033.

[261] S. Hu, S. Sun, Z. Feng, F. Wang, Y. Lv, Design and construction strategies to improve covalent organic frameworks photocatalyst' s performance for degradation of organic pollutants, Chemosphere 286 (2022) 131646, https://doi.org/10.1016/j.chemosphere.2021.131646.

[262] Q. Yuan, L. Chen, M. Xiong, J. He, S.L. Luo, C.T. Au, S.F. Yin, Cu$_2$O/BiVO$_4$ heterostructures: synthesis and application in simultaneous photocatalytic oxidation of organic dyes and reduction of Cr(VI) under visible light, Chem. Eng. J. 255 (2014) 394–402, https://doi.org/10.1016/j.cej.2014.06.031.

[263] Q. Liao, D. Wang, C. Ke, Y. Zhang, Q. Han, Y. Zhang, K. Xi, Metal-free Fenton-like photocatalysts based on covalent organic frameworks, Appl. Catal. B Environ. 298 (2021) 120548, https://doi.org/10.1016/j.apcatb.2021.120548.

[264] Y. Shen, C. Zhu, S. Song, T. Zeng, L. Li, Z. Cai, Defect-abundant covalent triazine frameworks as sunlight-driven self-cleaning adsorbents for volatile aromatic pollutants in water, Environ. Sci. Technol. 53 (2019) 9091–9101, https://doi.org/10.1021/acs.est.9b02222.

[265] G. Li, W. Wang, Y. Liu, Q. Fang, N. Lu, J. Chen, S. Xu, F. Liu, Solar-catalytic membranes constructed by graphene oxide and prussian blue@covalent triazine framework "active mega cubes" for ultrafast water transport, J. Memb. Sci. 644 (2022) 120156, https://doi.org/10.1016/j.memsci.2021.120156.

[266] Y. Shao, D. You, Y. Wan, Q. Cheng, Z. Pan, A novel molecularly expanded covalent triazine framework heterojunction with significantly enhanced molecular oxygen activation and photocatalysis performance under visible light, Dalton Trans. 52 (2023) 11272–11284, https://doi.org/10.1039/d3dt01726e.

[267] X. Yang, X. Bai, Y. Ma, D. He, X. Wang, Y. Guo, A solar light regenerated adsorbent by implanting CdS into an active covalent triazine framework to decontaminate tetracycline, Sep. Purif. Technol. 255 (2021) 117696, https://doi.org/10.1016/j.seppur.2020.117696.

[268] M. Roya, N. Azizi, M. Hekmati, M. Qomi, D. Esmaeili, ZnONPs/covalent triazine frameworks nanocomposite as high-performance photocatalysts for degradation of Congo red under visible light, Mater. Chem. Phys. 307 (2023) 128122, https://doi.org/10.1016/j.matchemphys.2023.128122.

[269] B. Yi, J. Zeng, W. Zhang, H. Cui, H. Liu, C.T. Au, Q. Wan, H. Yang, Enhanced hydrophilicity and promoted charge transfer in covalent triazine frameworks/ sepiolite complexed via hydrogen bonding for visible-light driven degradation of antibiotics, Appl. Clay Sci. 238 (2023) 106921, https://doi.org/10.1016/j.clay.2023.106921.

[270] X. Zhong, Q. Ling, S. Wang, B. Hu, Visible-light-driven 2D/2D bismuth oxyhalides/covalent organic framework heterojunctions for synchronous photocatalytic U(VI) reduction and bisphenol A degradation, J. Environ. Chem. Eng. 10 (2022) 108097, https://doi.org/10.1016/j.jece.2022.108097.

[271] H. Zhang, L. Zhang, S. Dong, X. Duan, D. Zhu, B.J. Ni, C. Lyu, Regulating energy band structures of triazine covalent organic frameworks with electron-donating/withdrawing substituents for visible-light-responsive photocatalytic tetracycline degradation and Cr(VI) reduction, J. Hazard Mater. 446 (2023) 130756, https://doi.org/10.1016/j.jhazmat.2023.130756.

[272] D. Lin, P. Duan, W. Yang, X. Huang, Y. Zhao, C. Wang, Q. Pan, Facile fabrication of melamine sponge@covalent organic framework composite for enhanced degradation of tetracycline under visible light, Chem. Eng. J. 430 (2022) 132817, https://doi.org/10.1016/j.cej.2021.132817.

[273] Y. Jia, Y. Zhang, X. Zhang, J. Cheng, Y. Xie, Y. Zhang, X. Yin, F. Song, H. Cui, Novel CdS/PANI/MWCNTs photocatalysts for photocatalytic degradation of xanthate in wastewater, Sep. Purif. Technol. 309 (2023) 123022, https://doi.org/10.1016/j.seppur.2022.123022.

[274] Y. Hou, F. Liu, C. Nie, Z. Li, M. Tong, Boosting exciton dissociation and charge transfer in triazole-based covalent organic frameworks by increasing the donor unit from one to two for the efficient photocatalytic elimination of emerging contaminants, Environ. Sci. Technol. 57 (2023) 11675–11686, https://doi.org/10.1021/acs.est.3c03711.

[275] K. Kamiya, R. Sugimoto, T. Tatebe, T. Harada, S. Nakanishi, Light-intensity-responsive changes of products in photocatalytic reduction of nitrous acid on a Cu-doped covalent triazine framework–TiO$_2$ hybrid, ChemSusChem 13 (2020) 3462–3468, https://doi.org/10.1002/cssc.202000687.

[276] X. Wang, S. Zhang, X. Li, Z. Zhan, B. Tan, X. Lang, S. Jin, Two-dimensional crystalline covalent triazine frameworksviadual modulator control for efficient photocatalytic oxidation of sulfides, J. Mater. Chem. A 9 (2021) 16405–16410, https://doi.org/10.1039/d1ta03951b.

[277] P. Liu, J. Yang, Y. Ai, S. Hao, X. Chen, F. Li, Recyclable covalent triazine framework-supported iridium catalyst for the N-methylation of amines with methanol in the presence of carbonate, J. Catal. 396 (2021) 281–290, https://doi.org/10.1016/j.jcat.2021.02.030.

[278] H. Hao, F. Zhang, X. Dong, X. Lang, 2D sp^2 carbon-conjugated triazine covalent organic framework photocatalysis for blue light-induced selective oxidation of sulfides with O$_2$, Appl. Catal. B Environ. 299 (2021) 120691, https://doi.org/10.1016/j.apcatb.2021.120691.